

Aus der Medizinischen Klinik und Poliklinik IV  
Klinik der Ludwig-Maximilians-Universität München  
Direktor: Prof. Dr. med. Martin Reincke

# **Metabolic comorbidities modulate kidney cholesterol crystal embolism**

Dissertation  
zum Erwerb des Doktorgrades der Humanbiologie  
an der Medizinischen Fakultät der  
Ludwig-Maximilians-Universität zu München

vorgelegt von

**Luying Yang**

aus Shandong, China

2023

**Mit Genehmigung der Medizinischen Fakultät  
der Ludwig-Maximilians-Universität München**

Berichterstatter : Prof. Dr. med. Hans-Joachim Anders

Mitberichterstatter : Prof. Dr. Daniel Teupser

Prof. Dr. Federico Tatò

Prof. Dr. Christian Weber

Mitbetreuung durch den

promovierten Mitarbeiter: Priv.-Doz. Dr. Stefanie Steiger

Dekan : Prof. Dr. med. Thomas Gudermann

Tag der mündlichen Prüfung : 03.04.2023

---

## Table of contents

<b>Declaration</b> .....	<b>ii</b>
<b>Zusammenfassung</b> .....	<b>iii</b>
<b>Summary</b> .....	<b>v</b>
<b>1. Introduction</b> .....	<b>1</b>
1.1 Cholesterol crystal embolism .....	1
1.2 Metabolic disorders and cholesterol crystal embolism .....	7
1.3 The role of the immune system in cholesterol crystal embolism.....	13
1.4 Animal models in metabolic disorders and cholesterol crystal embolism.....	17
<b>2. Hypotheses</b> .....	<b>22</b>
<b>3. Materials and Methods</b> .....	<b>23</b>
3.1 Materials.....	23
3.2 Mouse model procedures .....	28
3.3 Assessment of mouse kidney injury.....	31
3.4 Cell culture experiments .....	38
3.5 Analysis of platelet function in vitro .....	39
3.6 RNA analysis.....	40
3.7 Confocal microscopy imaging .....	43
3.8 Statistical analysis .....	43
<b>4. Results</b> .....	<b>44</b>
4.1 Type 1 diabetes worsens the outcomes in cholesterol crystal embolism .....	44
4.2 Hyperuricemia has vasoactive properties in cholesterol crystal embolism .....	57
<b>5. Discussion</b> .....	<b>77</b>
5.1 Overview .....	77
5.2 Type 1 diabetes worsens the outcomes in cholesterol crystal embolism .....	77
5.3 Hyperuricemia has vasoactive effects in cholesterol crystal-induced acute kidney injury ..	81
5.4 Limitations of this study .....	83
5.5 Summary and Conclusion .....	84
<b>6. References</b> .....	<b>85</b>
<b>7. Abbreviations</b> .....	<b>97</b>
<b>8. Acknowledgment</b> .....	<b>99</b>

***Declaration***

I hereby declare that all of the present work embodied in this thesis was carried out by me from 09/2018 until 03/2022 under the supervision of Prof. Dr. Hans Joachim Anders and Priv. Doz. Dr. Stefanie Steiger, Nephrologisches Zentrum, Medizinische Klinik und Poliklinik IV, Innenstadt Klinikum der Universität München. This work has not been submitted in part or full to any other university or institute for any degree or diploma.

Date: **03.04.2023**

Place: Munich, Germany

Signature: .....

(Luying Yang)

## **Zusammenfassung**

Die Cholesterinkristallembolie (CCE) ist eine häufige Komplikation der fortgeschrittenen Atherosklerose bei Patienten mit multiplen Begleiterkrankungen. Die CCE kann unter Umständen zu einer thrombotischen (Mikro-)Angiopathie führen und letztlich einen akuten Nierenschaden (AKI) mit ischämischer Nekrose verursachen. Das Ziel dieser Arbeit war es, die Pathomechanismen des CCE-induzierten AKI genauer zu untersuchen und inwiefern metabolische Begleiterkrankungen, wie Diabetes (Hyperglykämie) oder Hyperurikämie, den Nierenschaden, die Entzündung, Infiltration von Immunzellen, sowie den Verschluss von Arterien und Infarkt beeinflussen.

Um dies zu untersuchen, haben wir ein Tiermodell zur CCE etabliert. Hierbei wurden Cholesterinkristalle (CC) in die Nierenarterie von Mäusen injiziert und die CC-induzierte Niereninfarktgröße, Nierenfunktion, entzündliche Biomarker und Leukozyteninfiltration zu verschiedenen Zeitpunkten analysiert und quantifiziert. Diese Parameter wurden mit denen von Mäusen mit und ohne Hyperglykämie (Serumglukosespiegel  $\approx 500$  mg/dl) oder Hyperurikämie (Serumharnsäurespiegel  $\approx 9$  mg/dl) verglichen. Tubuläre Epithelzellen, Endothelzellen und gewaschene Thrombozyten wurden für mechanistische *in vitro* Studien unter erhöhten Glukose- oder Harnsäurebedingungen stimuliert.

Unsere Daten zeigten, dass die Hyperglykämie die Nierenfunktion nach CC Injektion sehr stark bei den Mäusen beeinträchtigt und vermehrt Niereninfarkte und -verschlüsse sowie Entzündung auftreten, was sich letztlich in erhöhten Entzündungsbiomarkern, vermehrte Leukozyteninfiltration, und beschleunigten Zelltod von Tubulusepithelzellen und Endothelzellen widerspiegelte. In *in vitro* Studien konnten wir zeigen, dass eine hohe Glukosekonzentration die Thrombozytenaggregation und -aktivierung im Vergleich zu normalen Bedingungen signifikant erhöht. Im Gegensatz dazu stehen die gefäßverengenden und antioxidativen Effekte der Hyperurikämie, welche zur Verbesserung der Nierenfunktion beitragen und die Niere vor ischämischen Infarkt und Gewebeschaden im Vergleich zu Tieren ohne Hyperurikämie nach CC-induzierten AKI schützt. Dies deutet auf einen kompensatorischen und autoregulatorischen physiologischen Mechanismus der Hyperurikämie zum Schutz der Niere hin.

---

Zusammenfassend lässt sich sagen, dass sowohl eine Hyperglykämie als auch eine Hyperurikämie einen AKI verschlimmern können, obwohl sie entgegengesetzte Auswirkungen auf den Niereninfarkt haben. Während die Hyperglykämie die Outcomes insbesondere bei Gewebsinfarkten in Mäusen nach CCE verschlechtert, vermindert die Hyperurikämie die Infarktgröße möglicherweise durch eine antioxidative Wirkung der löslichen Harnsäure und zeigt vasoaktive Effekte auf die Nierenfunktion in der kontralateralen Niere. Daher spiegelt der Grad der akuten Nierenfunktionsstörung möglicherweise nicht vollständig den Grad der Nierenschädigung bei der Hyperurikämie wieder. Insgesamt tragen die weit verbreiteten Komorbiditäten unabhängig voneinander zum Schweregrad der AKI und zum Ausmaß des Niereninfarkts bei CCE bei.

## Summary

Cholesterol crystal embolism (CCE) is a common complication of advanced atherosclerosis in patients with multiple comorbidities. CCE induces thrombotic (micro)angiopathy when affecting the kidney, causes acute kidney injury (AKI) and ischemic necrosis. We speculated that common metabolic comorbidities such as diabetes (hyperglycemia) or hyperuricemia would independently modulate pathomechanisms and affect the outcomes of CCE-induced AKI, e.g. kidney injury, inflammation, infiltration of immune cells, occlusion and infarction.

To investigate this, we induced experimentally CCE through injection of cholesterol crystal (CC) into the kidney artery of mice and analyzed CC-induced kidney infarct size, kidney function, inflammatory biomarkers and leukocyte infiltration at different timepoints. The parameters were compared with those from mice with and without hyperglycemia (serum glucose levels  $\approx 500$  mg/dl) or hyperuricemia (serum uric acid levels  $\approx 9$  mg/dl). Tubular epithelial cells, endothelial cells and washed platelets were stimulated under high glucose or high uric acid conditions *in vitro* for mechanistic studies.

Hyperglycemia contributed to impaired kidney function, increased kidney infarction and occlusion and inflammation as evidenced by elevated inflammatory biomarkers, leukocyte infiltration, accelerated cell death of tubular epithelial cells and endothelial cells as well as enhanced platelet aggregation and activation during CCE formation in a high glucose environment. In contrast, hyperuricemia had vasoconstrictive effects in the contralateral kidney by reducing kidney function, while at the same time protected mice from kidney infarction and tissue injury via anti-oxidative effects compared to non-hyperuricemic mice after CC-induced AKI. This suggests a compensatory and autoregulatory physiological mechanism of to protect the kidney.

In summary, both concomitant hyperglycemia and hyperuricemia can aggravate AKI despite having opposite effects on kidney infarction. While hyperglycemia worsens the outcome in particular tissue infarction in mice after CCE, hyperuricemia limits infarct size potentially via an anti-oxidative effect of soluble uric acid and shows vasoactive effects on kidney function in the contralateral kidney. Thus, the degree of acute kidney dysfunction may not fully reflect the

degree of kidney injury in hyperuricemia. Altogether, highly prevalent comorbidities independently contribute to the severity of AKI and the extent of kidney infarction in CCE.

## ***1. Introduction***

### ***1.1 Cholesterol crystal embolism***

Cholesterol crystal embolism (CCE) is a type of crystallopathy that occurs as a complication of severe atherosclerosis [1]. CCE may develop as a result of endovascular surgery, angiography or the use of anticoagulants, but may also develop spontaneously [2]. Whenever a large atherosclerotic plaque ruptures, the core material of the plaque containing CC may dislocate into the bloodstream. When entering smaller arteries and getting stuck in a certain location it may cause mechanical blockage of the artery and damage to the endothelium. Endothelial damage can trigger vascular obstruction, tissue ischemia and organ failure [3]. As a multi-system disease, CCE can affect a number of organs including the kidneys, skin, gastrointestinal tract, eyes, and muscles. The clinical features of CCE are diverse, which are mainly associated with the location of the atheromatous plaque and the obstructed arterial beds. CCE can present clinically as purple toes and in the kidneys as acute kidney injury (AKI).

#### ***1.1.1 Clinical studies of cholesterol crystal embolism***

That CCE can cause kidney disease was first described by Flory in 1945 [4]. With the development of medical technology, especially the popularity of kidney biopsy and the application of interventional cardiovascular therapies, cholesterol-induced multiple embolism has been found to be an increasingly important type of crystallopathies [1]. Because the disease generally requires a biopsy to confirm the diagnosis, patients who have not undergone biopsy or are asymptomatic are often not correctly diagnosed, indicating that the incidence of CCE to cause AKI is most likely underestimated.

#### ***Epidemiology and incidence***

Due to the diversity of symptoms, CCE is underdiagnosed [3, 5]. Flory performed autopsies on 267 patients with advanced atherosclerosis of which nine had CCE, and four cases of nine presented with CCE in the kidney arteries [4]. In a study of patients with thoracic aortic atherosclerotic plaques, 16 of the 519 patients (3%) were found peripheral CCE during follow-up of  $34 \pm 26$  months [6]. Yoshihiro Fukumoto and colleagues prospectively evaluated 1,789 patients after cardiac catheterization and 1.4% of them were diagnosed with CCE [7]. 19 of the 660 patients (2.9%) with abdominal aortic aneurysm were reported CCE in a mean of 15

---

months follow-up [8]. In a kidney biopsy study of AKI patients aged over 60, 7.5% of 259 cases revealed CCE [9].

Usually, CCE develops in people older than 60 years of age, often with clinical evidence of advanced atherosclerotic disease [5]. In a study of 354 renal CCE patients, 60% of them were older than 70 years of age and 90% had cardiovascular diseases [10]. CCE was reported to be a male-dominant disease with a sex ratio of 3.4:1 [11] or 83% [10]. Other risk factors for CCE include hypertension, tobacco usage, diabetes, angiographic procedures, anticoagulant treatment, and cardiovascular surgery [5, 12].

### ***Symptoms in the kidney***

The kidney is a common target organ for CC emboli, but only approximately 50% of patients present with clinical symptoms [13]. The time of presenting symptoms of AKI varies, for example, some patients develop symptoms shortly after CCE, while others show a delay of several weeks to months [12-14]. Kidney CCE manifests mostly in the following three conditions: 1) AKI that is often accompanied by symptoms from multiple sites or organs, resulting either from larger arteries or many emboli; 2) Subacute kidney injury that might be associated with an inflammatory response induced by CC emboli or successive lodging of new CC emboli; and 3) Chronic kidney disease (CKD) with renal vascular sclerosis or ischemic kidney disease that is often asymptomatic because CC emboli are only found in kidney biopsy or autopsy [3, 14]. Kidney ischemic injury and infarction, focal segmental necrotizing glomerulonephritis, and crescentic glomerulonephritis were observed in biopsies of patients with CCE of the kidney [15]. However, evaluating the role of CCE in CKD is rather difficult because patients often already have atherosclerotic kidney damage and urine analysis is often abnormal due to the underlying kidney disease. It is possible that CKD patients may have mild proteinuria and red and white blood cells or eosinophils in the urine sediment [14, 16].

### ***CCE in other organs***

Many factors influence the clinical features of kidney CCE, which involve the size and location of atherosclerotic plaques, lodging locations, the amount of CCs and the rupture frequency of plaques. CCE can occur in cerebral and retinal arteries, mainly derived from the ascending aorta and proximal aortic arch. It often presents with psychological disturbance, headaches, localized neurological deficits and amaurosis fugax, acute cerebrovascular disease, mild paralysis of the lower extremities, and mononeuropathy [17]. Arterial obstruction of the retina

---

can lead to retinal infarction, also known as Hollenhorst plaque, which is an additional diagnostic feature of CCE [18]. Emboli that mobilize to arteries of the kidneys and arteries below the abdomen such as in leg and feet are usually derived from the descending thoracic and abdominal aorta [17, 19]. Approximately 18% to 48% of CCE patients have gastrointestinal problems [20, 21]. Mucosal ulceration or infarction leading to gastrointestinal bleeding is more common and can also manifest as diarrhea, intestinal obstruction, stomach pain after eating and small intestine perforation. Moreover, skin lesions caused by CCE can be found in 35% to 96% of patients based on 6 case series [22]. Typical skin lesions include livedo reticularis (lower extremities and belly), cyanosis, infarction of the nail bed, toe gangrene, ulcers, and the appearance of blue-purple lesions (blue toe syndrome). In severe cases, penile and scrotal necrosis may occur [23]. In addition, hemoptysis, dyspnea, rhabdomyolysis, and femoral head necrosis can occur [24].

### ***Diagnosis of kidney CCE***

Histopathological confirmation of CC in kidney biopsies is the only option to confirm the diagnosis of CCE in the kidney [25]. CC emboli in the retina support the diagnosis and is more convenient to examine compared to kidney biopsy [26]. Kidney CC emboli can affect a variety of intrarenal arteries. Typical CCE occurs in medium-sized arteries, such as the arcuate and interlobular arteries, but can also occur in terminal capillaries [5]. The pathological morphology of CCE is a flat, convex needle shape. In paraffin-embedded tissue sections, CCs dissolve during tissue processing with alcohols leaving behind an empty cleft. If the tissue is treated with liquid nitrogen, CCs may appear birefringent under polarized light [3]. In the acute phase of CCE, CCs are often surrounded by eosinophils and accompanied by an inflammatory response in the surrounding interstitium. Fibrosis may develop around the arterial wall in the later stage. Usually, the vascular wall is inflamed without fibrinoid necrosis. It is also possible that CCs can be present in the glomerular capillaries, and complete obstruction of small arteries can lead to infarction or necrosis of the adjacent tissue, and incomplete obstruction can lead to localized ischemic atrophy of the kidney occurring distally [5].

The clinical manifestation of CCE does not only relate to organ damage but also to systemic inflammation. Inflammatory signs such as fever, weight loss, anorexia, fatigue, and myalgia are common in CCE patients [22]. Laboratory tests include abnormal inflammatory markers, such as increased white blood cells, erythrocyte sedimentation rate and C-reactive protein or

decreased serum complement levels. Patients may also have the potential to present anemia, thrombocytopenia and hypereosinophilia [22, 27, 28].

### **1.1.2 Pathophysiology of cholesterol crystal embolism**

#### ***Atherosclerotic plaque formation***

CCE occurs when small atheromas from major arteries including the aorta break and flush CC emboli into small arteries [1]. The atheromatous plaque or fibrofatty plaque is the central pathology of atherosclerosis. The atheromatous plaque forms in the intima layer. Low-density lipoprotein (LDL) particles are rich in cholesterol, covered by phospholipid with apolipoprotein B transport cholesterol through the bloodstream (Figure 1A). Barrier dysfunction of the endothelium favours LDL-C deposition in the intimal layer of arteries [29, 30]. LDL accumulates and aggregates with intimal proteoglycans and extracellular matrix macromolecules, and can enter smooth muscle cells through receptors [31, 32]. Cytokines released by endothelial cells and smooth muscle cells promote monocytes to migrate to endothelium lesions where they differentiate into macrophages. These macrophages for example express scavenger receptors that permit them from overloading cholesteryl ester and become foam cells, a hallmark of the early atherosclerotic lesion [33, 34]. Meanwhile, smooth muscle cells migrate from the tunica media layer into the intima by mediators released from leukocytes [35, 36]. Once atherosclerotic plaques are established they keep growing through the accumulation of lipid and lipid-filled cells such as macrophage foam cells.

Atherosclerotic plaques appear most commonly in the large arteries, especially in the ascending and abdominal aorta, arteria carotis and iliofemoral arteries [30]. Their formation and severity are strongly related to the lifestyle and dietary habits of individuals. For example, a high-fat and high-cholesterol diet as well as a sedentary office lifestyle are closely associated with advanced atherosclerosis. Other risk factors include monogenic disorders such as familial hypercholesterolaemia, diabetes, chronic inflammatory diseases and chronic kidney disease [37-40].

#### ***Atherosclerotic plaques rupture***

Usually atherosclerotic plaques remain stable for many years. However, they can gradually increase in size and ruptured plaques can damage the wall of arteries leading to coagulation and local thrombus formation(Figure 1B) [41]. Compared with ‘stable plaques’, which have

less lipid accumulation and thicker fibrous caps, ‘vulnerable plaques’ usually refer to lesions with large lipid cores covered by a thin fibrous cap ( $< 65 \mu\text{m}$ ) [42]. Numerous factors contribute to atherosclerotic plaques rupture including inflammation, sheering forces from blood flow (especially in hypertension), neovascularization around plaques, aneurysm, infection, anti-coagulation, surgery and vascular procedures [43].

### ***Lodging of the cholesterol crystal emboli***

CCE also referred to as atheromatous embolism is characterized by rupture of atherosclerotic plaques and multiple microemboli that contain CC fragments (Figure 1C). The material debris are released into the bloodstream and mobilize distally until they stuck in small arterioles that range from  $100 \mu\text{m}$  to  $200 \mu\text{m}$  in size [44, 45]. Compared with thromboemboli, CC emboli are smaller in size and occlude mainly end-organ arteries; thus, CC emboli are not easy to detect in the clinic. CCE can occur in brain and retinal arteries mainly derived from the ascending aorta and proximal aortic arch [18, 46]. Emboli that mobilize to arteries of the kidneys and arteries below the abdomen such as in leg and feet are usually derived from the descending thoracic and abdominal aorta [47].

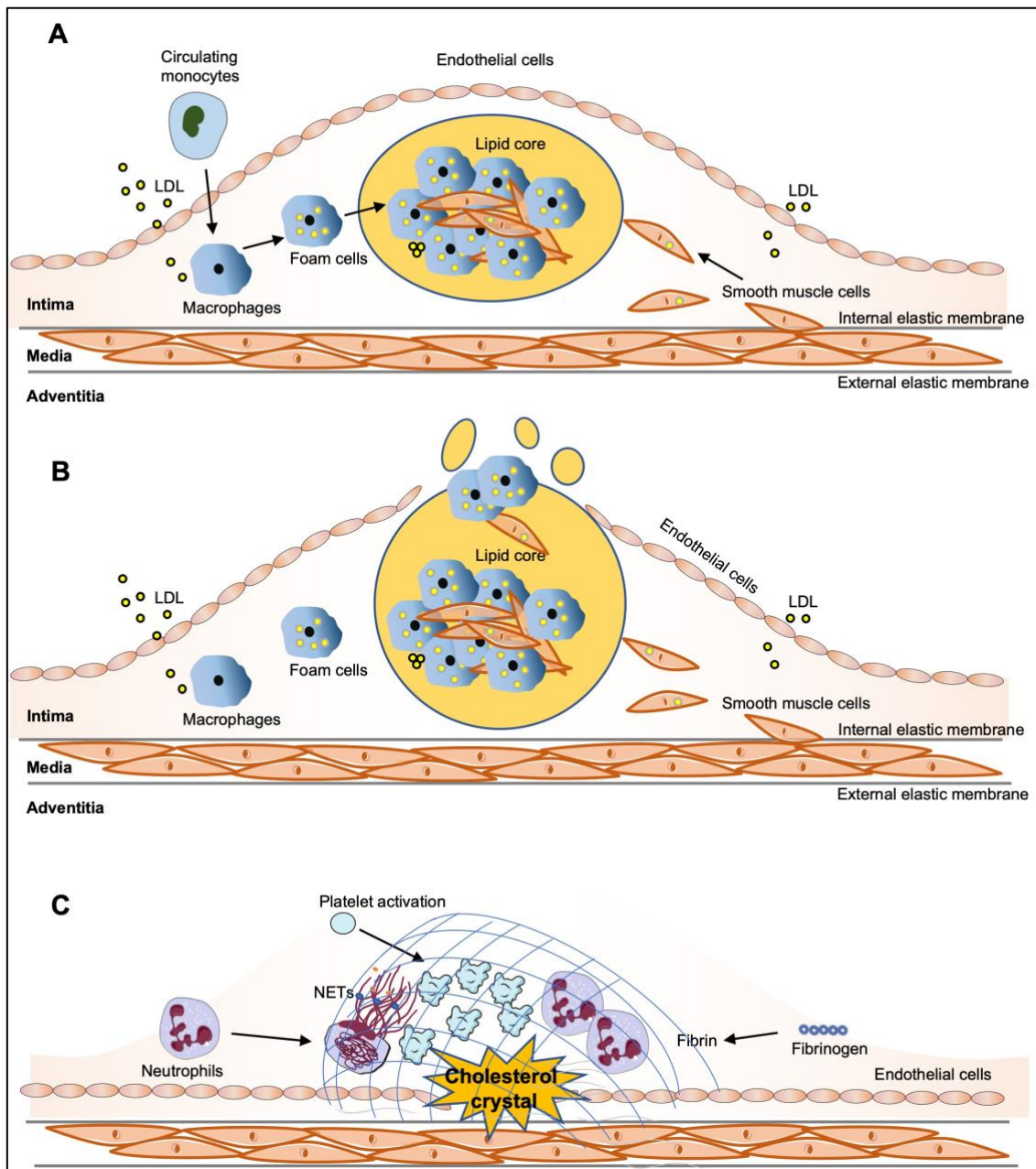


**Figure 1 Pathophysiology of cholesterol crystal embolism.** (A) Atherosclerotic plaque formation. In the early stages of lesion initiation, low-density lipoprotein (LDL) particles accumulate in the intima, which is composed of smooth muscle cells and elastin and collagen. In response to the pro-inflammatory effect of LDL, circulating monocytes migrate to the arterial wall and mature into macrophages. Macrophages in turn phagocytose LDL to become foam cells in the intima. Together with foam cells, smooth muscle cells migrate to the intima and form atherosclerotic plaque with lipid core eventually. (B) Atherosclerotic plaque rupture. With the expansion of the atherosclerotic plaque, the endothelium becomes thinner and eventually the plaque detaches from the arterial wall and enters the blood circulation. (C) Lodging and the inflammatory response of the cholesterol crystal emboli. Atherosclerotic plaque follows the blood flow and lodges in the arterial wall causing endothelial cells damage, collagen exposure, platelet activation, NET release, fibrin, etc., and eventually forming CCE.

---

### ***The inflammatory response in cholesterol crystal embolism***

When CC emboli obstruct the lumen of arterioles they promote a cascade of inflammatory responses including endothelium dysfunction, the release of cytokines, foreign body reaction, and intravascular thrombus formation that subsequently contribute to intimal fibrosis [41, 45]. Polymorphonuclear cells and eosinophils are the first cells that infiltrate the affected arterioles within the first 24 hours. Afterwards, monocytes infiltrate the affected lesion, differentiate into macrophages and form foreign body giant cells to phagocytose large CCs [45]. In addition, CC has been reported to activate the complement system through the lectin pathway in the inflammatory response [48]. In a recently established animal model of CCE in the kidney, extracellular traps were shown to have an important role during emboli formation [41].

### ***End-organ damage of cholesterol crystal emboli***

CC emboli are quite resistant to the breakdown efforts of macrophages and can remain in arterioles for up to 9 months [49]. Ultimately, the different extent of occlusion in the arterial lumen cause the tissue ischemic injury. End-organ damage can occur in any organ represented as skin necrosis, intestinal injury and acute kidney injury [5]. Clinical symptoms of CCE mostly relate to the location of the atheromatous plaque and the affected arterial beds. CC emboli released from the descending thoracic aorta may cause kidney failure, kidney infarction, mesenteric ischemia, while plaque rupture in the ascending aorta may also affect the brain and cause stroke-like symptoms [22].

## ***1.2 Metabolic disorders and cholesterol crystal embolism***

### **1.2.1 Metabolic syndrome**

Metabolic syndrome is a series of metabolic disturbances caused for example by insulin resistance, obesity and hyperlipidemia [50, 51]. The concept was first proposed one hundred years ago by Kylin, a Swedish physician, who defined hypertension, diabetes mellitus and gout as metabolic syndrome [52]. Over the past few decades, the prevalence of metabolic syndrome has strikingly increased worldwide due to the intake of high-calorie foods and the changing working patterns, which ranges from 20% to 25% in adults depending on different criteria [53, 54]. The Center of Disease Control (CDC) reported that 34.2% US adults had metabolic syndrome by 2012 [53]. In the general population, it increases the risks of cardiovascular disease. For example, people with metabolic syndrome have a 1.5 to 2-fold higher

cardiovascular risk than those without [55, 56]. As a hallmark of metabolic syndrome, insulin resistance promotes the development of type 2 diabetes. Other risk factors include stroke, hyperuricemia, hyperlipidemia and cardiovascular mortality [57, 58]. A better understanding of the pathomechanisms and treatment approaches are needed to prevent this global clinical problem.

Since diabetes mellitus, hyperuricemia and hyperlipidemia are complex comorbidities of an underlying disease or causally linked with each other, it is difficult to dissect the interrelationship and influence of different metabolic diseases in patients. Therefore, animal models are needed to explore the mechanistic changes between different metabolic diseases.

### **1.2.2 Diabetes**

Diabetes is a chronic metabolic disease with high blood glucose levels (hyperglycemia), leading over time to severe multi-organ injuries in the eyes, kidneys, nerves etc. According to the World Health Organization (WHO), about 422 million people all over the world suffer from diabetes and cause about 1.6 million deaths each year [59]. Diabetes usually results from insufficient production of the hormone insulin (type 1 diabetes, T1D) or an ineffective response of cells to insulin (type 2 diabetes, T2D). Other forms include gestational diabetes mellitus and specific types of diabetes such as drug- or chemical-induced diabetes. Diabetes can lead to various metabolic abnormalities in proteins, lipids and carbohydrates that eventually contribute to atherosclerosis [60].

#### ***Diabetes and atherosclerosis***

Diabetes is related to an increased risk of the development of atherosclerosis [61]. For example, studies reported an early development of atherosclerosis in T1D patients below 18 years old due to dyslipidemia, increased atherosclerotic LDL, hyperglycemia, oxidative stress and increased inflammation (Figure 2) [62]. Both large-scale clinical trials in T2D (the United Kingdom Prospective Diabetes Study) and T1D (the Diabetes Control and Complications) showed that patients without intensive blood glucose control had more risks of vascular complications [63].

Mechanistically, small dense LDL (sdLDL) particles play a pivotal role in atherosclerosis and studies have demonstrated that diabetes affects the levels of sdLDL. Although LDL is currently

---

considered a major source of intracellular lipid accumulation in atherosclerotic plaques, no significant lipid accumulation in cultured macrophages stimulated with native LDL particles has been observed [64]. Only alterations in the physical and chemical properties of LDL may trigger atherogenic lipid accumulation such as desialylation, which increases the particle density of LDL and reduces its volume followed by changes in the negative charge [64, 65]. After atherosclerotic low-density LDL accumulation in arterial lesions occurred, proteoglycans and LDL particles will be internalized mainly by macrophages in the lesion. The lower binding affinity of low-density LDL to the LDL receptor results in the accumulation of intracellular cholesterol in macrophages to form foam cells instead of degrading lipoprotein particles. Mette K Hagensen and colleagues illustrated that LDL from T1D patients showed increased subendothelial retention at atherosclerosis-prone sites in the arterial wall of mice [66]. A cross-sectional study reported that both T1D and T2D adolescents present a higher apolipoprotein B compared with the healthy control group [67]. Taken together, diabetes is an important comorbidity and risk factor of atherosclerosis.

### ***Diabetes in thrombosis and infarction***

Hyperglycemia can affect platelet reactivity, and consequently causes a hypercoagulable state in patients. Hyperglycemia can increase intracellular calcium mobilization and P-selectin exposure on the platelet surface, also increase the levels of circulating tissue factor in the blood, and inhibits platelet membrane fluidity and endothelial nitric oxide production [68-73]. Upregulation of systemic procoagulant factors increases the risk of arterial thrombosis such as coronary artery disease and cerebrovascular disease in diabetes. It was reported that 20%-40% of patients with T2D could finally develop cerebral blood vessel diseases [74]. Accordingly, mortality from ischemic infarction in patients with T1D or T2D is higher than in non-diabetic patients [75, 76]. In a retrospective cohort study based on 9 million adults, myocardial infarction was two to four times higher in diabetes than in those without diabetes [76]. Another study followed patients with diabetes for up to 9 years and reported that the risk of ischemic stroke was 3 times higher than in non-diabetic patients [77].

Currently, epidemiological studies between diabetes and CCE are missing. However, it is generally agreed that the risk factors for atherosclerosis including diabetes are also major risk factors for CCE [5, 13, 78]. In a prospective study of renal-CCE within 354 patients, diabetes was one of the significant predictors for death with an average of two years follow-up [10]. In diabetic db/db mice, treatment to prevent CC formation or to dissolve CC can markedly reduce

the progression of diabetic retinopathy [79]. Clinical and mechanistic studies between diabetes and CCE remain of utmost need.

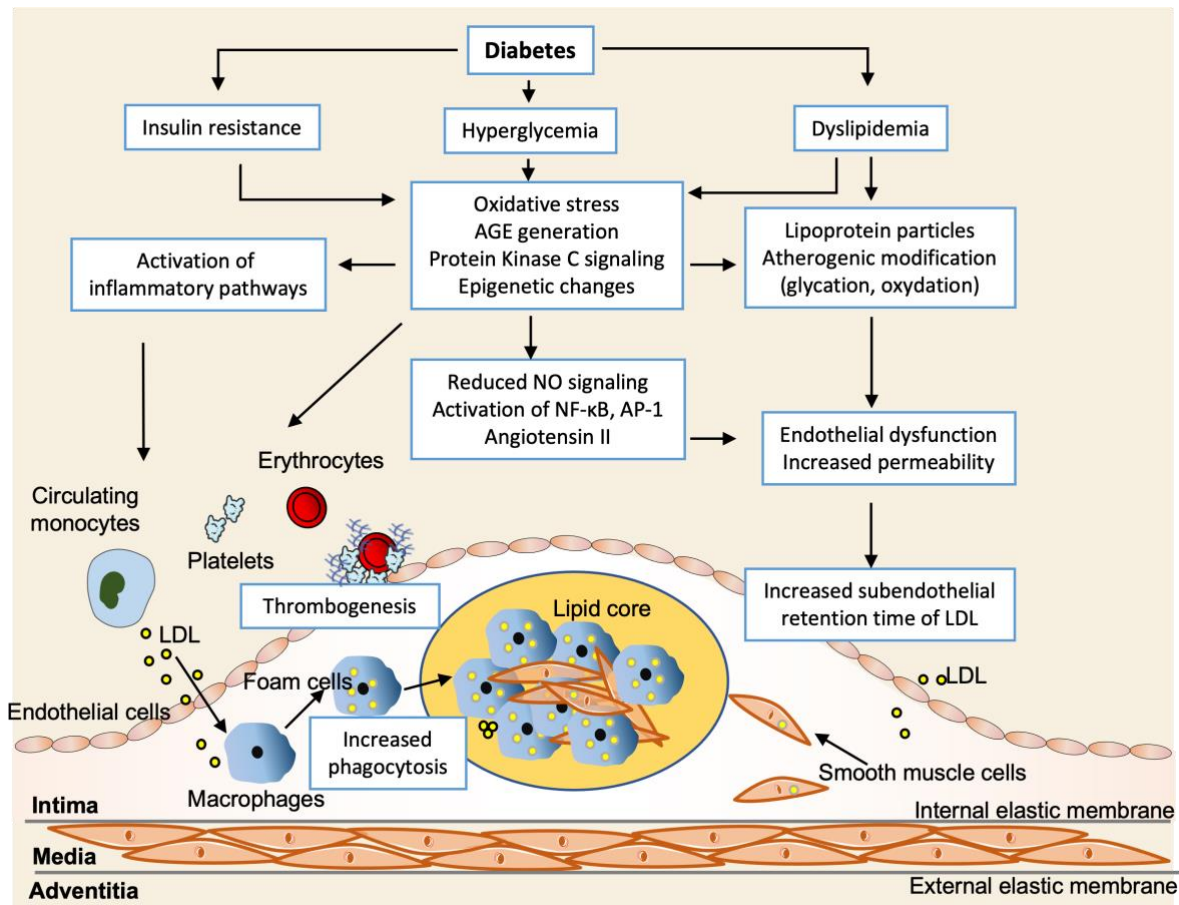


**Figure 2 Pathophysiology between diabetes and atherosclerosis.** Hyperglycemia, insulin resistance and dyslipidemia caused by diabetes can generate advanced glycation end products (AGE), activation of inflammatory pathways and lipoprotein particles atherogenic modification. In a hyperglycemic environment, many cellular activities promote atherosclerosis, such as endothelial cell dysfunction, migration of smooth muscle cells and macrophages, platelet activation and thrombosis formation.

### *Diabetes and acute kidney injury*

AKI refers to a rapid decline in kidney function within a few hours or days. Several human and animal studies demonstrate that diabetes contributes to the severity of AKI [80]. In a clinical trial in the UK with a median follow-up of 8.2 years, patients with T2D were more likely to develop AKI compared to non-T2D patients (48.6% versus 17.2%, respectively), and the prevalence of AKI was five times as high as in T2D patients who already had CKD as compared to patients without CKD [81]. A meta-analysis of cohort studies concluded that patients with diabetes in any level of estimated GFR and urine albumin-creatinine ratio (ACR) were at a higher risk of developing AKI [82]. Thus, diabetes is an independent risk factor for AKI.

---

Similarly, studies on the pathomechanisms of diabetes and AKI showed many similarities. For example, the hyperglycemic condition can upregulate Na/K ATPase activity and cause metabolic/hypoxic stress, which eventually results in impaired proximal tubular reabsorption and progression of kidney disease [83-85]. In addition, diabetes has many risk factors for AKI such as volume depletion caused by osmotic diuresis, potential nephrotoxic medications including inhibitors of the renin-angiotensin system and sodium-glucose cotransporter-2 (SGLT2) [86-88]. This is also evident by secondary immunodeficiencies related to kidney disease — for example glucosuria increases the risk for AKI from ascending urinary tract infection [89]. Furthermore, the kidney is a common target organ for CCE in patients with advanced atherosclerosis, which is an important comorbidity in diabetes. However, whether diabetes affects the outcomes after CC-induced AKI is currently unknown.

### **1.2.3 Hyperuricemia**

Uric acid (UA) is the end product of purine metabolism in humans. In contrast, to rodents, humans lost the enzyme uricase during evolution, which degrades UA into the more water-soluble allantoin. Therefore, humans have higher serum UA levels compared to other species. Approximately 70% of UA is excreted by the kidney and 30% by the gut. Genetic variants in urate transporters and kidney disease can cause an increase in serum UA levels, i.e., hyperuricemia. Hyperuricemia is defined as serum UA concentration of >7 mg/dL (>420  $\mu$ M) in men and >6 mg/dL (>360  $\mu$ M) in women. The definition threshold is chosen at 6.5 mg/dL because it is an approximation of the solubility of urate in water. However, in the plasma UA is more soluble and concentrations can increase up to >10 mg/dl (>600  $\mu$ m) without forming crystals.

#### ***The association between hyperuricemia and cardiovascular disease***

Whether hyperuricemia is causally related to metabolic comorbidities in humans has been of interest for many decades [90]. Epidemiological studies show that hyperuricemia associates with cardiovascular diseases. Indeed, serum UA concentrations are higher in individuals with coronary artery disease compared to healthy controls [91, 92]. In addition, several studies have shown that higher serum triglycerides, cholesterol and hyperglycemia are also associated with hyperuricemia [93-95].

However, a causal relationship between hyperuricemia and cardiovascular disease remains controversial. Data from animal studies and clinical trials are rather confounded because of the lack of a suitable animal model with clinically relevant serum UA concentrations or the outcome definitions in clinical trials. For example, a prospective cohort study in China investigated 2644 adults aged over 40 with a two-year follow-up. All participants with vascular stenosis were excluded. The results showed that individuals with hyperuricemia (serum UA levels >6 and >7 mg/dL for males and females, respectively) had a significantly higher cumulative incidence of stenosis compared with non-hyperuricemic patients, therefore increasing the risk for atherosclerosis [91]. Another single-center cross-sectional study included 4188 individuals without prior coronary artery disease or hyperuricemia-related disease. They found that serum UA levels were independently associated with the severity of coronary calcification measured by multidetector computed tomography [96]. *In vivo* studies using *Glut9* intestinal-specific knockout mice found that higher serum UA levels (175  $\mu$ M) were associated with early-onset metabolic syndrome and that treatment with urate-lowering therapy with allopurinol mitigated hypertension and dyslipidemia situation in knockout mice [97]. In contrast, Frederic Preitner *et al.* did not observe hypertension in liver-specific *Glut9* knockout hyperuricemic mice with serum UA levels of 300  $\mu$ M [98].

### ***The association of hyperuricemia and kidney disease***

Recent studies have demonstrated that asymptomatic hyperuricemia does not induce kidney injury nor contribute to the progression of CKD. Sellmayr *et al.* used a model of asymptomatic hyperuricemia with aristolochic acid I-induced CKD and showed no difference in kidney function between asymptomatic hyperuricemic mice with CKD (serum UA level: 15 mg/dL) and non-hyperuricemic mice with CKD after 42 days [99]. This is consistent with large multi-centre randomized control trials with urate-lowering therapy showing no benefit of allopurinol treatment in hyperuricemic patients with CKD [100, 101]. Only hyperuricemia with UA crystalluria causes tubular injury, inflammation and interstitial fibrosis that ultimately drives CKD progression [99, 102].

In addition, evidence now suggests that asymptomatic hyperuricemia with serum UA levels of 7–10 mg/dL can diminish tubular injury and inflammation, thus accelerating the recovery after acute kidney injury on day 14 suggesting an anti-inflammatory role of asymptomatic

hyperuricemia in AKI [103]. However, whether asymptomatic hyperuricemia exhibits similar effects also in CCE and improves the outcomes after CC-induced AKI is currently unknown.

### ***1.3 The role of the immune system in cholesterol crystal embolism***

Upon tissue damage and injury, several danger response programs are involved such as inflammation, clotting, epithelial healing and mesenchymal healing [104]. These protective response programs are necessary for humans to survive acute tissue injuries. For example during infections, clotting and inflammation occur rapidly to prevent further exacerbation of the injury. Although coagulation plays an important role in host defense against pathogens, the release of pro-inflammatory mediators and the activation of danger associated molecular patterns (DAMPs) contribute to thrombosis and tissue ischemia in the vasculature. The complex interplay between platelets, immune cells and CCs during CCE facilitates the closure of ruptured atherosclerotic plaques.

#### **1.3.1 From Vascular injury to thrombosis**

##### ***Platelet interaction with activated endothelium***

Under physiological conditions, pro and anti-thrombotic processes are kept in a balanced to maintain hemostasis, arresting bleeding in the accidentally opened vessel. The healthy endothelium limits platelet activation and adhesion by releasing NO and prostaglandin I<sub>2</sub> (PGI<sub>2</sub>) [105, 106]. Endothelial cells also express CD39 and CD73, which hydrolyse ADP to AMP and converts AMP to adenosine, and ADP to AMP, thereby inhibiting platelet aggregation to maintain vascular homeostasis [105].

Injured endothelium appears to diminish NO bioavailability and increases the adhesion of platelets as well as leukocytes [107]. Upon vessel injury, subendothelial matrix and von Willebrand factor (vWF) are exposed to the blood flow, that capture circulating platelets via vWF-collagen and glycoprotein Ib (GPIb)-IX-V—vWF interactions. Firm platelet adhesion to the injured endothelium is ensured by collagen interactions with platelet glycoprotein VI and integrin  $\alpha 2\beta 1$  [106]. Platelets also express several other integrins, such as  $\alpha \text{IIb}\beta 3$ ,  $\alpha \text{v}\beta 3$ ,  $\alpha 5\beta 1$  and  $\alpha 6\beta 1$  which can interact with various extracellular matrix proteins (mainly fibrinogen, vitronectin, fibronectin, laminin) and also mediate platelet attachment to the vessel wall [107]. Activated platelets release a variety of biologically active molecules, including adhesion

molecules (P-selectin, FGN, vWF), growth factors, chemokines, cytokines and coagulation factors from  $\alpha$  granules and ATP/ADP and serotonin from their dense ( $\delta$ ) granules along with thromboxane A<sub>2</sub> production [108]. These secondary mediators also contribute to the recruitment of platelets by increasing the affinity of integrin  $\alpha$ IIb $\beta$ 3 for fibrinogen and vWF, thereby inducing clot formation.

In the presence of CC, the hemostatic balance is disturbed by the rupture of endothelial layer. The vascular extracellular matrix is exposed, which further trigger platelet adhesion and thrombin induce platelet activation, thereby inducing glycoprotein VI (GPVI) and protease-activated receptor-G $\alpha_q$  (PAR-Gq) signalings, resulting in inside out activation of integrin  $\alpha$ IIb $\beta$ 3 [109, 110]. CC can also enhance platelet attachment to the endothelial cells, thereby amplifying platelet reactivity through P-selectin exposure, fibrinogen and ATP release from activated platelets, increasing the attachment of circulating platelets to the CC-induced thrombi [111].

### ***Activation of the coagulation cascade***

Following the process of blood clot formation, the second wave of a hemostatic process initiated by activated platelet mediators, induces the coagulation cascade. Activation of Factor XII caused by exposed collagen can trigger intrinsic coagulation pathways [112]. Injured endothelial cells also release tissue factors, which trigger extrinsic coagulation pathways [113]. The conversion of prothrombin to thrombin by prothrombinase complex is located on the activated platelet surface. Once thrombin is formed, conversion of fibrinogen to fibrin occurs immediately [114]. The fibrin network entraps circulating platelets, red blood cells and plasma proteins, thereby consolidating fibrin rich-thrombi. Upon CC-induced thrombus formation, activated platelets can release high amount of fibrinogen from  $\alpha$  granules, thereby inducing a fibrin-rich blood clot.

## **1.3.2 Thrombo-inflammation: interplay between immune cells and platelets**

### ***Platelet interaction with immune cells***

Clotting and inflammation are intimately linked and induce and amplify each other to limit fatal bleeding and pathogen invasion upon traumatic injuries [109-111]. Recent studies have

shown that platelets are not only involved in coagulation but also have an immune function and are actively involved in the inflammatory process [112]. Once immune cells are recruited to the site of injury, the interaction between activated platelets and immune cells is strongly influenced by interactions of surface receptors. First, neutrophils adhere to the exposed endothelial matrix through selectins and their ligands, e.g.  $\beta_2$  integrins and intercellular adhesion molecule 1 [113]. Activated platelets release P-selectin from  $\alpha$ -granules and transfer them to the cell surface. P-selectin glycoprotein ligand-1 (PSGL-1) is expressed on the membrane of leukocytes such as neutrophils, monocytes, dendritic cells and subclasses of lymphocytes [114]. The efficient association/dissociation interactions between P-selectin and PSGL-1 mediate physical interactions between platelets and leukocytes, which are crucial for the initial tethering and rolling of leukocytes to the vascular injuries. Afterward, the mixed platelet-leukocyte conjugates form in the blood [114].

In addition, activated platelets release biological molecules with hemostatic and non-hemostatic functions from  $\alpha$ -granules, dense granules, and lysosomes. Of these three,  $\alpha$ -granules are most important. During platelet activation,  $\alpha$ -granules fuse with the cell membrane and therefore increase the expression of inflammatory proteins and coagulation mediators on the surface as well as the release of soluble molecules. For example, platelet factor-4 released from  $\alpha$ -granules can induce neutrophil activation and phagocytosis as well as respiratory burst in monocyte [115]. Chemokine (C-X-C motif) ligand 1 (CXCL1) mediates monocyte recruitment along the endothelium under flow *in vitro* and this can be inhibited by blocking C-X-C motif chemokine receptor 2 (CXCR2) function [116]. ADP and ATP released from platelet dense granules may modulate oxygen respiratory burst in neutrophils by leukocyte purinergic receptors [117, 118].

### ***Release of extracellular traps***

A breakthrough in the field of immunothrombosis was the discovery of immune cells releasing extracellular traps during infection, i.e., neutrophil extracellular traps (NETs). Extracellular traps are composed of DNA, histones and granules from injured immune cells that act as pro-thrombotic DAMPs and provoke coagulation and fibrin formation [119]. These structures are formed by chromatin trapped red blood cells, platelets and coagulation factors including tissue factor and fibrin. These processes trigger platelet activation and induce procoagulant and prothrombotic effects on the vasculature that ultimately cause the release of extracellular DNA, MPO, neutrophil elastase and histones in neutrophils or monocytes [120]. Studies indicate that

extracellular traps from neutrophils and monocytes induce endothelial dysfunction and drive clotting, which contributes to organ failure [121]. Injecting anti-histone antibodies and activated protein C in mice prevented acute tissue injury, while platelets stimulated with thrombin receptor agonists induced NETosis, a form of cell death, in neutrophils suggesting a direct contribution of activated platelets and their mediators in this process [122].

In addition to immune cells, apoptotic platelets and damaged endothelial cells can also release extracellular DNA, therefore the provenance of extracellular traps remains controversial *in vivo* [111, 123]. Indeed, neutrophils, circulating extracellular DNA and neutrophil elastase are elevated in stroke patients implying that neutrophils play an important role in extracellular trap formation. Similarly, our published data showed that neutrophil depletion by anti-Ly6G antibody protects from ischemic tissue infarction during CCE-induced AKI in mice. However, this had no significant effect on the glomerular filtration rate (GFR) decline or arterial obstructions [111]. While recombinant DNase I inhibited clot formation and protected from GFR loss during CCE suggesting that extracellular DNA is not only released from neutrophils but also from other cells. Therefore, more studies are needed to unravel the contribution of immune cells, endothelial cells and platelets during CCE formation.

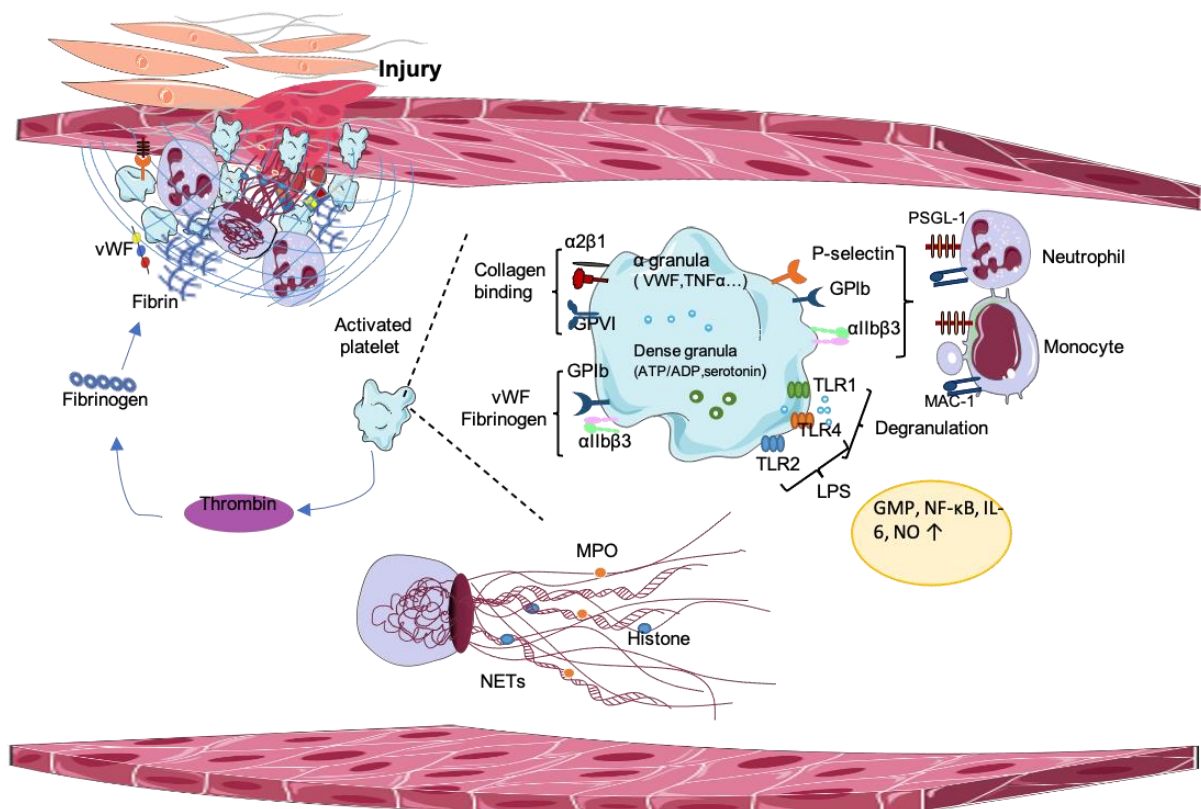


**Figure 3. Central paradigms of immunothrombosis.** Damaged vessel walls and injured endothelial cells release tissue factor (TF) and extracellular matrix molecules, inducing functional crosstalk between platelets and leading to platelet aggregation. Activated platelets promote thrombin formation thereby enhancing platelet degranulation and fibrin formation. Activated platelets release proinflammatory cytokines from  $\alpha$ -granules, which promotes platelet-neutrophil interaction and triggers the release of the NETs. vWF, von Willebrand Factor; GPIb, glycoprotein Ib; GPVI, glycoprotein VI; TLR, toll-like receptor; LPS, lipopolysaccharides; NO, nitric oxide; GMP, guanosine monophosphate; NF- $\kappa$ B, nuclear factor- $\kappa$  beta; IL-6, interleukin 6; MPO, myeloperoxidase; NETs, neutrophil extracellular traps; MAC-1, macrophage antigen 1. Figure is reprinted and adapted by permission from Frontiers. Reprinted from Front Immunol. 2020 Oct 7. Shi C, Yang L, Braun A, Anders HJ. Extracellular DNA-A Danger Signal Triggering Immunothrombosis.

## 1.4 Animal models in metabolic disorders and cholesterol crystal embolism

### 1.4.1 Animal models of arterial thrombosis

Photothrombosis model of cerebral stroke. The cerebral infarct model was induced by a photochemical reaction after injecting photosensitive dyes such as rose Bengal into rats [124, 125]. The photochemical reaction caused the formation of oxygen and superoxide radicals, which can damage the surrounding endothelium, promote platelet degranulation and aggregation, lead to occlusion and ischemic infarction in the cerebral arteries by platelet-rich thrombi. The modification includes targeting the specific individual brain arteries or implanting optical fibers to induce infarction in the desired brain area. The benefits of this model is that

the animals are freely moving without anesthesia before the acute stroke occurs. This makes it possible to observe the brain function and behavior of animals in real-time [126, 127].

Thromboembolic stroke model. This model, which can be induced by injecting thrombus-like material into cerebral vessels and internal carotid arteries, is the most popular model for studying thromboembolic stroke [128-130]. According to the diameter and quantity of injected material, this model leads to the occlusion of one or more arteries followed by ischemic infarction in the corresponding area. This model induces a well-defined penumbra around the cerebral infarct with a large variation in infarct size and is suitable for studying the pathogenesis of arterial immune thrombosis and the role of thrombolytic drugs during this process [131].

Microsphere/macrosphere embolic stroke model. Embolic stroke can be triggered by injecting synthetic microsphere/macrospheres spheres (between 20 and 400  $\mu\text{m}$  in diameter) into cerebral arteries. Various materials such as silicone, collagen and titanium dioxide have been utilized to provoke embolic stroke *in vivo* [131]. This model leads to permanent ischemia due to the artificial spheres that may not be dissolved by the fibrinolytic system. In contrast to thrombosis, microspheres can suddenly obstruct arteries leading to a rapid development of edema and redistribution of blood flow [132]. However, the disadvantage is the unavailability to study thrombolytic drugs.

Cholesterol embolism model. We recently established a novel CCE model by injecting 100  $\mu\text{L}$  of CCs into the artery of the kidney in mice [41]. Depending on the amount of CCs, intravascular injection causes occlusion of multiple microvascular emboli and subsequent ischemic tissue infarction. Histological analysis revealed that not the CCs themselves but the clots surrounding the crystals cause vascular occlusion, tissue ischemia and kidney failure. The advantage of this model is the kidney function is sensitively associated with the amount of crystals injected, although the size of kidney infarction was highly variable in the injured kidney.

#### **1.4.2 Animal models of hyperuricemia**

Developing mouse models of asymptomatic hyperuricemia with clinically relevant serum UA levels has been challenging because rodents express the enzyme uricase. However, several mouse models of hyperuricemia have been developed including genetically modified mouse models and environmentally induced mouse models that are described below [133].

### ***Environmentally induced and surgical mouse models***

To induce increased serum UA levels, rodent diets can be modified with supplements such as UA precursor substances including drugs or diets containing xanthine, hypoxanthine, yeast and sardines. Other approaches that have been described are injection of rodents with exogenous UA or oral administration of potassium oxonate. Although injecting intraperitoneally 250 mg/kg UA for 7 days increased serum UA levels from 3 mg/dL to 7 mg/dL in mice 1 hour after the final administration [134] or applying potassium oxonate orally increased serum UA levels by 1.5 to 2.1 fold within 7 days [135-138], both approaches can only maintain elevated serum UA levels for a very short period of time or don't reach serum levels similar to those observed in hyperuricemic patients. In addition, surgical animal models have also been described that induce serum UA levels between 2-5 mg/dL including unilateral ureteral obstruction, ischemia reperfusion injury and uninephrectomy with diabetes-induced kidney disease [139, 140]. Thus, in vivo studies investigating the role of hyperuricemia are impossible with such models.

### ***Genetically induced mouse models.***

Uricase-related models. In 1994, Wu et al. first reported a uricase-knockout mouse *Uox*<sup>-/-</sup>, which was developed with embryonic stem cells (ESC)-targeting technology [141]. In these mice, the activity of uricase was knocked out, which resulted in high serum UA levels (11.0 ± 1.7 mg/dL) and the development of a severe phenotype. Approximately 65% of mice died by 4 weeks of age due to UA crystal nephropathy, urolithiasis and/or hyperuricosuria. Lu et al. set up another *Uox*-knockout mouse model based on deleting 28 base pairs in exon 3 of the *Uox* gene [142]. These mice had serum UA levels of 7-9 mg/dL but also developed a strong phenotype with 40% of mice dying at 5 weeks of age.

ABCG2-related models. In humans, *ABCG2* encodes a secretory urate transporter that regulates urate excretion primarily in the gut. Ichida K. et al. generated *ABCG2*-knockout mice where the gut excretion of urate was reduced with only caused a very low increase in serum UA levels from 2.8 mg/dL in *ABCG2*-knockout mice compared with 2.2 mg/dL in healthy control mice [143].

SLC2A9-related models. *SLC2A9*, also known as GLUT9, is a urate transporter protein expressed primarily in the liver but also kidney. Preitner et al. generated whole body *Slc2a9*-knockout mice (G9KO) as well as liver-specific *Slc2a9*-knockout mice (LG9KO, Alb-

creERT2;*Glut9*<sup>lox/lox</sup>) and showed that LG9KO mice had higher serum UA levels (2.0 mg/dL in male and 3.1 mg/dL in female) but did not develop kidney disease compared with G9KO mice [144]. However, feeding LG9KO mice a purine-rich diet with inosine for 3 days caused an increase in serum UA to 300  $\mu$ M, while feeding a combination of high-fat diet with inosine further increased serum UA levels to 500  $\mu$ M and caused acute UA crystal-induced nephropathy [145].

Taken together, developing a mouse model of asymptomatic hyperuricemia with serum UA concentrations that mimic human hyperuricemia has been a vast challenge for scientists in the past decades. To overcome this issue, a novel mouse model has been established within our institute in which LG9KO mice when placed on a standard chow diet with inosine developed asymptomatic hyperuricemia with serum UA levels that can reach up to 15 mg/dl dependent on the length of the feeding time without causing kidney dysfunction [99]. This mouse model opened up new avenues to finally study the role of asymptomatic hyperuricemia in CCE-induced kidney injury.

### 1.4.3 Animal models of diabetes

Several rodent models to study diabetes and its complications have been established and are widely used. Leptin-deficient mice (*ob/ob*, C57BL/6J genetic background) and leptin receptor-deficient mice (*db/db*, C57BLKS/J genetic background) are the most common models to study T2D [146-148]. *Ob/ob* mice develop mild diabetes but severe obesity, while *db/db* mice develop moderate obesity with severe diabetes (hyperglycemia). Of note, if both mouse strains are on the same genetic background, they develop an identical phenotype [149]. *Db/db* mice are hyperphagic, hypothermic and have less energy expenditure as a result of reduced brown adipose tissue [149]. Serum leptin levels are extremely high in *db/db* mice and they show limitations in linear growth due to insufficient growth hormone [150].

To study the pathogenesis of T1D, most animal models are based on inducing T1D by chemical approaches, such as streptozotocin (STZ) or alloxan, which target the insulin-secreting  $\beta$ -cells. Both drugs are cytotoxic glucose analogues with high affinity for the GLUT2 transporter. STZ is mostly used compared to alloxan due to its stability and lower toxicity. STZ induces T1D and other complications including diabetic nephropathy. STZ is cheap, has a short gestation time and high genetic homology with humans [151, 152]. However, the disadvantage of this

model is that STZ is also toxic to renal tubular epithelial cells, so it is possible that kidney damage may occur due to STZ toxicity [153, 154].

It is essential to select appropriate animal models for scientific questions, to explore specific pathological mechanisms and to identify potential adverse effects and toxicity. To further investigate the effect of metabolic disorders on kidney injury after atherosclerotic plaque rupture, we finally choose the STZ-induced T1D model and the asymptomatic hyperuricemic model using Alb-creERT2;*Glut9*<sup>lox/lox</sup> mice and performed surgery to induce CCE.

## 2. *Hypotheses*

Numerous observational studies have reported an association between metabolic disorders and cardiovascular disease where atherosclerosis is a leading cause [30, 155, 156]. In advanced atherosclerosis, CCE is a life-threatening complication with an average mortality of 62.8% [157]. In a new model of CCE-induced AKI, we recently found that fibrin clots form around CCs, obstruct peripheral arteries and cause tissue infarction and organ failure. However, metabolic disorders such as diabetes and hyperuricemia are common comorbidities and their role in modulating CCE-induced AKI is currently unknown. We hypothesized that metabolic disorders would have an impact on the outcomes of CC-induced AKI.

Accordingly, the specific aims of this thesis were:

1. To investigate whether hyperglycemia affects CC-induced AKI *in vivo* during experimental T1D and CC-induced AKI, e.g. kidney injury, inflammation, infiltration of immune cells, occlusion and infarction.
2. To investigate whether asymptomatic hyperuricemia affects the outcomes of CC-induced AKI by exerting anti-inflammatory and vasoactive effects on kidney injury, inflammation, infiltration of immune cells, occlusion and infarction.

### 3. *Materials and Methods*

#### 3.1 *Materials*

##### 3.1.1 Instruments

###### Balance:

Analytic Balance, BP 110 S	Sartorius
Mettler PJ 3000	Mettler-Toledo

###### Cell Incubator:

Heracell Type B5060 EC-CO <sub>2</sub>	Heraeus Sepatech
--	------------------

###### Centrifuges:

Heraeus, Minifuge T	VWR International
Centrifuge 5424	Eppendorf
Centrifuge 5810R	Eppendorf
Heraeus, Sepatech Biofuge A	Heraeus Sepatech

###### ELISA-Reader:

Tecan, GENios Plus	Tecan
--------------------	-------

###### Microscopes:

Light microscope Leitz DM II	Leica Microsystems
CCD-Camera	Tröndle
Libra 120	Carl-Zeiss
Light microscope Zeiss AxioPlan 2	Carl-Zeiss

---

Axiocam HR Carl-Zeiss

Aggregometer:

APACT 4004 Semi-automated LABiTec  
4-channel platelet aggregometer

TaqMan Sequence Detection

System:

ABI prism™ 7700 sequence Beckman Coulter  
detector

qRT-PCR syber green LC-480 PE Biosystems

Flow cytometer

FACS Calibur Becton Dickinson

FACS Canto II Becton Dickinson

Other Equipments:

Microtome HM 340E IKA GmbH

Nanodrop Roche

pH meter WTW Microm

Thermomixer 5436 WTW GmbH

Vortex Genie 2™ Eppendorf

Water bath HI 1210 Bender & Hobein AG

Miniaturized imager device Mannheim Pharma & Diagnostics GmbH

Miniaturized battery Mannheim Pharma & Diagnostics GmbH

### 3.1.2 Chemicals and reagents

Chemicals and reagents	Source
DMEM-medium	Biochrom KG
RT-PCR primers	Metabion
RNeasy Mini Kit	Qiagen GmbH
Fetal calf serum	Biochrom KG
Trypsine	PAN Laboratories GmbH
Penicillin Streptomycin	PAN Laboratories GmbH
Activated form of integrin $\alpha$ IIb $\beta$ 3 (JON/A-PE)	Emfret Analytics
P-selectin antibodies conjugated to fluorescein isothiocyanate (FITC)	Emfret Analytics
Fibrinogen (ab27913)	Abcam
Rat anti-mouse neutrophils	Serotec
CD31 (DIA-310, Dianova)	Abcam
Alpha smooth muscle actin ( $\alpha$ -SMA) (M0852)	Dako Deutschland
Ly6B2+ (MCA771G)	Bio-Rad AbD Serotec Limited
Blood urea nitrogen (BUN) kit	DiaSys Diagnostic System
Mouse albumin	Bethyl Laboratories
Uric acid assay kit	BioAssay systems
LDH cytotoxicity assay	Roche
Creatinine FS	DiaSys Diagnostic System
Urea FS	DiaSys Diagnostic System
TMB Substrate Reagent Set	Becton Dickinson
Mouse IL-6 ELISA kit	Becton Dickinson

---

AEC Substrate Packing	Biogenex
Apyrase (grade III)	Sigma
Bovines Serum Albumin	Roche Diagnostics
Collagen	Kollagenreagent Horm
Collagen suspension	Takeda
Collagen-related peptide (CRP)	Sigma
DMSO	Merck
EDTA	Calbiochem
30% Acrylamide	Carl Roth
Eosin	Sigma
Ethanol	Merck
FITC-sinistrin	Medi Beacon
Formalin	Merck
Glucose	Roth
Prostacyclin(PGI <sub>2</sub> )	Calbiochem
Streptomycin	Sigma, Deisenhofen
Thrombin	Roche Diagnostics
Uric acid	Invivogen
Water, nuclease free	Roth
Xylol	Merck
Microbeads	Miltenyl Biotech
Cell Titer 96 Proliferation Assay	Promega
Needles	Becton Dickinson
Pipette's tip 1-1000µL	Eppendorf
Syringes	Becton Dickinson
Cell culture dishes	Techno Plastic Products AG

Tubes 1.5, 2, 15 and 50 mL

Techno Plastic Products AG

---

**Buffers**

---

*Tyrode's buffer (pH 7.3)*

NaCl	137 mM
KCl	2.7 mM
NaHCO <sub>3</sub>	12 mM
NaH <sub>2</sub> PO <sub>4</sub>	0.43 mM
Glucose	0.1 %
Hepes	5 mM
BSA	0.35 %
CaCl <sub>2</sub>	2 mM
MgCl <sub>2</sub>	1 mM

---

*ELISA coating buffer for mouse albumin (pH 9.6)*

Na <sub>2</sub> CO <sub>3</sub>	0.0157 M
NaHCO <sub>3</sub>	0.3430 M

---

*ELISA wash buffer for mouse albumin (pH 8.0)*

Tris	50 mM
NaCl	0.14 M
Tween20	0.05 %

---

*ELISA sample diluent buffer for mouse albumin (pH 7.0)*

Tris	50 mM
NaCl	0.14 M
BSA	1 %
Tween20	0.05 %

---

*ELISA blocking buffer for mouse albumin (pH 8.0)*

Tris	50 mM
------	-------

---

NaCl	0.14 M
BSA	1 %

---

***ELISA coating buffer for mouse IL-6 (pH 9.5)***

Na <sub>2</sub> CO <sub>3</sub>	1.59 g to 1 L
NaHCO <sub>3</sub>	7.13 g to 1 L

---

***Phosphate-Buffered Saline (PBS) 1L (pH 7.0)***

NaCl	8 g
Na <sub>2</sub> HPO <sub>4</sub>	1.16 g
KH <sub>2</sub> PO <sub>4</sub>	0.2 g
KCL	0.2 g

---

***Assay diluent for mouse IL-6 (pH 7.0)***

PBS	
FBS	10 %

---

***Wash buffer for mouse IL-6 (pH 7.0)***

PBS	
Tween20	0.05 %
Citrate buffer 0.1M	pH 7.0
Sodium citrate	0.1 M 40 %
Citrate	0.1 M 60 %

---

## ***3.2 Mouse model procedures***

### **3.2.1 Housing conditions and ethical approvals**

C57BL/6N background wild type mice were ordered from Charles River (Sulzfeld, Germany), and Alb-creERT2;*Glut9*<sup>lox/lox</sup> mice and *Glut9*<sup>lox/lox</sup> control mice were kindly provided by Frédéric Preitner and Bernhard Thorens (University of Lausanne, Center for Integrative Genomics, Lausanne, Switzerland).

The provisions of the German Animal Welfare Act (Tierschutzgesetz) were always applied during the experiments. All animal experiments used were approved by the local government (Regierung von Oberbayern) prior to the study (AZ: ROB ROB-55.2Vet-2532.Vet\_02-19-79) based on the EU directive for the Protection of Animals Used for Scientific Purposes (2010/63/EU) and reported according to the ARRIVE guidelines [158].

Mice were kept in groups of up to 5 mice inside clean cages with a red mouse house and aspen wood litter. Under SPF standard conditions, the temperature of the mouse facility was kept at  $22 \pm 2$  °C with a 12 hour light/ dark cycle. All mice had unlimited access to water and standard chow diet (Sniff, Soest, Germany) ad libitum. The mice cages were changed once a week by a trained laboratory animal care keeper. Cages, lids, bedding, houses, nestle, food, and water were sterilized by autoclaving before use.

### **3.2.2 Animal models**

#### ***Mouse model of cholesterol crystal embolism***

To induce CCE, 9 weeks old mice were given injection of CCs into the left kidney artery according to a procedure as recently reported [41]. In brief, male and female mice were anesthetized by injecting medetomidine (0.5 mg/kg), midazolam (5 mg/kg), and fentanyl (0.05 mg/kg) i.p.. To maintain the body temperature, in a heating chamber was employed. After a laparotomy, the left kidney artery was cannulated from across the aorta using a 34-Gauge needle and 100  $\mu$ L CC stock solution or normal saline was injected. The successful CC injection was visually verified by the color change of the injured kidney (Figure 4). Afterwards, the needle was removed and a cotton swab was immediately placed on the wound with a light local pressure for 3 to 5 minutes. A small sponge made from pig gelatine was gently stick on the wound to close the artery. Finally, standard absorbable sutures were used to close the abdominal wall and skin, followed by subcutaneous injection of atipamezole (2.5 mg/kg) and flumazenil (0.5 mg/kg) to antagonize the anesthesia. For pain management, buprenorphine (0.05 mg/kg) was subcutaneously injected every 8 hours.

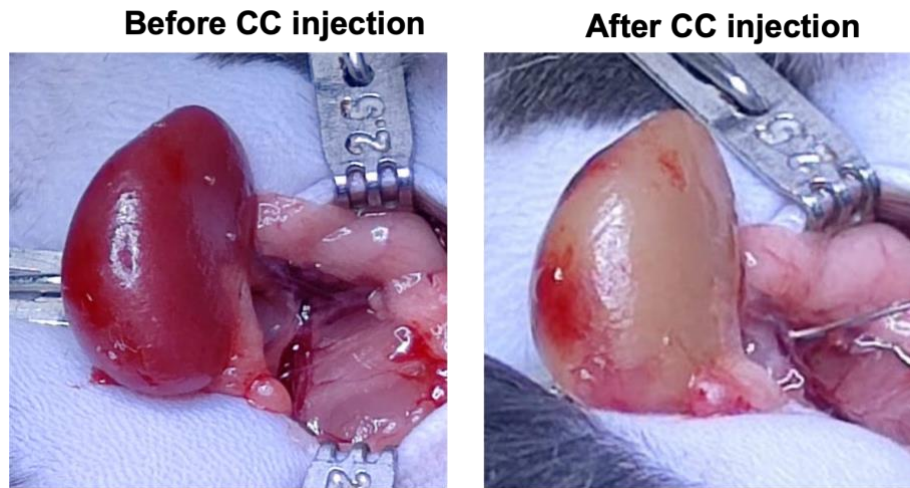


**Figure 4. Mouse model of cholesterol crystal embolism. (Left image)** Before CC injection, the kidney was red. **(Right image)** The successful CC injection was visually verified by the color change.

#### ***Type 1 diabetic mouse model with cholesterol crystal embolism***

Six-week old wild type C57BL/6N mice were injected intraperitoneally (i.p.) with streptozotocin (STZ) dissolved in 0.1 M citrate buffer to induce T1D [127] (Figure 5). Mice were administered with 50 mg/kg STZ i.p. for five consecutive days (final dose per mouse 250 mg/kg). Blood glucose levels as well as body weight were determined before every injection because it was essential to adjust the quantity of STZ if necessary. T1D was established when blood glucose levels were  $> 400$  mg/dL, afterwards CC-induced AKI was induced. Control mice without T1D were injected 5 times with citrate buffer. Afterwards, mice with and without T1D were injected with CC solution as described above. The experiment groups were as follow: T1D+CC and WT+CC.

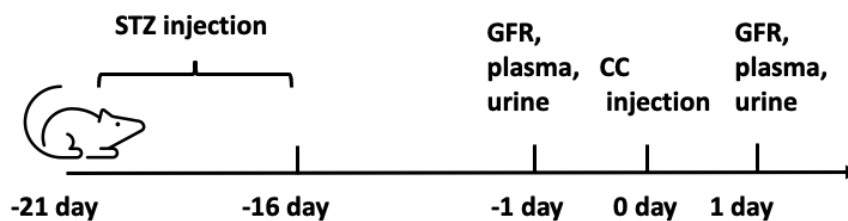


**Figure 5. Schematic of study design for type 1 diabetes with cholesterol crystal embolism**

All mice were sacrificed 24 hours after CC-induced AKI. Urine and plasma were collected and GFR was measured before and 24 hours after surgery. After sacrifice, the injured and

contralateral kidney were harvested and one half of the kidney fixed in 4% formalin for histological analysis and the other half of the kidney used for TTC staining.

### **Mouse model of asymptomatic hyperuricemia**

Six-weeks old Alb-creERT2;*Glut9*<sup>lox/lox</sup> mice and *Glut9*<sup>lox/lox</sup> control mice (on a C57BL/6N background) were injected i.p. with tamoxifen every alternative day for one week to knockdown *Glut9* expression in hepatocytes in the liver [145]. Both groups of mice received a standard chow diet enriched with 25.6 g/kg inosine (Ssniff, Soest, Germany) to induce asymptomatic hyperuricemia without any renal impairment for two weeks (Figure 6) [99]. *Glut9*<sup>lox/lox</sup> mice did not develop hyperuricemia and served as control group. Afterward, mice with and without asymptomatic hyperuricemia were injected with CC solution or PBS (control), as described above. The experiment groups were as follow: Healthy+CC and HU+CC.

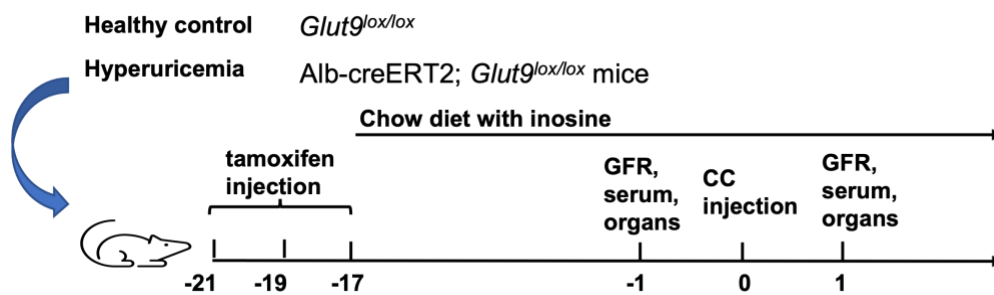


**Figure 6. Schematic of study design for hyperuricemia with cholesterol crystal embolism.**

Mice were sacrificed after 24 hours or 14 days after surgery. Urine and plasma were collected and GFR measured before and after (1 or 14 days) surgery. After sacrifice, the injured and contralateral kidney were harvested and one half of the kidney was fixed in 4% formalin for histological analysis and the other half of the kidney was used for TTC staining.

## **3.3 Assessment of mouse kidney injury**

### **3.3.1 Primary endpoint**

As primary endpoint, the GFR was measured in conscious mice to assess kidney function as previously described [159]. Briefly, the exogenous GFR tracer sinistrin conjugated with fluorescein-isothiocyanate (FITC) was used to measure the kidney excretion kinetics. FITC-sinistrin was prepared at 30 mg/mL in 0.9% sodium chloride. Mice were anesthetized in a isoflurane chamber with 20% oxygen. The light sensor device (Medibeacon, Germany) with

battery was attached on the back of the mouse and the baseline was recorded when the light began flashing (Figure 7A). After waiting for 10 minutes for baseline recording, FITC-sinistrin solution was administrated intravenously at a dose of 0.15 mg/g mouse of body weight. The measurement period was approximately 90 minutes. After removing the sensor device, the MPD Lab software (Medibeacon, Germany) was used to analyze the data (Figure 7B). The GFR was calculated using the formular reported previously [160].

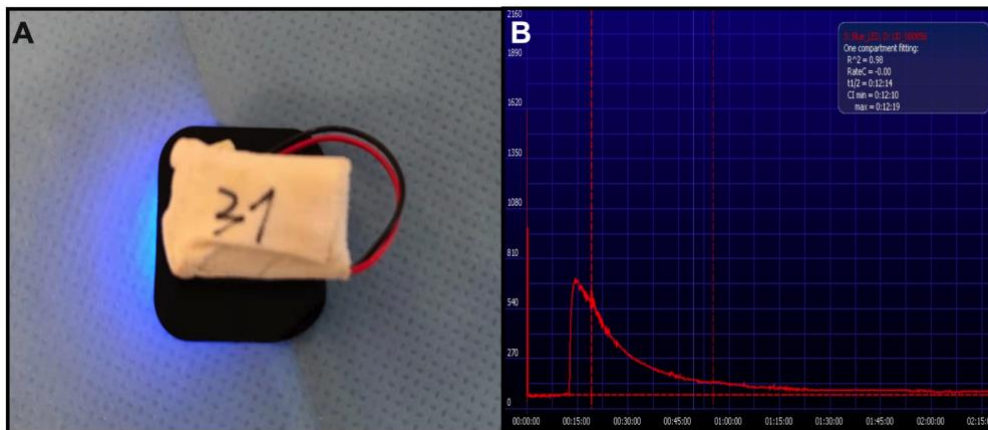


**Figure 7. Transcutaneous glomerular filtration rate measurement method. (A)** Kidney excretion kinetics measuring device with the light sensor and attached battery. **(B)** The sinistrin half-life data.

### 3.3.2 Secondary endpoints

#### TTC staining and infarct size

At the end of the animal study, both injured and contralateral kidneys were harvested from mice and sagittally sectioned half of each kidney. Then the kidneys were labeled and incubated with 1% 2,3,5-triphenyl tetrazolium chloride (TTC) for 15 minutes at 37°C. Subsequently, they were be fixed in 4% formalin for 2 hours at room temperture. The infarct size (white color) was calculated via percentage of the kidney with Image J software.

#### Serum BUN, creatinine, glucose and UACR

Blood was collected before the experiment and at the end of the study prior to sacrifice. Mouse was placed into a mouse restrainer and a tail vein puncture performed (with a 30 G needle) without anesthesia. Five drops of blood were collected in a 1.5 mL Eppendorf tube containing ethylenediaminetetraacetic acid (EDTA) (10  $\mu$ L of 0.5 M solution) to get plasma for aim 1 and blood were collected without EDTA to get serum for aim 2. After blood collection, the bleeding was stopped by applying pressure with a sterile gauze. Blood samples were centrifuged at 8000 rpm for 8 minutes to get plasma. For serum collection, blood samples were put at 37°C for 2

hours and then at 4°C for 1 hour, centrifuged at 5000 rpm for 5 minutes. Supernatant was collected and stored at -20°C until further use.

Blood glucose levels were measured before STZ injection, before CC injection and at the end of the study using an ACCU-CHEK device.

Creatinine levels in the urine and plasma were detected using a Creatinine FS kit (DiaSys Diagnostic system, GmbH, Holzheim, Germany). Urine samples were diluted 4 - 20 times with distilled water and plasma samples were used undiluted. The calculation formula is the same as the published article [159].

Blood urea nitrogen (BUN) levels were detected via a Urea FS kit (DiaSys Diagnostic system, GmbH, Holzheim, Germany). The calculation formula is the same as the published article [99].

The urinary albumin to creatinine ratio (UACR) was calculated as follow:

UACR = albumin content for each sample (mg/dL) / creatinine content (mg/dL) for the same sample [161]

Urinary albumin levels were measured using an albumin ELISA kit from Bethyl Laboratories.

### **Serum UA level**

To determine serum UA levels, blood was collected without EDTA because EDTA can influence the UA assay. Serum UA levels were detected using a QuantiChrom™ Uric Acid Assay kit from BioAssay Systems according to manufacturer's instruction. 5 µL of sample, blank and standard were transferred in duplicates into 96-well plate and mixed with 200 µL working reagent. The plate was incubated for 30 minutes at room temperature in the dark and optical density read at 590 nm using an ELISA reader (Tecan, GENios Plus). The serum UA concentrations were calculated as follow:

$$\text{UA (mg/dl)} = (\text{OD sample} - \text{OD bland}) / (\text{OD standard} - \text{OD bland}) \times 10$$

### **Serum interleukin-6 levels**

Serum interleukin-6 (IL-6) levels were measured using an mouse-specific ELISA kit from RayBiotech according to manufacturer's instructions. Serum samples were diluted 5 times with assay diluent. Capture antibody (goat anti-mouse IL-6, 1:100) was diluted in coating buffer

(carbonate-bicarbonate, pH 9.6) in a Nunc Maxisorb flat bottom 96-well plate and incubated overnight at 4°C. Then aspirate the liquid and wash three times with wash buffer. 100 µL standard or sample was added to a 96-well plate and incubated 2 hours at room temperature. After washing 5 times with wash buffer, working detector, substrate solution and stop solution were added as the same method as before [162]. The data was read at 450 nm within 30 minutes using an ELISA reader (GENios Plus, Tecan).

### **3.3.3 Immunohistochemistry**

For tissue analysis, one sagittal half was cut with a tissue slicer (HSMS001-2, Zivic Instr.) to obtain 1 µm slices. Infarct size planimetry upon staining with TTC that red staining indicates viable tissue [163]. The other half was processed for histology and immunostaining such as PAS staining for tissue injury, CD31 staining for vascular injury, α-SMA/fibrinogen co-staining for quantifying vascular occlusions and vasoconstriction, Ly-6B<sup>2+</sup> immunostaining staining for inflammation.

For immunohistological analysis, the sagittal half of the tissue was fixed in 10% formalin overnight, then paraffin blocks prepared using tissue processors (Leica). 2 µm thick paraffin-embedded sections were cut with Microtome HM 340E. The de-paraffinization and staining method as previously described. The primary antibodies used in the study are mentioned above (section 3.1.2).

#### **Leukocyte staining:**

The percentage area of infiltrated leukocytes was quantified in each kidney stained with the Ly-6B<sup>2+</sup> antibody (Serotec MCA771G, 1:200 diluted). Healthy kidneys without injury served as control. All quantifications were performed in Fiji software.

#### **CD31 staining:**

Kidney sections were stained with CD31 antibody (DIA-310, Dianova) to show the injury on endothelial cells. The percentage of the positive area in the injured kidney was quantified. Analysis and statistical method were the same as neutrophils staining.

#### **Alpha-smooth muscle actin (α-SMA) / fibrin staining**

We performed  $\alpha$ -SMA (M0852, Dako ) and fibrinogen (ab27913, Abcam) co-immunostaining to quantify the CC-induced occlusion and vasoconstriction ratio in renal artery. The total number of arteries in one kidney were quantified by  $\alpha$ -SMA positive staining, thrombosis occlude arteries were quantified by fibrin positive indication.

### **3.3.4 Periodic acid Schiff staining and kidney injury score**

For Periodic acid Schiff (PAS) staining, kidney in paraffin were cut to 2  $\mu$ m sections via tissue processors. Then section slides were de-paraffinized in xylene (5 minutes each time with 3 times) and re-hydrated in 100% ethanol (3 minutes each time with 3 times). Then sections were in 95% ethanol (3 minutes each time with 2 times), and 3 minutes in 70% ethanol. After washing with distilled water (5 minutes each time with 2 times), sections can be used for PAS staining.

First, we incubated kidney sections in periodic acid (2%) for 5 minutes and washed with distilled water for 5 minutes. Next, sections were incubated with Schiff reagent for 20 minutes at room temperature. Then the sections were washed with distilled water for 6 minutes, counterstained with Hematoxylin solution for another 2 minutes, and washed with tap water for 5 minutes. In the end, sections were put in 90% ethanol, then dried and mounted with coverslips.

Mice kidney injury was measured based on tubular and interstitial injury. The quantification includes four different parameters and each parameter has six levels, as follows (Table 1). 15-20 pictures were taken per kidney with a light microscope Leica DII to cover the whole section, and scored 4 parameters about tissue injury in each photo according to injury percentage. The kidney injury score in one picture is the sum from these four parameters and the core for one mouse is the mean value from all pictures in this kidney.

		Tubular necrosis	Tubular dilation	Cast formation	Interstitial edema
Kidney injury level	0				
	1 ( $\leq 20\%$ )				
	2 (21% to 40%)				
	3 (41% to 60%)				
	4 (61% to 80%)				
	5 (81% to 100%)				

**Table 1. Kidney injury score system for one picture of the kidney section.**

### 3.3.5 Vasoconstriction ratio

All kidney sections of  $\alpha$ -SMA and fibrin co-immunostaining were taken pictures under a light microscope Leica DII. Then each cross-sectional artery area (artery area include lumen) and the lumen area of this artery was quantified with Photoshop 21.0 software. For the formula, each artery lumen area was calculated as S1, and the cross-sectional artery area was calculated as S2. The ratio of lumen/artery area =  $S1/S2$ , as follows (Figure 8).

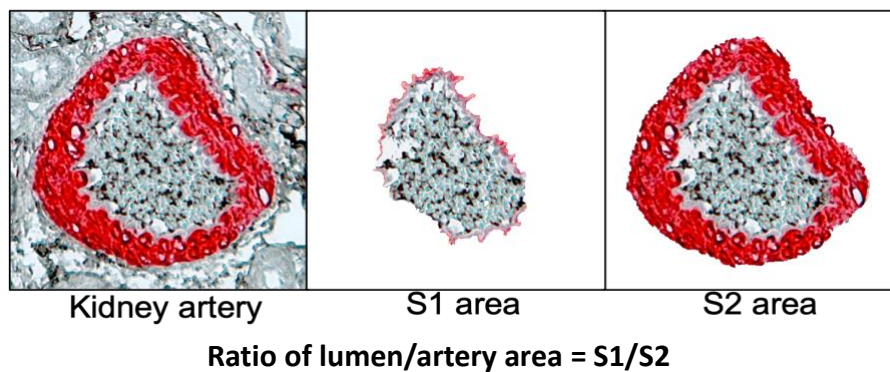


**Figure 8. Schematic of the vasoconstriction ratio calculation in the kidney artery.**

### 3.3.6 Assessment of arterial occlusion

All kidney sections of  $\alpha$ SMA and fibrin co-immunostaining were taken pictures of under a light microscope Leica DII. Based on the different size of arteries in the kidney, they can be divided into interlobar, arcuate and interlobular (Figure 9). CC-induced clot formation was quantified according to three morphological abnormalities: no occlusion (0% of the lumen),

partially occluded (1 - 80% of the lumen), completely occluded (81% - 100% of the lumen) (Table 2).

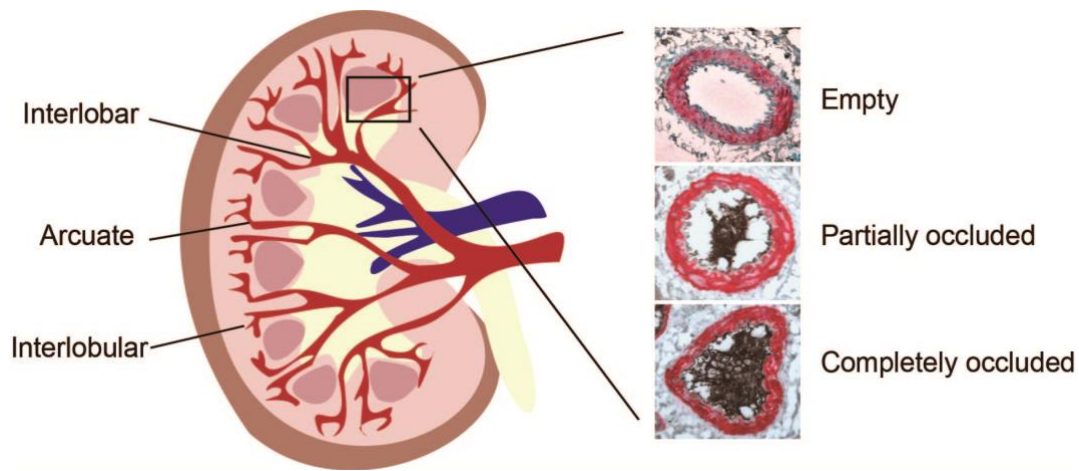


Figure 9. Schematic illustration of kidney vascular tree and obstruction levels.

		Interlobar artery (number)	Arcuate artery (number)	Interlobular artery (number)
Artery conditions of occlusion	Empty	A	D	G
	Partially	B	E	H
	Completely	C	F	I

Table 2. Schematic of the assessment of arterial occlusion.

Mice were labeled in one group as 1, 2, 3, 4... So,  $A(\text{total}) = A1 + A2 + A3 + A4\dots$

Total number of the interlobar arteries is  $\text{Sum}(\text{interlobar}) = A(\text{total}) + B(\text{total}) + C(\text{total})$

Finally, results of each group were showed as bellow:

		Interlobar artery (Ratio)	Arcuate artery (Ratio)	Interlobular artery (Ratio)
Artery conditions of occlusion	Empty	$A(\text{total}) / \text{Sum}(\text{interlobar})$	$D(\text{total}) / \text{Sum}(\text{arcuate})$	$G(\text{total}) / \text{Sum}(\text{interlobular})$
	Partially	$B(\text{total}) / \text{Sum}(\text{interlobar})$	$E(\text{total}) / \text{Sum}(\text{arcuate})$	$H(\text{total}) / \text{Sum}(\text{interlobular})$
	Completely	$C(\text{total}) / \text{Sum}(\text{interlobar})$	$F(\text{total}) / \text{Sum}(\text{arcuate})$	$I(\text{total}) / \text{Sum}(\text{interlobular})$

Table 3. The caculation method of arterial occlusion.

### **3.4 Cell culture experiments**

#### **3.4.1 Cell culture for mice endothelial cells and human proximal tubular cells.**

Mouse glomerular endothelial cells (GEnC) and human kidney proximal tubular epithelial cells (HK2) were cultured with standard cell culture procedure. We used Dulbecco's Modified Eagle Medium (DMEM) with 10% fetal calf serum (FCS) and 1% penicillin-streptomycin (PS). When cells reached 80-90% confluence in the plate, they were detached from the plate and used for the experiments like LDH assay, platelet adhesion assay etc.

#### **3.4.2 Preparation of soluble uric acid solution**

50 mg of UA powder (Sigma-Aldrich) was added into 29.75 mL distilled water. Then 0.2 - 0.6 mL of 1N NaOH was added and shaken until the solution became clear. Finally the PH of the solution was adjusted to 7.4 following that the solution was filtered sterile with a 0.22  $\mu$ m filter. The UA concentration was checked by kit (around 100 mM) [164].

#### **3.4.3 Cholesterol crystal stock solution**

10 mg cholesterol powder was suspended in the 5 mL sterile PBS, sonicated them with ultrasonic destructor for 1 hour. After that, CC solution was filtered through a 34 Gauge needle and autoclaved. Finally the CC concentration was 2 mg/mL. Always shaken the solution before using for experiments.

#### **3.4.4 Stimulation assay of HK2 cells**

HK2 cells were incubated at 37°C for 90 minutes in the presence of 10 mg/dL UA or 30 mM glucose. Rasburicase (0.3 mg/dL, 1 mg/dL and 1.5 mg/dL) was added to deplete UA in the culture medium 1 hour prior to H<sub>2</sub>O<sub>2</sub> stimulation. For UA experiments, cells were incubated with 10 mM H<sub>2</sub>O<sub>2</sub> for 3 hours. For high glucose experiments, cells were incubated with 5 mg/mL CC for 24 hours. 1% triton was used as a positive control. After stimulation, supernatants were transferred into a new 96 well plate and cell death was quantified according to lactate dehydrogenase (LDH) release using the LDH cytotoxicity assay kit (Cytotoxicity Detection Kit, Roche). Values from the triton group were set to 100% and the cytotoxicity in experimental groups was calculated and normalized to the percentage of the positive control.

### 3.5 Analysis of platelet function in vitro

#### 3.5.1 Purification of platelets from whole blood of mice

Blood was collected from wild type mice in Eppendorf tubes containing 100  $\mu\text{L}$  heparin (20 U) and 200  $\mu\text{L}$  Tyrode's buffer without  $\text{Ca}^{2+}$ . Then bloods were centrifuged for 5 minutes at 1300 rpm. Subsequently, the upper part containing erythrocytes was removed into a new Eppendorf tube and centrifuged for 6 minutes at 800 rpm. After centrifugation, supernatants were transferred and centrifuged again for 5 minutes at 2500 rpm to get platelet pellets. To further purify platelets, platelets were washed with Tyrode's buffer without  $\text{Ca}^{2+}$  containing 5  $\mu\text{L}/\text{mL}$   $\text{PGI}_2$  (0.1  $\mu\text{g}/\text{mL}$ ) and 5  $\mu\text{L}/\text{mL}$  apyrase (0.02 U/mL), and centrifuged for 5 minutes at 2500 rpm. The samples were washed twice. After washing, the number of platelets was counted using a hemocytometer. The platelets were suspended at  $1 \times 10^6$  platelets/ $\mu\text{L}$  in Tyrode's buffer without  $\text{Ca}^{2+}$  containing 1  $\mu\text{L}/\text{mL}$  apyrase (0.02 U/mL). Before further experiments, platelets rested for 10-20 minutes. Washed platelets from healthy mice were incubated with different UA concentrations (5 mg/dL and 10 mg/dL) or glucose (5.5 mM and 30 mM) at  $37^\circ\text{C}$  for 1.5 hours [165]. Afterwards, platelets were stimulated with 2.5 mg/mL CC. FACS was used to quantify the effect of CC, UA and glucose on platelets activation and degranulation. A four-channel aggregometer ATRACT 4004 aggregometer was used to test platelet aggregation. RT-PCR data showed *Glut9* expression in platelets from human and mice, murine megakaryocytes, kidney and liver.

#### 3.5.2 Platelet aggregation assay

After incubating platelets with different glucose or UA concentrations for 90 minutes at  $37^\circ\text{C}$ , we added 40  $\mu\text{L}$  platelets stock solution ( $1 \times 10^6$  platelets per  $\mu\text{L}$  in Tyrode's buffer without  $\text{Ca}^{2+}$ ) into 160  $\mu\text{L}$  Tyrode's buffer with human fibrinogen (50  $\mu\text{g}/\text{mL}$ ) in the presence or absence of 2.5 mg/mL CC. A four-channel aggregometer (ATRACT 40004, Hamburg) calculated the suspension of washed platelets by light transmission for 10 minutes. After 55 seconds, different agonists such as collagen, collagen-related peptide (CRP) and thrombin were added into the well. The light transmission of 200  $\mu\text{L}$  Tyrode buffer with human fibrinogen was calculated as 100% aggregation.

#### 3.5.3 Platelet integrin activation and degranulation

After incubating platelets with glucose and UA for 90 minutes at  $37^\circ\text{C}$ , 50  $\mu\text{L}$  platelets stock solution ( $1 \times 10^6$  platelets per  $\mu\text{L}$  in Tyrode's buffer without  $\text{Ca}^{2+}$ ) from each group was added

into 450  $\mu\text{L}$  Tyrode's buffer with  $\text{Ca}^{2+}$  in the presence or absence of 2.5mg/mL CC and stimulated for 15 minutes. Platelets from WT mice under normal conditions were incubated at the same time in the presence or absence of 2.5 mg/mL CC and served as control. Platelets were incubated with fluorophore-conjugated antibodies directed against activated  $\alpha\text{IIb}\beta\text{3}$  integrins (PE-conjugated JON/A) as well as P-selectin or CD62P (FITC-labeled WUG 1.9). Afterwards, different agonists such as CRP and thrombin were added in low or high dose concentrations. CRP activates platelets through Glycoprotein VI, while thrombin signals via G protein-coupled receptors (GPCR). After incubation for 7 minutes at 37°C and 7 minutes at room temperature in the dark, the reactions were stopped by adding 0.5 mL PBS to each tube. This experiment monitored the signaling-dependent activation of  $\alpha\text{IIb}\beta\text{3}$  integrin and the process of degranulation (determined by P-selectin exposure). The samples were analyzed through flow cytometry using the BD FACSCanto II and data were analyzed with the FlowJo software.

### **3.6 RNA analysis**

#### **3.6.1 RNA isolation**

RNA isolation was conducted with the RNA isolation kit from Ambion (Ambion, CA, USA). Cells were transferred into 0.6 mL lysis buffer with 1% 2-mercaptoethanol. The samples were kept on ice all the time. 700  $\mu\text{L}$  of the sample was taken to homogenate with the same amount of 70% ethanol and mixed thoroughly. Total RNA was isolated by using Qiagen mRNA extraction kit following instructions. Isolated RNA was quantified using Nano drop. The purified RNA was stored at -80°C for storage.

#### **3.6.2 RNA reverse transcription**

RNA samples were dissolved in RNase-free water and diluted to get a concentration of 2  $\mu\text{g}$  total RNA in 22.45  $\mu\text{L}$  reaction. Then, the prepared master mix was prepared as indicated below and added to the sample prior to incubation at 42°C for 90 minutes and 90°C for 5 minutes. Samples were stored at 4°C.

Preparation master mix:

---

<b>Master mix:</b>	<b>Volume (<math>\mu\text{L}</math>)</b>
5x buffer	4.5
0.1M DTT	1
25 mM dNTPs	0.45
Rnasin and ribonuclease inhibitor (40 u/ $\mu\text{L}$ )	0.5
Acrylamide (15 $\mu\text{g}/\text{mL}$ )	0.25
10x Hexanucleotide Mix	0.25
Superscript II (200 u/ $\mu\text{L}$ )	0.5
Sample (2 $\mu\text{g}$ )	15
Total	22.45

---

### 3.6.3 Quantitative real-time PCR

The mRNA was determined using quantitative real-time PCR (RT-qPCR) with the SYBR Green Dye Detection System on a Light Cycler 480. The cDNA samples were diluted at 1:100 for real-time PCR. The prepared master mix was incubated at the following settings with Light Cycler 480: Pre-incubation: 95°C for 5 minutes. Amplification was as follow: 95°C for 15 seconds, 60°C for 15 seconds and 68°C for 20 seconds by running 40 cycles. Melting curve: 95°C for 5 seconds and 65°C for 60 seconds. Cooling: 40°C for 30 seconds. The CT values were calculated and the results normalized with the reference gene (18s rRNA) for each sample.

Preparation master mix:

---

Master mix	Volume ( $\mu\text{L}$ )
Mix SybrGreen	10
Taq polymerase (5000 u/mL)	0.16
Forward primer (10 $\mu\text{M}$ )	0.6
Reverse primer (10 $\mu\text{M}$ )	0.6
cDNA	0.2
ddH <sub>2</sub> O	8.44
Total	20

---

### 3.6.4 Oligonucleotide primers used for endpoint PCR and quantitative RT-PCR

The following oligonucleotide primers were used in the study.

---

Gene	Sequence
Mouse <i>18s</i>	Forward: GCAATTATTCCCATGAACG
	Reverse: AGGCCTCACTAAACCATCC
Mouse <i>Slc2a9 1</i>	Forward: TTCGGGTCCTTCCTTCCTCTA
	Reverse: GGACACAGTCACAGACCAGA
Mouse <i>Slc2a9 2</i>	Forward: TGCTTCCTCGTCTTCGCCACAATA
	Reverse: CTCTTGGCAAATGCCTGGCTGATT
Human <i>SLC2A9</i>	Forward: GCTCTTGGAGAAGCACAACGAG
	Reverse: ACACCAGGCGGATGCTCCTCT
<i>GAPDH</i>	Forward: GTCTCCTCTGACTTCAACAGCG
	Reverse: ACCACCCTGTTGCTGTAGCCAA

---

### ***3.7 Confocal microscopy imaging***

To determine whether glucose influences necrotic cell death in kidney tubular cells in the presence of CCs, cells were incubated in the presence of 0.1  $\mu$ M Sytox Green dye prior to confocal microscopy. Sytox Green is an extracellular DNA dye. Thus, the release of extracellular DNA from dying cells can be identified in green using a LSM 510 microscope and LSM software.

### ***3.8 Statistical analysis***

All scientific analyses were completed with Prism 8 (GraphPad Software, San Diego, CA). Data were checked for normal distribution before every statistical analysis using the Kolmogorov-Smirnov test. Normally distributed data were used to compare two groups via unpaired Student's t-test or via one-way ANOVA followed by Fisher's LSD test for multiple comparisons. Not normally distributed data sets were compared by using the Mann-Whitney test for two groups comparisons. Data are presented as means  $\pm$  SD or means  $\pm$  SEM. A value of  $p < 0.05$  was considered to indicate statistical significance. \*  $p < 0.05$ , \*\*  $p < 0.01$ , \*\*\*  $p < 0.001$ , #  $P < 0.05$ , ##  $P < 0.01$ , ###  $P < 0.001$ .

## 4. Results

### 4.1 Type 1 diabetes worsens the outcomes in cholesterol crystal embolism

To answer the question how hyperglycemia affects CCE-induced AKI and ischemic cortical necrosis, we induced experimental T1D and CCE-related AKI *in vivo*. As primary endpoint, the GFR was measured and showed that hyperglycemia aggravated the decline in kidney function. Kidney injury, inflammation, infiltration of immune cells, occlusion and infarction were evaluated to gain more insights into the pathomechanisms.

#### 4.1.1 Establishment of a mouse model of type 1 diabetes and cholesterol crystal embolism

To investigate the impact of hyperglycemia in CC-induced AKI, we established a suitable mouse model by injecting 6 weeks old C57BL/6N mice either with streptozotocin (STZ) to induce T1D or citrate buffer as control, as described in section 3.2.2. At baseline, blood glucose levels ranged between 160-220 mg/dL (Figure 10A). After STZ injection, blood glucose levels significantly increased up to 500 mg/dL compared with the two groups at baseline and the citrate-injected group after 3 weeks (Healthy) indicating that these mice developed T1D (Figure 10A). Both groups of mice were then injected with CC. As shown in Figure 10B, the blood glucose levels remained low 24 hours after CC injection in non-diabetic mice (Healthy+CC) similar to levels found prior to surgery. However, blood glucose levels remained significantly high in mice with T1D 24 hours after CC injection (T1D+CC) (Figure 10B).

Previous reports showed that STZ-induced T1D mice gain less body weight (T1D), which was consistent with our findings [166] (Figure 10C), while CCE surgery did not significantly alter body weight (T1D+CC). Similarly, CC injection had a statistically negative effect on kidney weight, although injured kidneys were slightly heavier than the contralateral kidneys (Figure 10D).

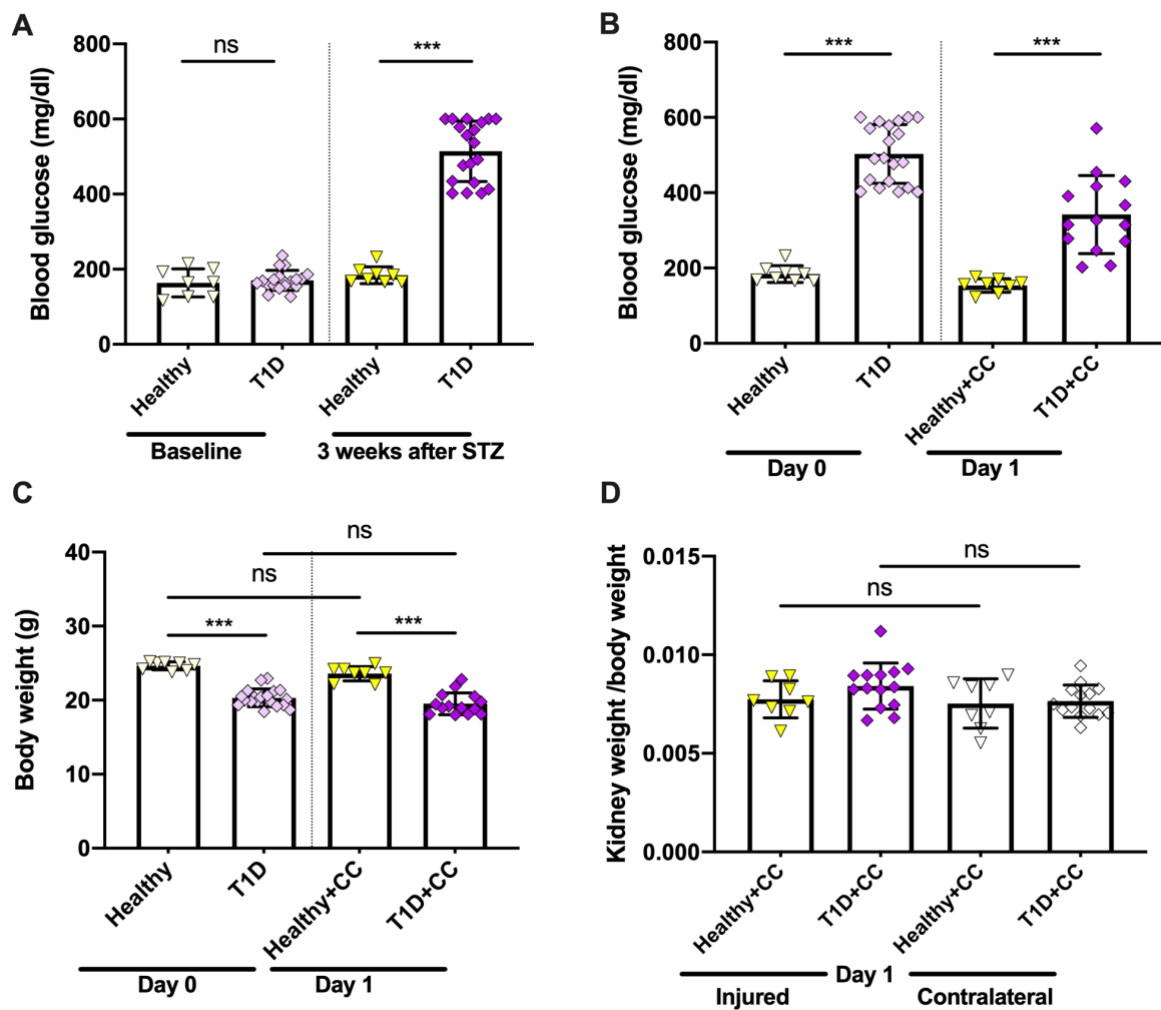


**Figure 10. Induction of hyperglycemia and cholesterol crystal embolism in mice.** (A) Blood glucose levels at baseline and diabetic (T1D) mice after STZ injection. (B and C) Blood glucose levels (B) and body weight (C) before surgery and 24 hours after CC injection. (D) Kidney weight/body weight values from both injured and contralateral kidneys after CC injection. n = 8-19 per group. All quantitative data are means ± SD, ns = not significant, \*\*\* P < 0.001 by one-way ANOVA.

#### 4.1.2 Type 1 diabetes aggravates the decline of kidney excretory function after cholesterol crystal embolism

In order to investigate the effect of hyperglycemia on kidney function after CCE, we measured the following functional kidney parameters: GFR, serum BUN, the urinary albumin to creatinine ratio (UACR) in diabetic and nondiabetic mice after CC injection. The data showed that the GFR significantly decreased in diabetic mice (T1D+CC) after CC injection compared with CC-injected non-diabetic mice (Healthy+CC) as indicated by a decrease in delta GFR

(Figure 11A and 11B). Consistent with a decline in GFR, CC injection induced an increase in urinary albumin/creatinine ratios (UACR) in both groups of mice on day 1 as a result of increasing hyperfiltration in the remnant nephrons, while T1D amplified proteinuria in mice after CCE (T1D+CC) (Figure 11C). Serum BUN levels increased in non-diabetic mice on day 1 after CC injection (Healthy+CC) although not significant, while diabetic mice presented with significantly higher serum BUN levels following CC injection on day 1 (T1D+CC) (Figure 11D). Our data indicate that hyperglycemia worsened kidney function, specifically GFR and UACR in CCE.

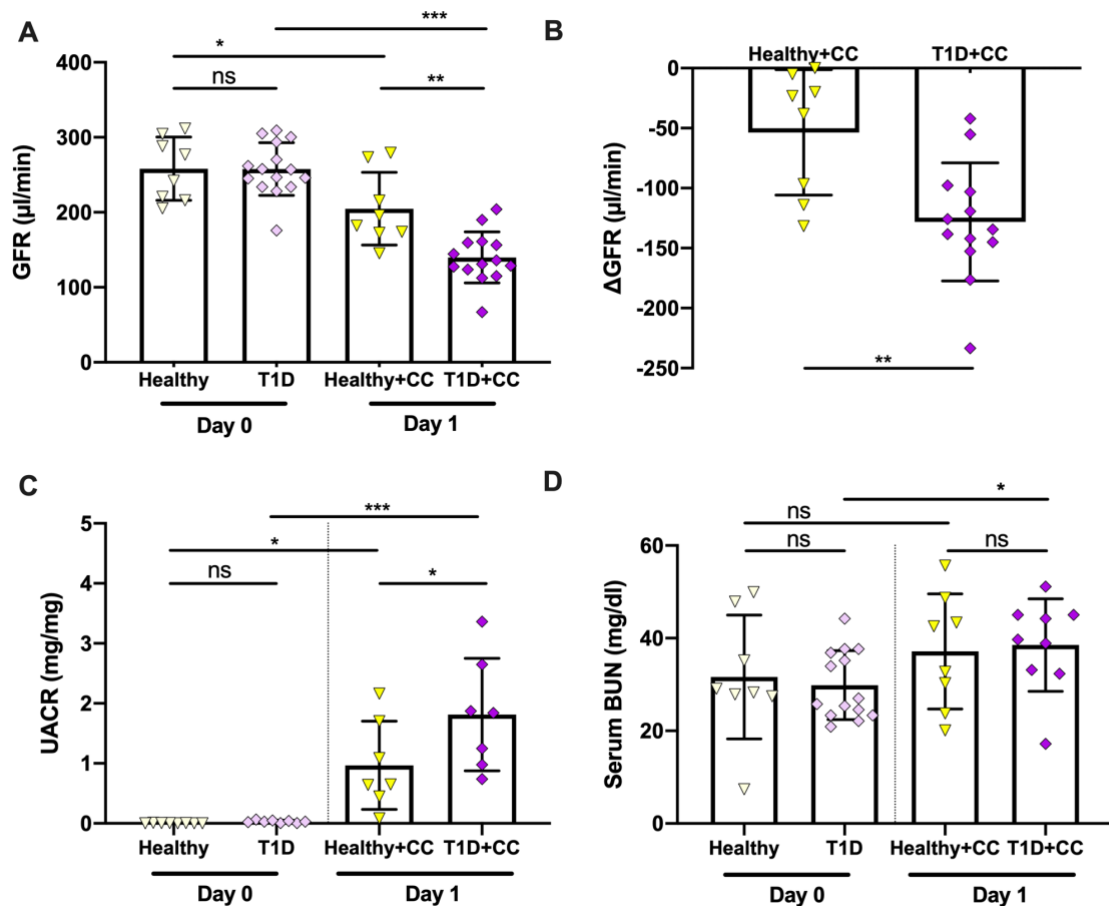


**Figure 11. Type 1 diabetes aggravates the decline of kidney excretory function after cholesterol crystal embolism.** (A) the GFR values in different groups (n = 8-15 per group, one-way ANOVA). (B) the  $\Delta$ GFR is the GFR values 24 hours after CCE subtract the values at the baseline (n = 8-13 per group, Student's t-test). (C and D) The urinary albumin to creatinine ratio (UACR) (C) and serum BUN levels (D) in diabetic and non-diabetic mice (n = 7-14 per group, one-way ANOVA). All quantitative data are means  $\pm$  SD, ns = not significant, \* p < 0.05, \*\* p < 0.01.

### 4.1.3 Diabetic mice display increased kidney infarct size and artery occlusion after cholesterol crystal embolism

After injecting diabetic and non-diabetic mice with CC, we collected kidneys to assess kidney infarct size after 24 hours via TTC staining as described in section 3.3.2. TTC staining showed that CC injection into the left kidney artery induced diffuse (Healthy+CC) or complete (T1D+CC) kidney infarction in mice as illustrated by a color change from red to white in the injured kidney but not in the contralateral kidney (Figure 12A). This suggests that CC injection impaired blood perfusion in the kidney and caused ischemic injury [167]. When quantifying kidney infarct size, we found that diabetic mice (T1D+CC) presented with an overall greater area of kidney infarct compared with non-diabetic mice (Healthy+CC) (Figure 12B). One should mention here that the kidney infarct size after CC injection varied between mice even within the same experimental group due to the difficult surgery; therefore, the number of mice per group was relatively large to be able to perform statistical analysis (Figure 12B).

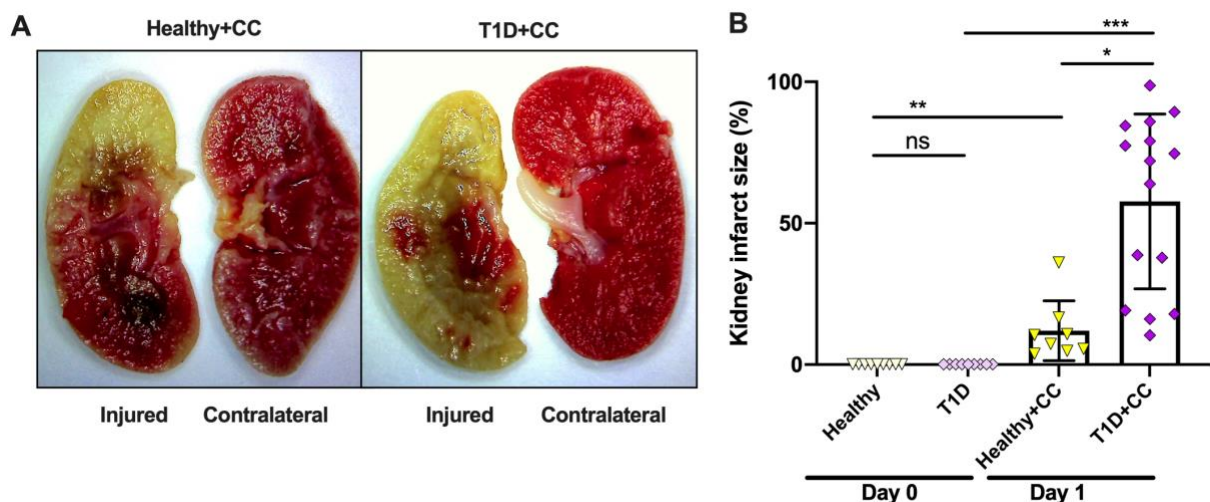


**Figure 12. Diabetic mice display increased kidney infarct size after cholesterol crystal embolism.** (A-B) Both injured and contralateral kidneys were collected from diabetic and non-diabetic mice at 24 hours after CCE and stained with TTC for 15 minutes at 37°C. (A) Representative TTC stained kidneys from different groups on day 1. (B) Kidney infarct sizes from different groups were quantified by Fiji software (n = 8-15 per group). All quantitative data are means ± SD, ns = not significant, \* p < 0.05, \*\* p < 0.01, \*\*\* P < 0.001 by one-way ANOVA.

To quantify the ratio of occluded arteries in diabetic and non-diabetic mice with CCE, kidney sections were stained with  $\alpha$ -SMA and fibrin and the ratio of occluded interlobar, arcuate, and interlobular renal arteries was assessed as described in section 3.3.6. Co-immunostaining staining of  $\alpha$ -SMA and fibrin showed that intrarenal arteries were either completely and partially occluded by CC clots or remained empty (Figure 13A). Interestingly, T1D mice presented with more completely and partially interlobar and arcuate kidney arteries after CC injection compared with non-diabetic mice with CCE (Healthy+CC) suggesting that T1D contributes to worsens immunothrombosis (Figure 13B).

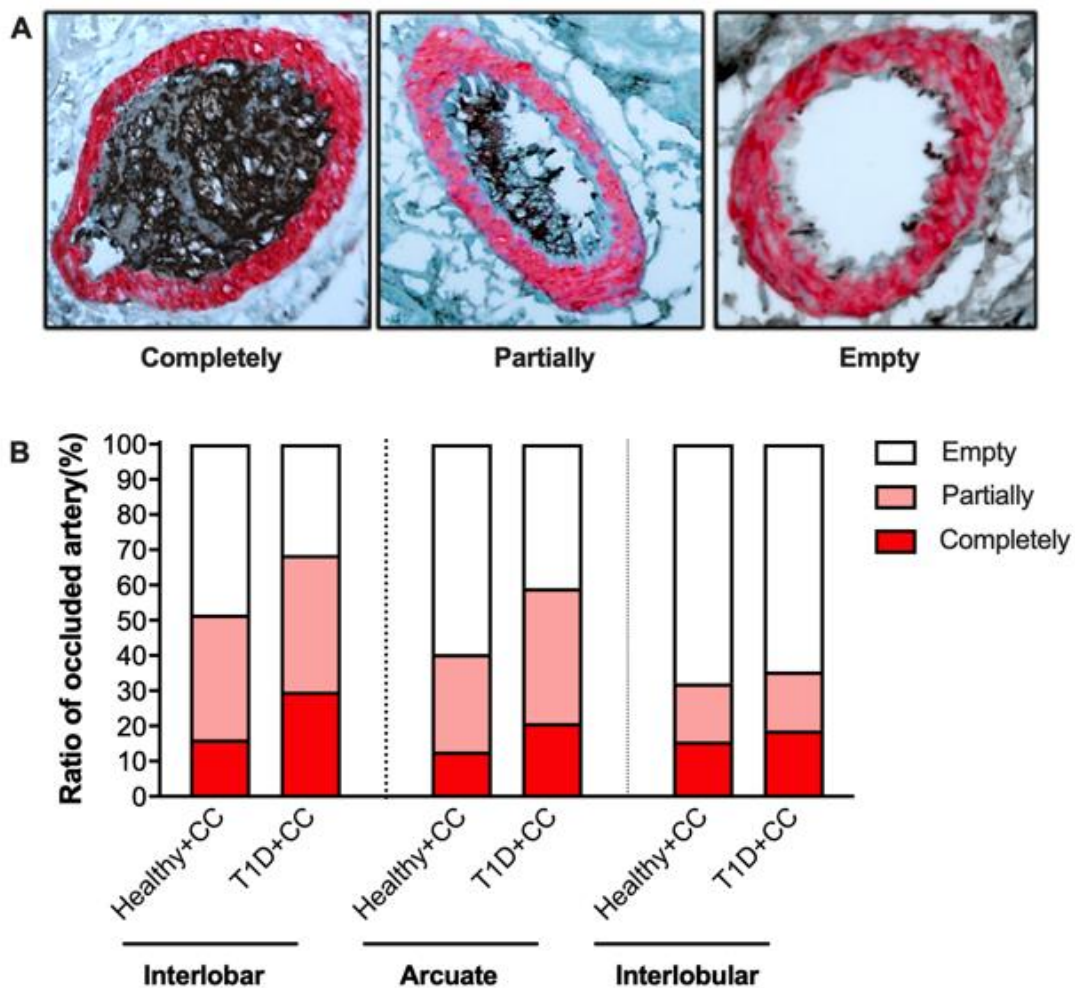


**Figure 13. Quantification of CC-induced occlusion of intrarenal arteries from different sizes. (A)** Illustration of the severity of CC-induced obstruction in the kidney arteries. **(B)** Ratio of CC-induced occluded arteries in diabetic and non-diabetic mice according to the size of arteries (n = 8-15 per group). Data analyzed with the formula described in 3.3.6.

#### 4.1.4 Type 1 diabetes has no effect on vasoconstriction in cholesterol crystal embolism

Recent studies indicate that diabetes mellitus can lead to constriction in vascular smooth muscle cells not only in the aortic tissue but also in the kidney [168, 169]. To investigate a potential contribution of T1D on vasoconstriction in CCE, we stained kidney sections with  $\alpha$ -SMA and fibrin, and vasoconstriction (ratio of lumen/artery area, S1/S2) was verified as described in section 3.3.5. Representative images of renal arteries before (empty) and after (occluded) CCE are shown in Figure 14A. The ratio of lumen/artery area slightly increased although not significantly in the CC-injured kidney compared with the contralateral kidney in control mice (Healthy+CC) (Figure 14B). We found no difference in the ratio of lumen/artery area between the CC-injured and contralateral kidney in T1D+CC mice (Figure 14B). When looking at the interlobar and arcuate arteries in more detail, we did also not observe any differences in the ratio of lumen/artery area in the CC-injured kidney in all groups of mice (Figure 14C). The data indicated that T1D has no significant effect on vasoconstriction in CCE-induced thrombotic angiopathy.

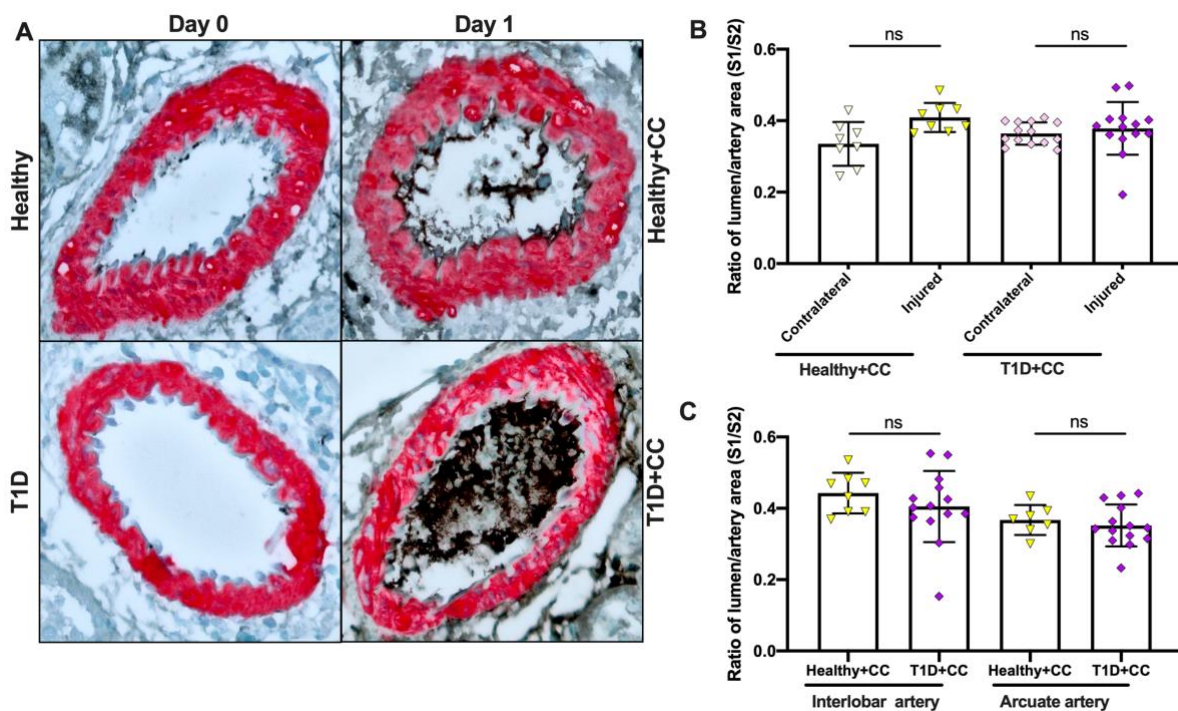


**Figure 14. Type 1 diabetes has no effect on vasoconstriction in cholesterol crystal embolism. (A)** Representative images of  $\alpha$ -SMA/fibrin-stained renal arteries from different groups. **(B)** Ratio of lumen/artery area analyzed from both injured and contralateral kidneys on day 1. **(C)** Ratio of lumen/artery area analyzed of interlobar and arcuate arteries from injured kidneys on day 1.  $n = 7-14$  per group. All quantitative data are means  $\pm$  SD, ns = not significant by one-way ANOVA.

### 4.1.5 Type 1 diabetes aggravates kidney injury during cholesterol crystal embolism

Kidney injury was quantified on PAS-stained kidney section 24 hours after CC injection as described in section 3.3.4. The results showed that CC caused tubular injury in diabetic and non-diabetic mice on day 1 (Healthy+CC) compared with control mice (Healthy) on day 0 as illustrated and quantified by increased tubular necrosis, tubular dilation and cast formation respectively (Figure 15A and 15B). However, diabetic mice (T1D+CC) displayed severe tubular necrosis and tubular dilation as compared to non-diabetic mice after CC injection (Healthy+CC), while T1D+CC mice with similar tissue edema (Figure 15C) suggesting that T1D worsened CC-induced AKI.

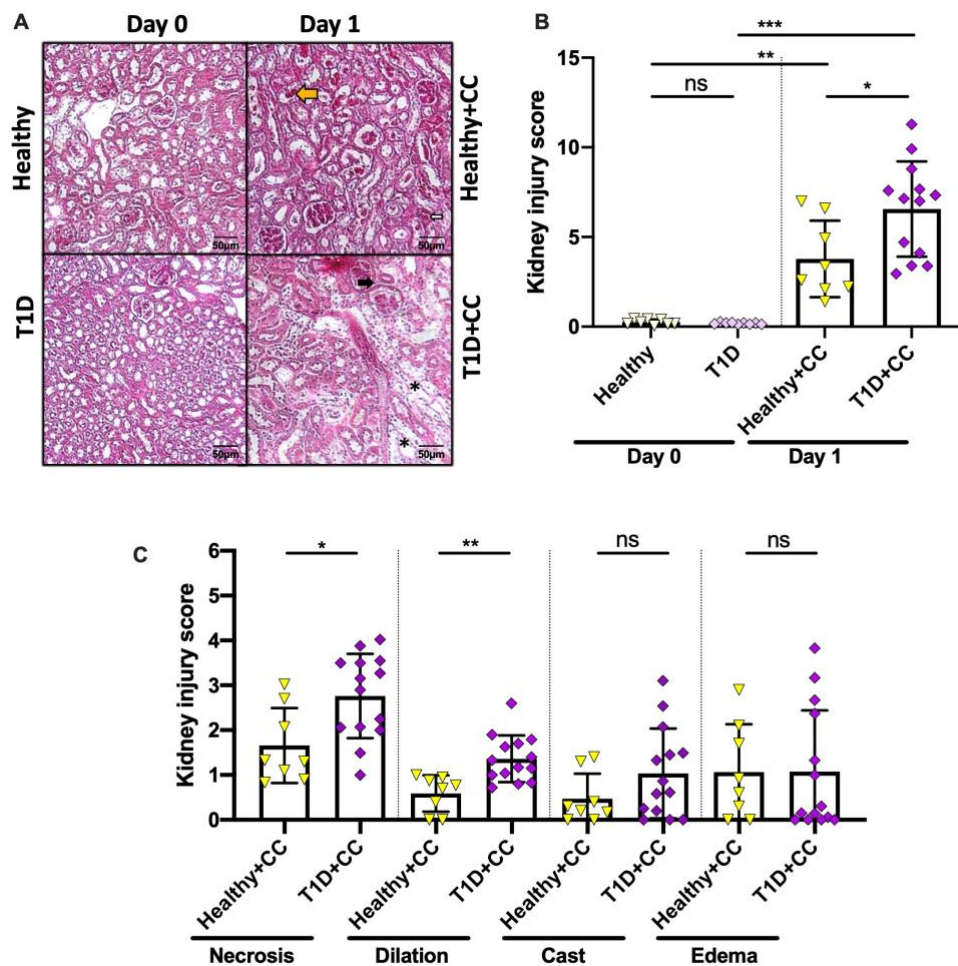


**Figure 15. Type 1 diabetes induces more kidney injury in mice with cholesterol crystal embolism.** (A) Representative images of PAS staining from different groups on day 0 and day 1. \* is indicated tubular necrosis, ➔ is tubular dilation, ➤ is cast respectively. (B) Kidney injury analysis score from sum of the four evaluations including tubular necrosis, tubular dilation, cast formation and tissue edema. (C) Kidney injury analysis score in different parameters. n = 8-13 per group. All quantitative data are means ± SD, ns = not significant, \* p < 0.05, \*\* p < 0.01, \*\*\* P < 0.001 by one-way ANOVA.

---

#### **4.1.6 Type 1 diabetes aggravates necroinflammation in mice with cholesterol crystal embolism**

To investigate whether T1D could enhance the inflammatory response during CC-induced immunothrombosis, serum levels of the pro-inflammatory cytokine IL-6 were measured before and after CC injection. As shown in Figure 16A, serum IL-6 levels significantly increased following CC injection in diabetic and non-diabetic mice of which diabetic mice had significantly elevated IL-6 levels compared to the control group (Figure 16A).

Neutrophils play an essential role during AKI and immunothrombosis [170, 171]. To look for a potential contribution of T1D on leukocytes infiltration, kidney sections were stained with the anti-Ly6B2+ antibody and the percentage of Ly6B2+ leukocytes in the kidney was quantified as described in section 3.3.3. As illustrated in Figure 16B, leukocytes infiltrated the kidney after CC injection on day 1 as compared to the control groups on day 0. Leukocytes were predominantly located near the renal arteries (Figure 16B). Quantification of kidney sections revealed a significant increase in the number of leukocytes in mice with CCE of which diabetic mice had two-fold higher leucocyte numbers after 24 hours than non-diabetic mice (Figure 16C). Taken together, T1D aggravated necroinflammation in mice after CCE.

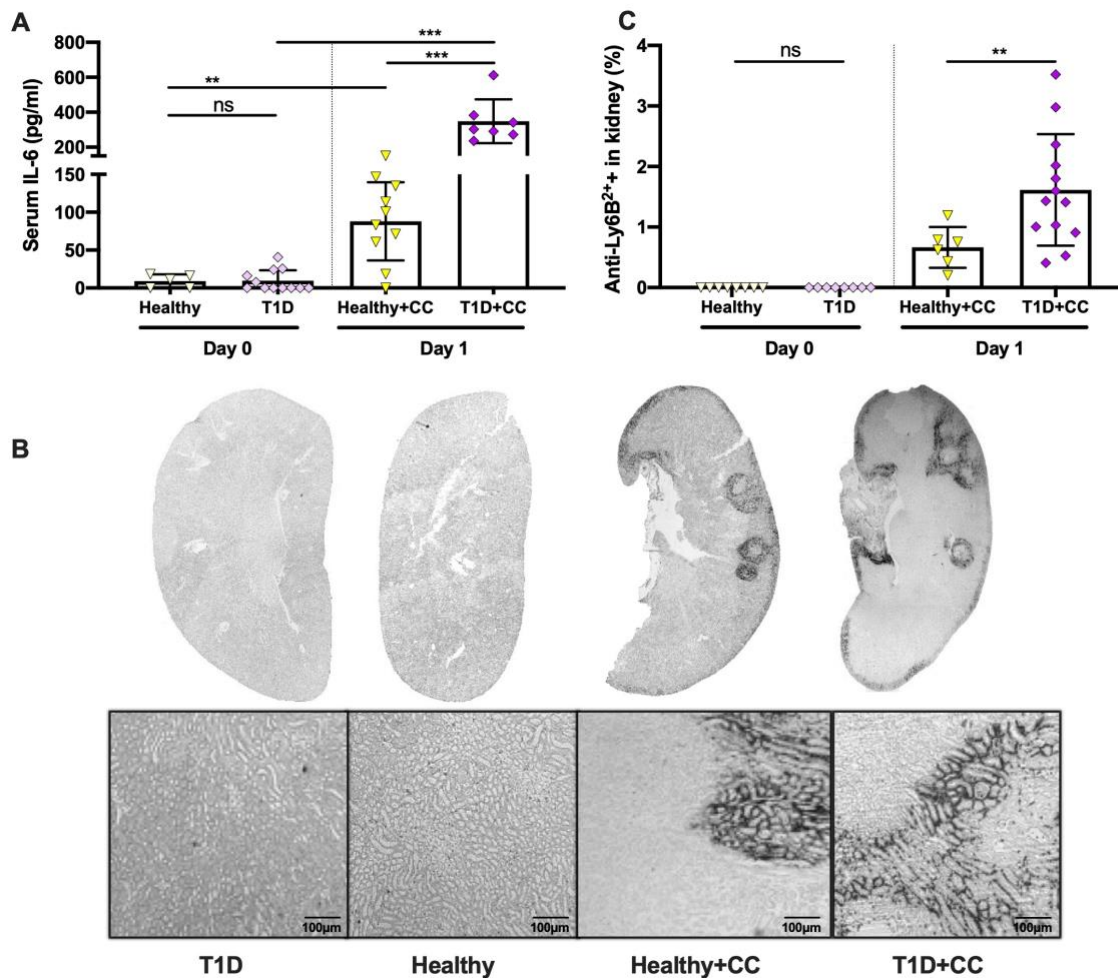


**Figure 16. Type 1 diabetes aggravates necroinflammation in mice with cholesterol crystal embolism.** (A) Serum IL-6 levels from different groups on day 0 and day 1 (n = 5-10 per group). (B) Representative images of Ly6B2+ stained kidney sections before and after CCE injury and zoom in images are shown below. (C) Quantified Ly6B2+ positive staining of the healthy or CCE-injured kidneys (n = 6-12 per group). All quantitative data are means ± SD, ns = not significant, \*\* p < 0.01, \*\*\* P < 0.001 by one-way ANOVA.

#### 4.1.7 Type 1 diabetes has no effect on endothelial injury in cholesterol crystal embolism

Previous reports have shown that CC can destroy the integrity of the vasculature and cause endothelial injury during clot formation [41]. To determine whether T1D would aggravate endothelial injury during CCE, we performed CD31 immunostaining of kidney sections and confirmed that CC reduced the intensity of CD31 (Figure 17A) as well as the percentage (%) of CD31 positive area (Figure 17B) in the kidney from diabetic and non-diabetic mice as compared to the control groups without CC injection. However, there was no statistical

difference between diabetic (T1D) and non-diabetic (Healthy) mice after CCE (Figure 17B), indicating that T1D does not worsen endothelium injury in CC-induced AKI.

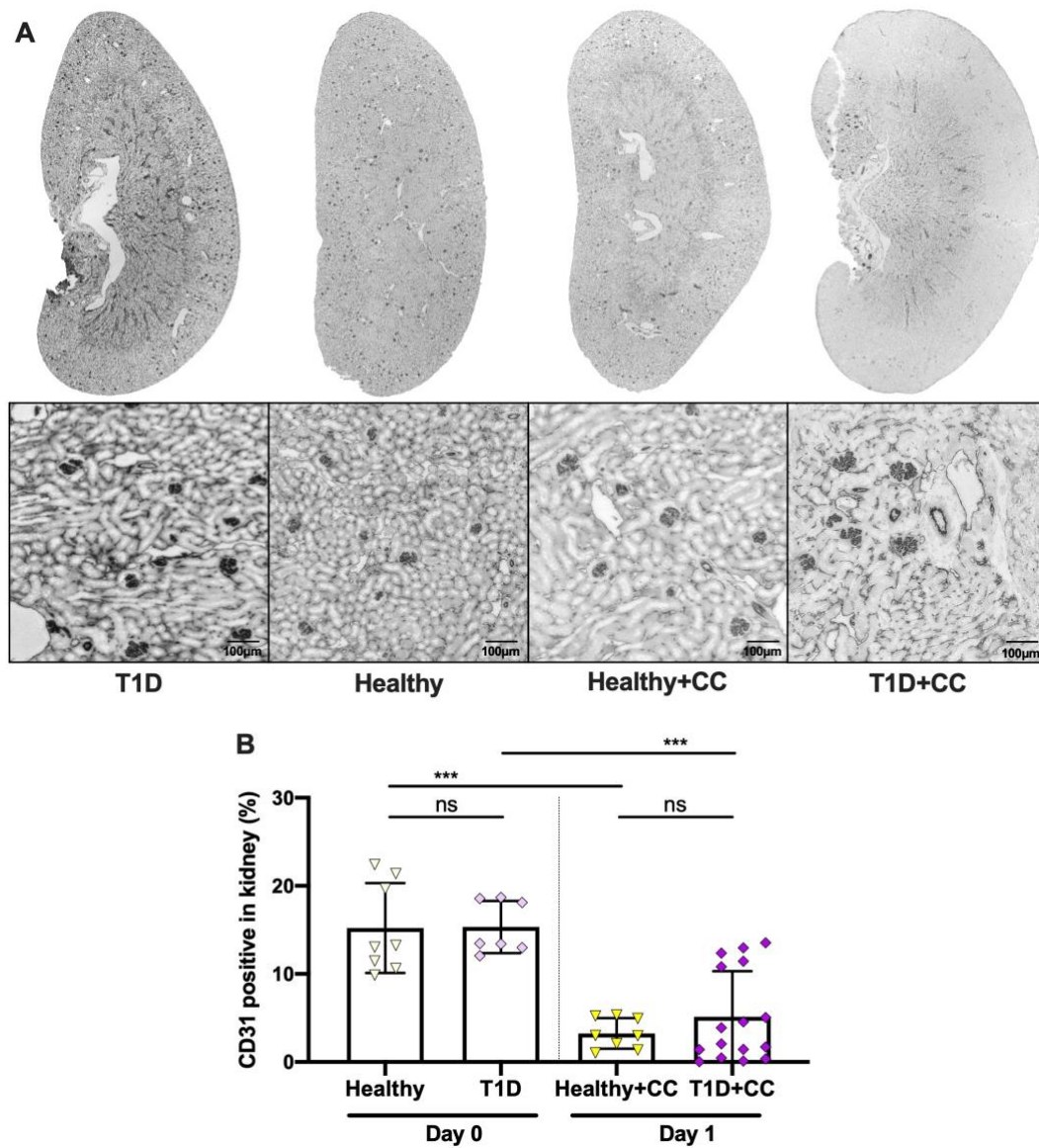


**Figure 17. Type 1 diabetes has no effect on endothelial injury in cholesterol crystal embolism. (A)** Representative CD31 staining sections before and after CCE injury and the zoomed-in details are shown below. **(B)** Quantification of CD31 positive area of the healthy or CCE-injured kidneys (n = 7-16 per group). All quantitative data are means ± SD, ns = not significant, \*\*\* P < 0.001 by one-way ANOVA.

---

#### 4.1.8 High glucose concentration promotes cholesterol crystal-induced platelet aggregation *in vitro*

In CC embolism model, vascular collagen matrix is an important element inducing local platelet adhesion and thrombus growth. Furthermore, CC embolism induce fibrin accumulation and neutrophil recruitment, tthereby leading to the vascular occlusions [41]. Published articles showed that blood glucose can affect platelet function in multiple ways *in vitro* [172]. Similarly, diabetic patients have a higher risk to suffer from coronary artery disease [173]. To investigate whether T1D contributes to collagen-driven platelet activation and aggregation during crystal clot formation and to verify our *in vivo* findings, we isolated platelets from C57BL/6N wild type mice and stimulated them with glucose and/or CC *in vitro* as described in section 3.5.2. Afterward, collagen, a GPVI-selective agonist was added to all four groups and platelet aggregation responses were recorded. As shown in Figure 18A, incubating platelets with CC increased collagen-induced platelet aggregation compared to untreated platelets (control). However, stimulating platelets with glucose also induced platelet aggregation (HG) that was even more pronounced in platelets stimulated with glucose and CC (CC+HG) in the presence of collagen (Figure 18B) indicating that combined CC+HG treatment can amplify CC-induced platelet aggregation in response to collagen.

Next, we studied platelet activation and degranulation in the presence of glucose with or without CC. For this, washed mouse platelets were pre-incubated with or without glucose and/or CC, and stimulated with collagen-related peptide (CRP), which only activates glycoprotein VI-immunoreceptor tyrosine-based activation motif (GPVI-ITAM) pathway in platelets. In resting platelets,  $\alpha$ IIB $\beta$ 3 integrin is constrained in inactive confirmation. Upon stimulation with agonists, transduction of inside-out signaling, resulted in  $\alpha$ IIB $\beta$ 3 integrin activation, to adopt a high affinity conformation, and leads to platelet activation. In this study, the JON/A-PE antibody was used to detect only the active form of  $\alpha$ IIB $\beta$ 3 integrin in murine platelets. Flow cytometric analysis showed that CC or glucose treatment increased inside-out activation of  $\alpha$ IIB $\beta$ 3 integrin compared to resting platelets, that was further increased in platelets stimulated with both glucose and CC (HG+CC) (Figure 18C).

We also investigated the effect of CC and glucose on P-selectin exposure, recognized marker of platelet  $\alpha$ -degranulation. Flow cytometric analysis showed that CC induced degranulation

in platelets as indicated by an increase in P-selectin levels (Figure 18D). Similar results were obtained in the presence of glucose alone (HG) and platelet degranulation was further enhanced in response to glucose plus CC (HG+CC) (Figure 18D). Taken these results together, our *in vitro* findings support the *in vivo* results showing that hyperglycemia promotes CC-induced clot formation and infarct size in the kidney due to multiple functional changes in platelets including aggregation,  $\alpha$ IIb $\beta$ 3 integrin activation and platelet degranulation.

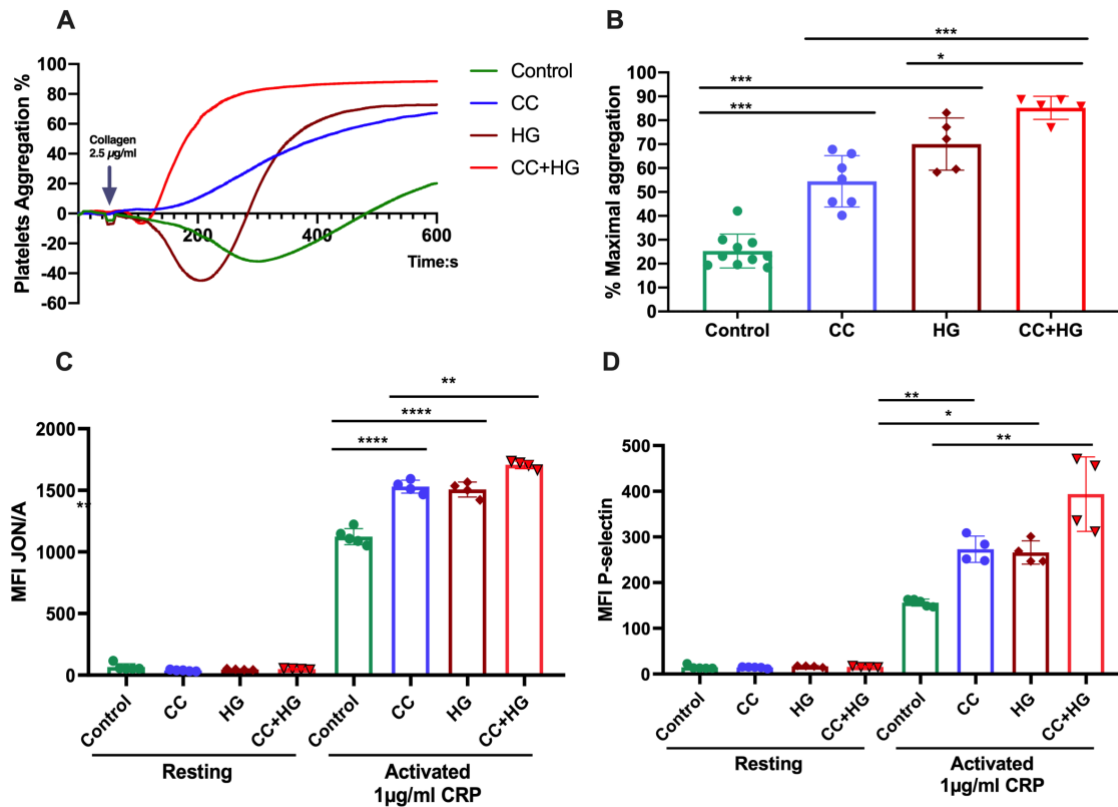


**Figure 18. Glucose promotes cholesterol crystal-induced platelet aggregation *in vitro*.** (A and B) Washed platelets from BL6N WT mice were stimulated with glucose and/or CC *in vitro* as described in section 3.5.2. Platelets aggregation was quantified by light transmission. Platelet-poor-plasma in Tyrode’s buffer with human fibrinogen was set as 0% aggregation and 200  $\mu$ L Tyrode buffer with human fibrinogen was set as 100%. (A) Platelet aggregation curves in represent light transmission over time with adding collagen 2.5  $\mu$ g/mL at 60 seconds. (B) Maximal platelet aggregation in different groups with adding collagen 2.5  $\mu$ g/mL at 60 seconds (n = 5-10 per group). (C and D) Platelet  $\alpha$ IIb $\beta$ 3 integrin activation (C) and P-selectin exposure (D) serving as measure for  $\alpha$ -granule release and were determined by flow cytometry (n = 4-5 per group). All quantitative data are means  $\pm$  SD, ns = not significant, \* p < 0.05, \*\* p < 0.01, \*\*\* P < 0.001 by one-way ANOVA. CRP: collagen-related peptide.

### 4.1.9 High glucose aggravates tubular and endothelial cells death caused by CC injury

As previously shown on PAS-stained kidney sections, T1D mice (T1D+CC) presented with more necrosis in the kidney than the control group (Healthy+CC). To further explore whether hyperglycemia can increase necrosis in tubular epithelial and glomerular endothelial cells in the presence of CC *in vitro*, we pre-incubated HK2 cells and GEnC with or without glucose (30 mM) prior to CC stimulation (2.5 mg/mL). Images of extracellular DNA were taken and cell cytotoxicity analyzed as mentioned in section 3.4.4. As shown in Figure 19A, CC and glucose (HG) increased cytotoxicity in HK2 cells and GEnC. However, glucose further enhanced this effect in the presence of CC (HG+CC). Similarly, tubular epithelial and glomerular endothelial cells released significantly more extracellular DNA in the presence of glucose and CC (CC+HG) than the other groups in GEnC (Figure 19B). The data indicated that glucose aggravates cell death caused by CC, which was consistent with the *in vivo* results that hyperglycemia increased necrosis in tubular epithelial cells during CCE-induced kidney injury.

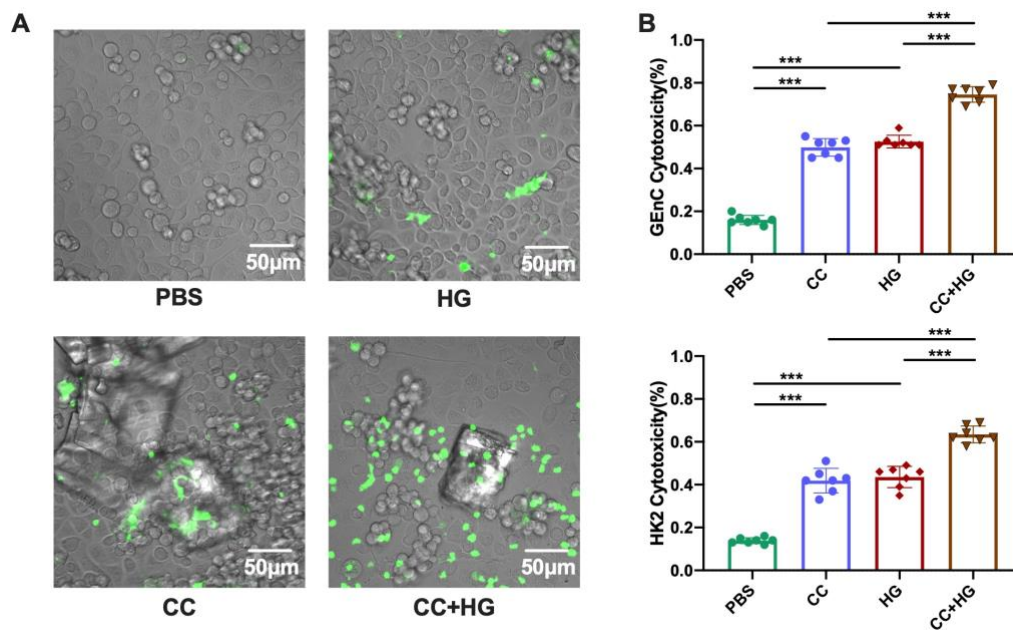


**Figure 19. High glucose aggravates tubular epithelial cells and glomerular endothelial cells death caused by CC injury.** (A) Representative pictures of extracellular DNA in cultured GEnC stained by Sytox Green. (B) GEnC and HK2 cells cytotoxicity in different conditons (n = 7 per group). All quantitative data are means ± SD, \*\* P < 0.01, \*\*\* P < 0.001 by one-way ANOVA.

## 4.2 *Hyperuricemia has vasoactive properties in cholesterol crystal embolism*

To investigate whether asymptomatic hyperuricemia, an important metabolic disorder, would affect the outcomes of CC-induced AKI, the CCE experiments were performed in hyperuricemic mice model *in vivo*. We observed anti-inflammatory and vasoactive effects of asymptomatic hyperuricemia in this context. The occlusion in kidney arteries and ischemic tissue infarction were quantified. In addition, the effects of soluble UA in response to CC were also evaluated in washed platelets from BL6N WT mice and human tubular cells *in vitro*.

### 4.2.1 Establishment of a mouse model of asymptomatic hyperuricemia and cholesterol crystal embolism

To generate a model of asymptomatic hyperuricemia with CCE, we first checked whether asymptomatic hyperuricemia had an impact on body weight and kidney function in male and female Alb-creERT2;*Glut9*<sup>lox/lox</sup> mice. Alb-creERT2;*Glut9*<sup>lox/lox</sup> and *Glut9*<sup>lox/lox</sup> control mice were injected with tamoxifen and placed on a standard chow diet enriched with inosine for two weeks as described in section 3.2.2. As shown in Figure 20A, Alb-creERT2;*Glut9*<sup>lox/lox</sup> mice (HU) developed hyperuricemia as indicated by a significant increase in serum UA levels (7-12 mg/dL) in both female and male mice, while the serum UA levels remained normal in *Glut9*<sup>lox/lox</sup> control mice (Healthy). No difference in body weight between healthy and hyperuricemic female mice was observed (Figure 20B). Similar results were noticed in male mice. Of note, female mice were in general smaller than male mice. Importantly, hyperuricemia did not induce a decrease in GFR in male and female Alb-creERT2;*Glut9*<sup>lox/lox</sup> mice as compared to healthy *Glut9*<sup>lox/lox</sup> mice (Figure 20C) indicating that asymptomatic hyperuricemia did not induce kidney injury independent of the sex. Therefore, both female and male mice were used throughout the study.

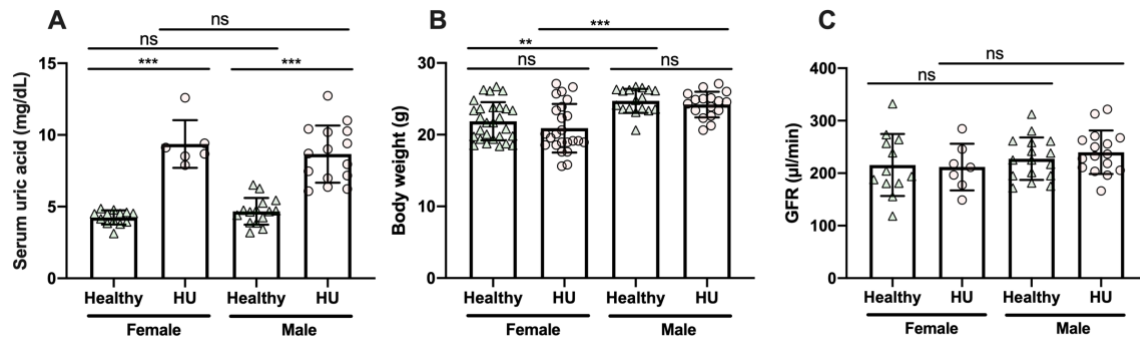


**Figure 20. Establishment of a mouse model of asymptomatic hyperuricemia.** AlbcreERT2;*Glut9*<sup>lox/lox</sup> (HU) and *Glut9*<sup>lox/lox</sup> control mice (Healthy) were injected with tamoxifen and placed on a standard chow diet enriched with inosine for two weeks as described in section 3.2.2. After that serum uric acid levels (A), body weight (B) and GFR (C) were tested in both male and female mice before CCE surgery. n = 6-28 per group. All quantitative data are means ± SD, ns = not significant, \*\* p < 0.01, \*\*\* P < 0.001 by one-way ANOVA.

Next, we injected hyperuricemic and healthy mice with CC. Our results showed that hyperuricemia nor CCE induced a drop in body weight in mice (Figure 21A). After CC injection into the left kidney artery, the kidney weight slightly increased on day 1 compared with healthy and hyperuricemic (HU) mice on day 0 (Figure 21B), while kidney weights significantly decreased on day 14 after CC surgery in both groups of mice (Figure 21B). We did not observe differences in the weight of the contralateral kidneys between both groups indicating that hyperuricemia may not promote hypertrophy (Figure 21B).

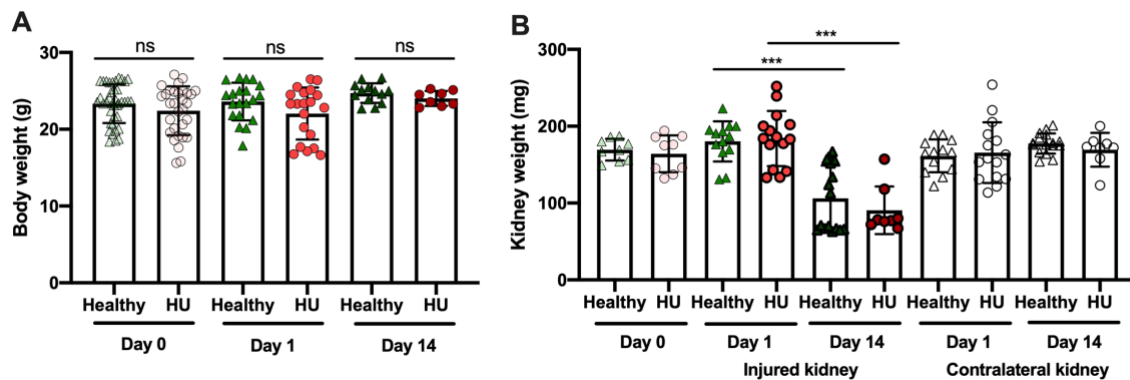


**Figure 21. Body and kidney weight in different groups.** (A) No loss of body weight occurred during the experiments in both groups of mice. (B) CC-injured kidney atrophy occurred in both groups only on day 14. n = 8-25 per group. All quantitative data are means ± SD, ns = not significant, \*\*\* P < 0.001 by one-way ANOVA.

After injecting mice with CC, serum UA levels increased in hyperuricemic mice from 9 to 15 mg/dL and in the healthy (non-hyperuricemic) from 5 to 7 mg/dL on day 1 compared to day 0

due to the impaired urinary UA clearance as a result of kidney injury (Figure 22). However, serum UA levels returned to baseline after 14 days.

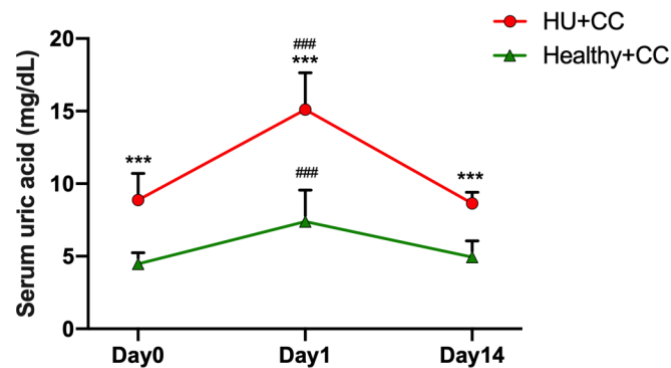


**Figure 22. Serum uric acid level before and after cholesterol crystal injection.** Serum UA levels on day 0, 1 and day 14 after CCE in both HU and control mice.  $n = 8-16$  per group. All quantitative data are means  $\pm$  SD, \*\*\*  $P < 0.001$  compared between two groups at the same time points, ###  $P < 0.001$  compared with day 0 baseline, by one-way ANOVA.

#### 4.2.2 Hyperuricemia contributes to a greater decline in kidney excretory function after cholesterol crystal embolism

Next, we looked at the effect of asymptomatic hyperuricemia on kidney function after CCE. As shown in Figure 23A, GFR and delta-GFR significantly decreased in control mice (Healthy) and even more than 60% in hyperuricemic mice (HU+CC) after CC injection on day 1 (Figure 23A and 23B). After 14 days, the kidney function fully recovered in control mice (Healthy+CC), while the GFR remained low in hyperuricemic mice (HU+CC) (Figure 23A and 23B). Consistent with the GFR measurement, serum BUN levels were higher in hyperuricemic mice compared to control mice after CC injection on day 1 and 14 (Figure 23C). Taken together, the data suggested that asymptomatic hyperuricemia contributes to a greater reduction in kidney function after CCE possibly due to a compensatory vasoactive effect.

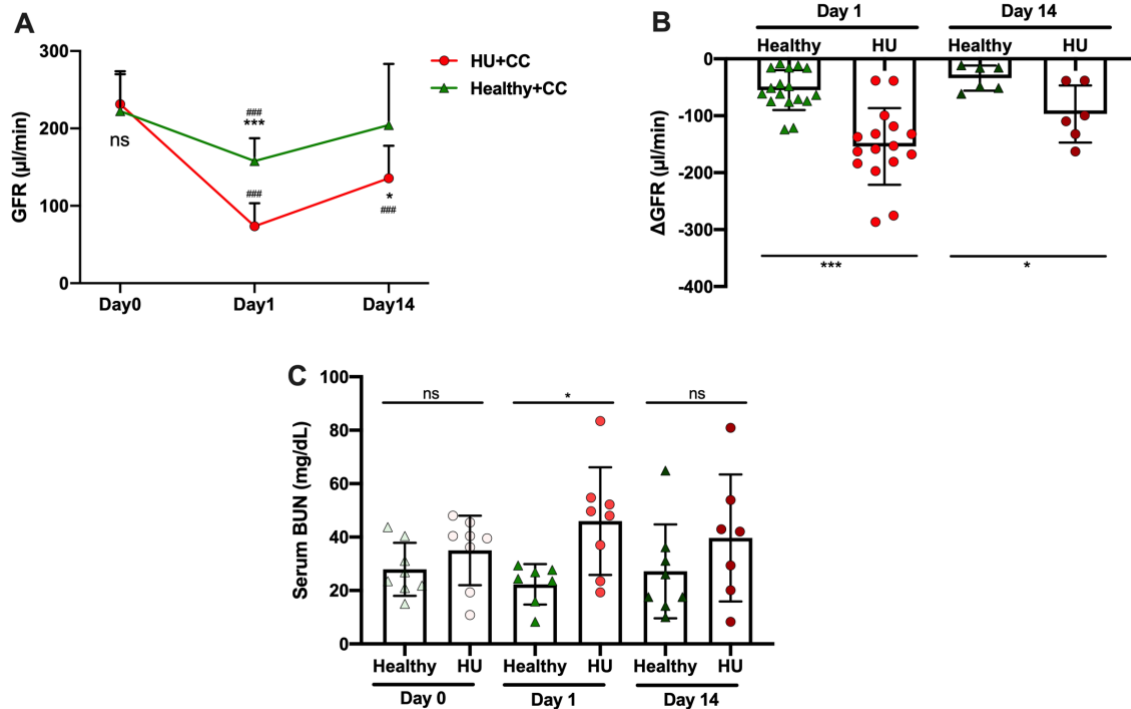


**Figure 23. Hyperuricemia contributes to a greater reduction in kidney excretory function after CC-induced AKI.** (A) GFR values on day 0, 1 and 14 after CCE in both hyperuricemic HU and control mice (n = 8-17 per group, \* compared between two groups at the same days, # compared with day 0 baseline, by one-way ANOVA). (B) the  $\Delta$ GFR is the GFR values on day 1 or day 14 after CCE subtract the values on day 0 from each mice (n = 6-17 per group, Student's t-test). (C) Serum BUN levels from different groups (n = 7-8 per group, one-way ANOVA). All quantitative data are means  $\pm$  SD, ns = not significant, \* p < 0.05, \*\* p < 0.01, \*\*\* P < 0.001, #### P < 0.001.

#### 4.2.3 Hyperuricemia decreases kidney infarction and artery occlusion in the early but not the late phase after cholesterol crystal embolism

After injecting hyperuricemic (HU) and control (Healthy) mice with CC, we collected kidneys to assess kidney infarction on day 1 and day 14 using TTC staining as previously described in section 3.3.2. TTC staining showed that CC injection into the left kidney artery induced diffuse or complete kidney infarction in mice as illustrated by a color change from red to white in the injured kidneys but not in the contralateral kidney (Figure 24A). When quantifying kidney infarct size, we found that hyperuricemic mice (HU+CC) had significantly less kidney infarct size than healthy mice on day 1, an effect that disappeared on day 14. This suggests that CC injection reduced renal blood flow more in healthy mice (Healthy+CC) than in hyperuricemic mice and that hyperuricemia diminished ischemic tissue infarction on day 1 (Figure 24B).

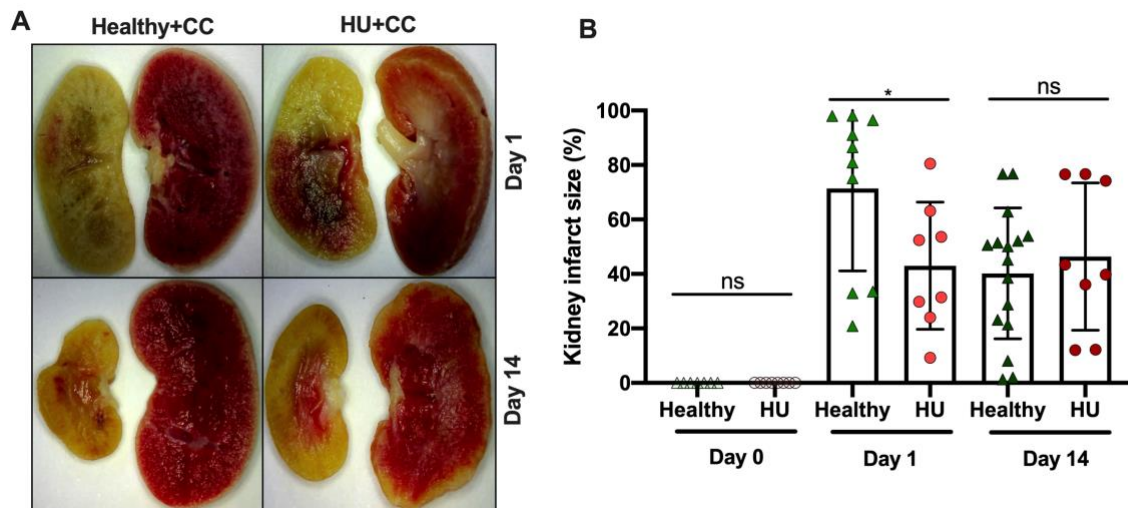


**Figure 24. Hyperuricemia decreases kidney infarction in the early but not the late phase after cholesterol crystal embolism. (A and B)** Both injured and contralateral kidneys were collected from HU and control (Healthy) mice on day 1 and day 14 after CCE and stained with TTC for 15 minutes at 37°C. **(A)** Representative TTC stained kidneys from different groups. **(B)** Kidney infarct size from different groups were quantified by Fiji software (n = 8-16 per group). All quantitative data are means ± SD, ns = not significant, \* p < 0.05 by one-way ANOVA.

To quantify the ratio of occluded arteries in hyperuricemic and control mice after CCE, kidney sections were stained with  $\alpha$ -SMA and fibrin and the ratio of occluded interlobar, arcuate and interlobular renal arteries was assessed as described in section 3.3.6. Co-immunostaining staining of  $\alpha$ -SMA and fibrin showed that intrarenal arteries were either completely and partially occluded by CC clots or remained empty (Figure 25A). The mean values of the artery conditions from each groups were quantified and are shown in Figure 25B for day 1 and Figure 25C for day 14. The results displayed that CC caused occlusion in renal arteries in both groups of mice. However, hyperuricemic mice (HU+CC) had less completely occluded interlobar and arcuate arteries but more partially arcuate arteries and completely interlobular arteries than control mice (Healthy+CC) on day 1 (Figure 25B) suggesting that in hyperuricemic mice the CC clots may obstruct deeper the kidney arteries. In addition, both hyperuricemic and healthy mice presented with a similar ratio of occluded interlobar renal arteries, while hyperuricemic mice had more occluded arcuate and interlobular arteries compared with healthy mice on day 14 after CCE (Figure 25C).

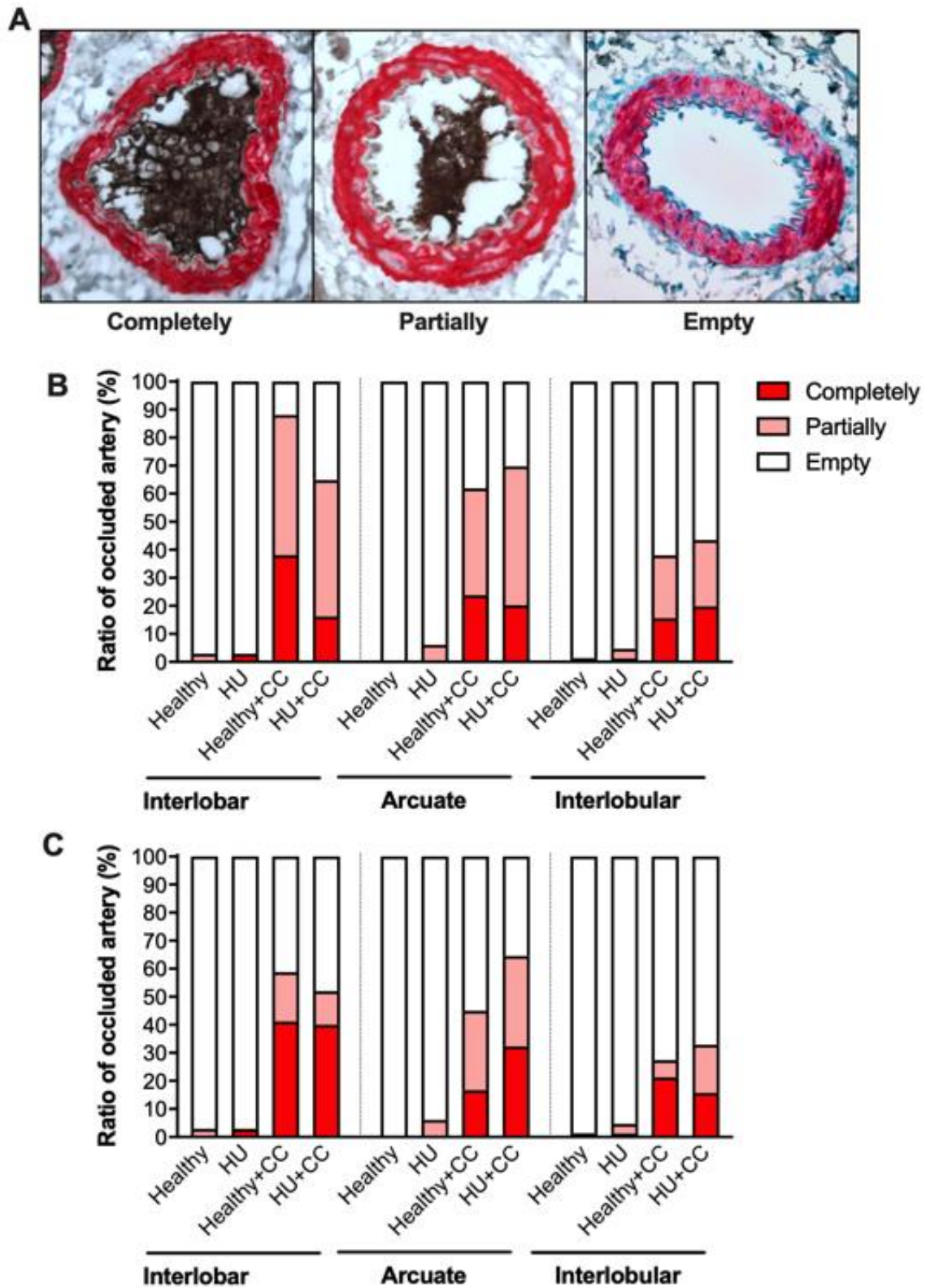


**Figure 25. Quantification of CC-induced arterial occlusions from different groups.** (A) Illustration of the severity of CC-induced obstruction in the kidney arteries. (B and C) Ratio of CC-induced occluded arteris in hyperuricemic (HU) and healthy mice according to the size of arteries on day 1 (B) and day 14 (C). n = 8-16 per group. Data analyzed with the formula described in 3.3.6.

---

#### **4.2.4 Hyperuricemic mice display a higher vasoconstriction ratio on both kidneys after cholesterol crystal embolism**

To better understand why the kidney function (GFR) in hyperuricemic mice declined by more than 60% after CCE compared to baseline (before CCE) and the healthy group, we stained kidney sections with  $\alpha$ -SMA and fibrin, and quantified the ratio of lumen/artery area (S1/S2) as described in section 3.3.5. Representative images of renal arteries from the injured and contralateral kidney on day 0, 1 and 14 after CCE are shown in Figure 26A. After CC injection, the ratio of lumen/artery area decreased in the contralateral kidney in healthy mice after CCE on day 1 compared with day 0 and returned to baseline on day 14 (Figure 26B and 26C). Interestingly, the ratio of lumen/artery area decreased in both injured and contralateral renal arteries in hyperuricemic mice compared with healthy mice on day 1 (Figure 26B and 26C). This was more pronounced in the contralateral arteries in hyperuricemic mice on day 1 as indicated by a 50% drop in the ratio of lumen/artery area compared with baseline values before surgery and a 30% drop compared with the injured kidneys. However, 14 days after CC injection, vasoconstriction of the contralateral kidney arteries returned to baseline ratios in hyperuricemic mice, while the ratio remained low in the CCE injured kidney (HU+CC injured). Taken together, the results suggested that hyperuricemia induced vasoconstriction of the arteries in the injured and even more in the contralateral kidney after CCE providing an explanation for the significant decline in kidney function.

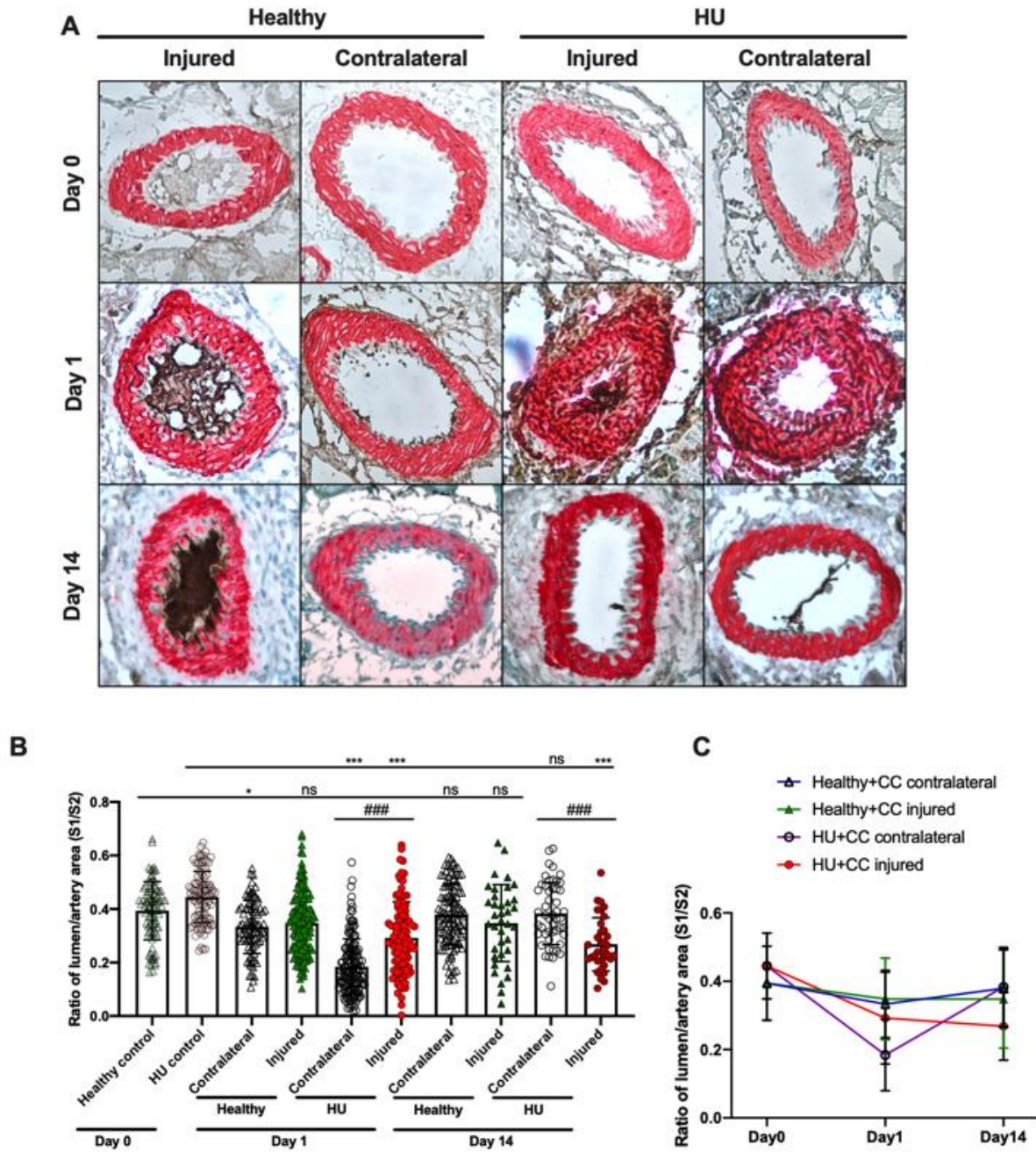


**Figure 26. Hyperuricemic mice display a higher vasoconstriction ratio in both kidneys after cholesterol crystal embolism. (A)** Representative images of  $\alpha$ -SMA/fibrin-stained renal arteries from different groups. **(B and C)** Ratio of lumen/artery area analyzed from both injured and contralateral kidneys on day 0, day 1 and day 14.  $n = 37$ -200 arteries per group. All quantitative data are means  $\pm$  SD, ns = not significant, \*  $p < 0.05$ , \*\*  $p < 0.01$ , \*\*\*  $P < 0.001$ , ###  $P < 0.001$  by one-way ANOVA.

---

#### **4.2.5 Hyperuricemia reduces kidney injury on day 1 but worsens on day 14 after cholesterol crystal embolism**

To investigate the contribution of hyperuricemia on kidney injury, we performed PAS staining of kidney sections and quantified tissue injury on day 1 and 14 after CC injection as described in section 3.3.4. As illustrated in Figure 27A and quantified in Figure 27B, PAS staining revealed less kidney injury in hyperuricemic (HU+CCE) mice compared to healthy mice (Healthy+CCE) after CCE on day 1. In particular, we observed significantly less tubular necrosis and renal interstitial edema in hyperuricemic mice (Figure 28A), while tubular dilation and cast formation were similarly affected between hyperuricemic and healthy mice at day 1 after CCE. However, this was different on day 14 after CCE. Hyperuricemic mice presented with a higher kidney injury score than healthy mice after CCE, in particular cast formation significantly increased in kidneys from hyperuricemic mice as compared with healthy mice (Figure 28B). No difference was observed in interstitial edema, tubular necrosis and tubular dilation between both groups of mice on day 14. Taken together, hyperuricemia reduced CC-induced acute kidney injury during the early phase but worsened kidney injury on day 14.

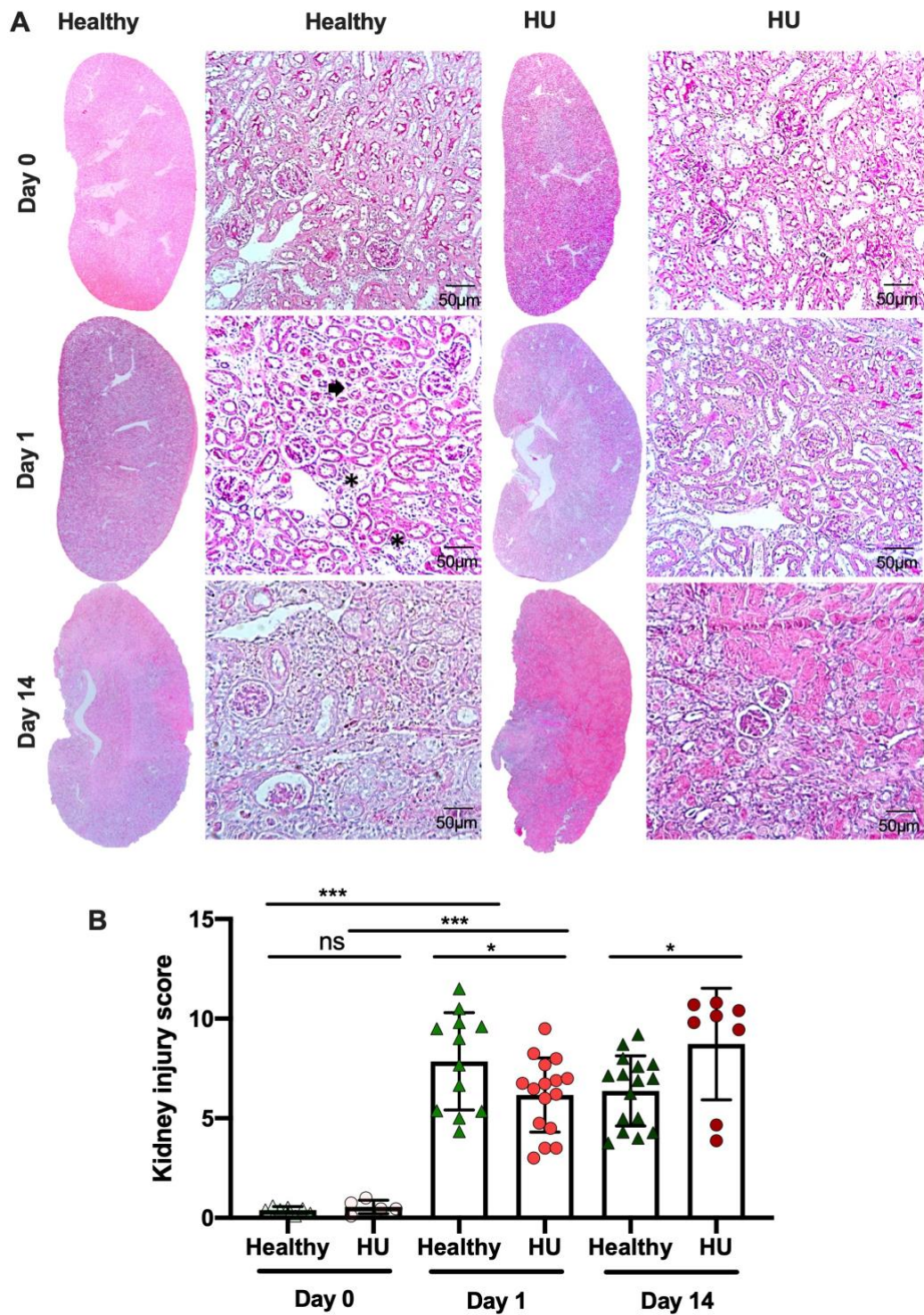


**Figure 27. Hyperuricemia reduces kidney injury on day 1 but worsens the outcome on day 14 after cholesterol crystal embolism. (A)** Representative images of PAS-stained kidneys from healthy and hyperuricemic mice on day 0, 1 and 14 after CCE. \* is indicated tubular necrosis,  $\blacktriangleright$  is tubular dilation respectively. **(B)** Quantification of the total kidney injury score evaluated for tubular necrosis, tubular dilation, cast formation and tissue edema. n = 8-17 per group. All quantitative data are means  $\pm$  SD, ns = not significant, \* p < 0.05, \*\* p < 0.01, \*\*\* P < 0.001 by one-way ANOVA.

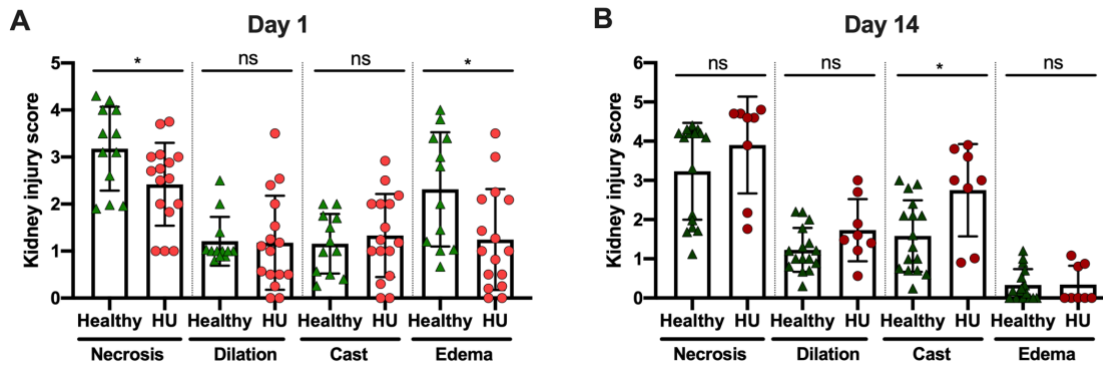


**Figure 28. Kidney injury score after cholesterol crystal embolism.** (A) Kidney injury score evaluated according to tubular necrosis, tubular dilation, cast formation and tissue edema on day 1. (B) Kidney injury score on day 14. n = 8-17 per group. All quantitative data are means ± SD, ns = not significant, \* p < 0.05 by one-way ANOVA.

#### 4.2.6 Hyperuricemia increases serum IL-6 levels but not leukocyte counts in mice after cholesterol crystal embolism

To investigate whether asymptomatic hyperuricemia would affect the inflammatory response during CC-induced immunothrombosis, serum levels of the pro-inflammatory cytokine IL-6 were measured before and after CC injection. As shown in Figure 29A, serum IL-6 levels increased in both hyperuricemic (HU+CCE) and healthy (Healthy+CCE) mice after CCE on day 1 and returned to baseline on Day 14 (Figure 29A). However, serum IL-6 levels were four-times higher in hyperuricemic mice compared with healthy mice at day 1 after CCE (Figure 29A).

One hallmark of inflammation is the infiltration of immune cells to the site of tissue injury. To address whether asymptomatic hyperuricemia modulates leukocyte infiltration, we stained kidney sections with the anti-Ly6B2 antibody as described in section 3.3.3 and found that the percentage of Ly6B2+ leukocytes increased in hyperuricemic and healthy mice on day 1 after CC injection as illustrated in Figure 29B. Leukocytes were mainly observed in the areas of injured arteries and the surrounding ischemic tissue (Figure 29B). However, the percentage of infiltrating Ly6B2+ leukocytes decreased on 14 days compared to day 1, whereas no difference was found between hyperuricemic and healthy mice after CCE (Figure 29C).

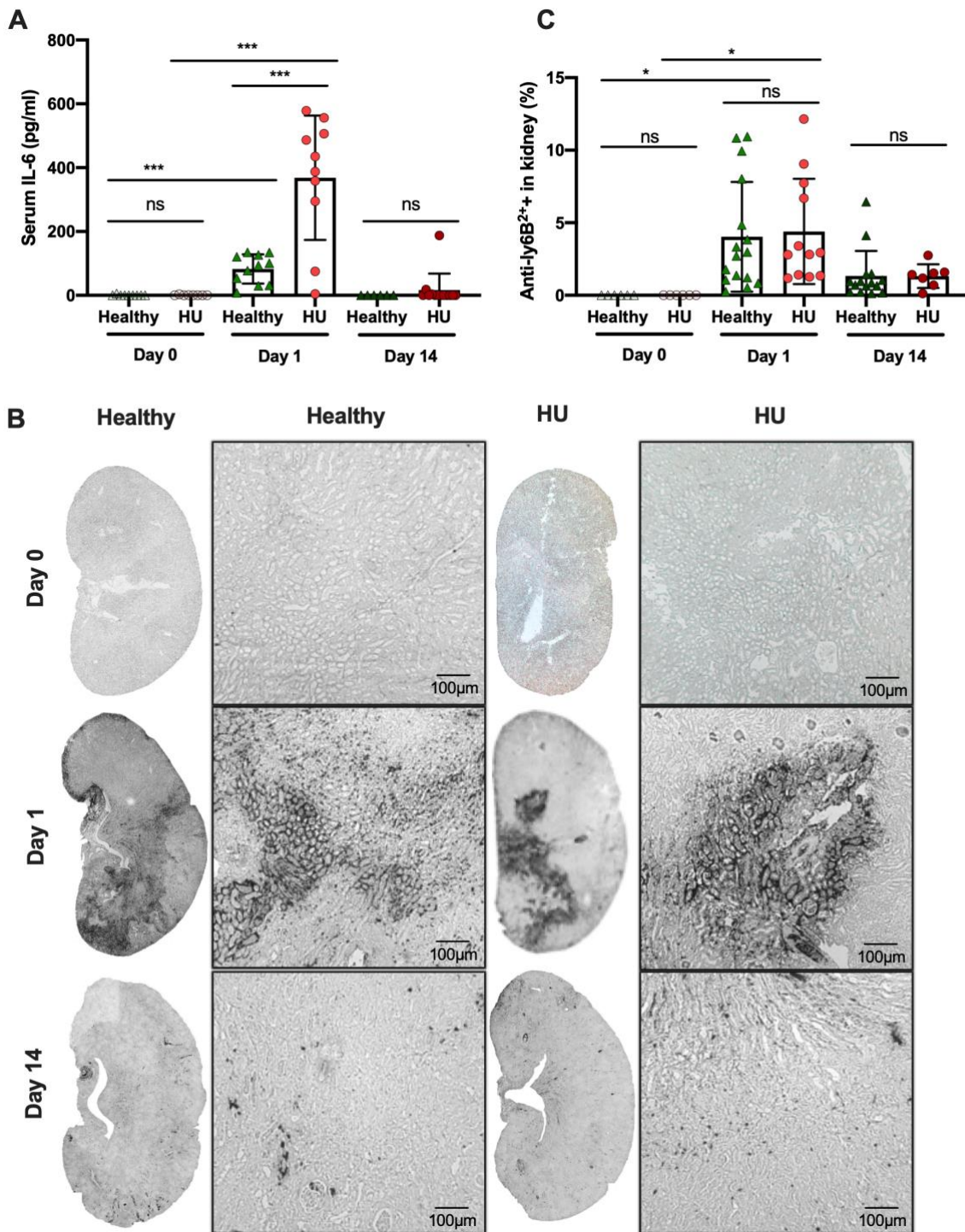


**Figure 29. Hyperuricemia increases serum IL-6 levels without affecting leukocyte infiltration in mice after cholesterol crystal embolism. (A)** Serum IL-6 levels from different groups on day 0, day 1 and day 14 (n = 8-11 per group). **(B)** Representative images of Ly6B2+ stained kidney sections before and after CCE injury and zoomed-in images are shown on the right. **(C)** Quantified Ly6B2+ positive area of the healthy or CCE-injured kidneys (n = 6-16 per group). All quantitative data are means ± SD, ns = not significant, \* p < 0.05, \*\*\* P < 0.001 by one-way ANOVA.

---

#### **4.2.7 Hyperuricemia did not affect endothelial injury in cholesterol crystal embolism**

To determine whether asymptomatic hyperuricemia contributes to endothelial injury during CCE, we performed CD31 immunostaining of kidney sections and found that CC caused a significant decrease in the intensity of CD31 (Figure 30A) as well as the percentage of CD31 positive area in the kidney of both hyperuricemic and healthy mice 1 day after CCE (Figure 30B). However, the percentage of CD31+ area increased again on day 14 in both groups of mice (Figure 30B), while no differences were observed between the groups after CCE indicating that hyperuricemia does not affect endothelial injury in CC-induced AKI.

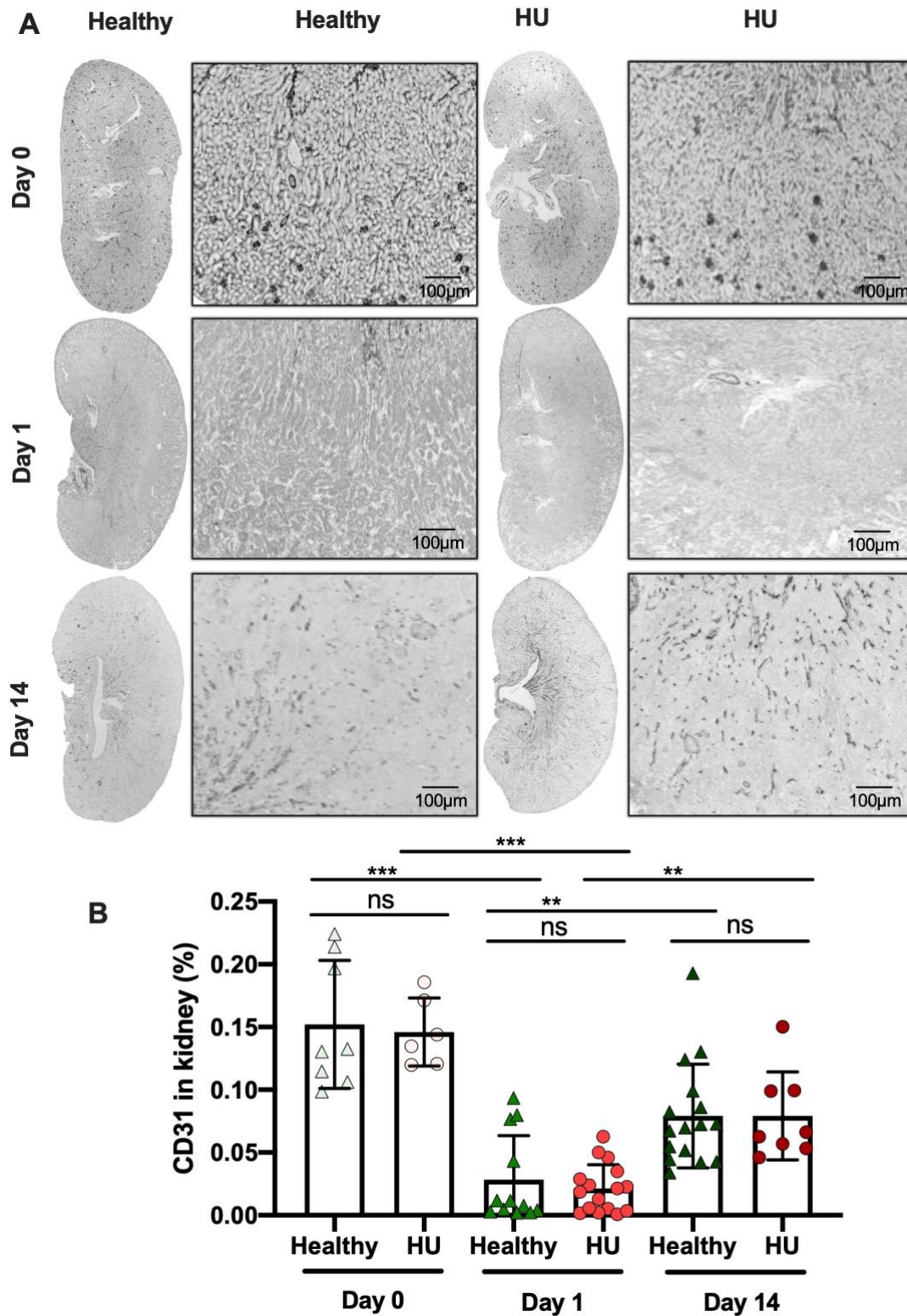


**Figure 30. Hyperuricemia is dispensable on endothelial injury in cholesterol crystal embolism.** (A) Representative images of CD31-stained kidney sections before and after CCE injury and the zoomed-in details are shown on the right side. (B) Quantified CD31 positive staining of the CCE-injured kidneys at different time points (n = 6-16 per group). All quantitative data are means ± SD, ns = not significant, \*\* p < 0.01, \*\*\* P < 0.001 by one-way ANOVA.

---

#### **4.2.8 Soluble uric acid has no effect on CC-induced platelet aggregation, activation and degranulation *in vitro***

Platelets play an important role in the vascular occlusion after CCE [41]. Clinical evidence suggests that the concentration of serum UA serves as a negative predictor of platelet reactivity [174]. However, whether asymptomatic hyperuricemia and soluble UA have effects on platelet function and activity in CCE is currently unknown. To investigate this and to verify our *in vivo* findings, we isolated platelets from BL6N WT mice and stimulated them in the presence or absence of soluble UA prior to stimulation with CC as described in section 3.5.2. Platelet agonists such as collagen, U46619 or CRP were also added to activate platelet aggregation. As shown in Figure 31A and 31B, CC included a significant increase in platelet aggregation in control and soluble UA-treated platelets over time compared with unstimulated platelets (control and UA) in the presence of 2.5  $\mu\text{g}/\text{mL}$  collagen. However, no difference was observed in platelet aggregation between control and soluble UA-treated CC-activated platelets (Figure 31A and 31B). Similar results were obtained in the presence of 5  $\mu\text{g}/\text{mL}$  collagen (Figure 31C) and 1.5  $\mu\text{M}$  U46619 (Figure 31D) over time compared to untreated platelets (Control), which confirmed the association between platelet activation and CC thrombotic angiopathy. In addition, soluble UA did not enhance platelet aggregation under normouricemic (5 mg/dL UA) and hyperuricemic condition (10 mg/dL UA) in response to 0.025  $\mu\text{g}/\text{mL}$  and 0.05  $\mu\text{g}/\text{mL}$  CRP compared with control platelets (Figure 31E and 31F). This suggests that hyperuricemia does not affect platelet aggregation in response to CC activation *in vitro* as well as platelet aggregation and fibrin formation during CC-induced embolism *in vivo*.

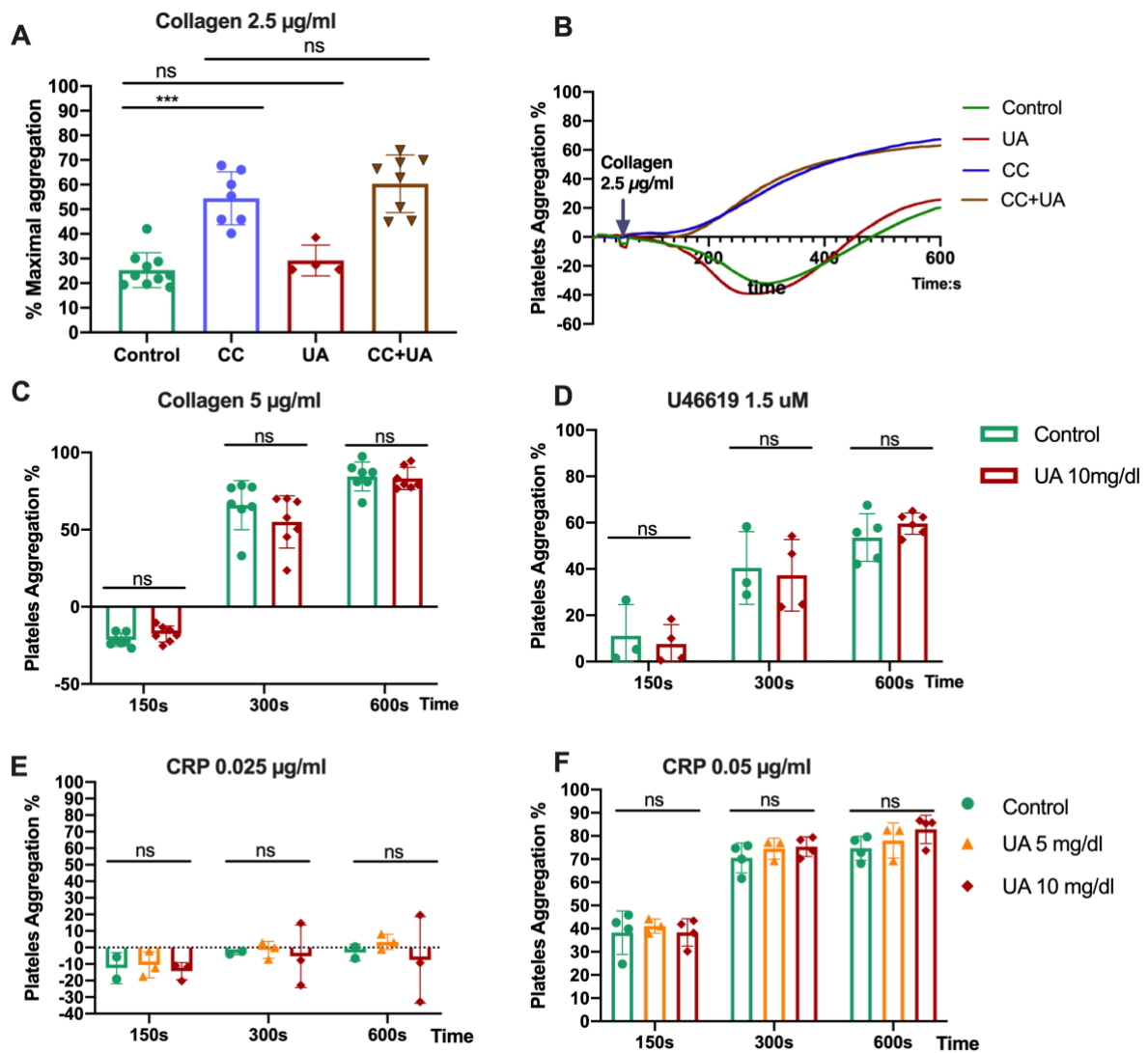


**Figure 31. Soluble uric acid has no effect on CC-induced platelet aggregation *in vitro*.** (A-F) Washed platelets from BL6N WT mice were stimulated with soluble UA and/or CC *in vitro* as described in section 3.5.2. Platelet aggregation was quantified via light transmission in platelet-poor-plasma in Tyrode’s buffer with human fibrinogen that was set as 0% aggregation and 200  $\mu\text{L}$  Tyrode buffer with human fibrinogen that was set as 100%. (A) Maximal platelet aggregation in different groups (n = 4-10 per group). (B) Curves represent light transmission over time. (C-F) Platelet aggregation over time with different aggregation agonists under normouricemic (5 mg/dL UA) and hyperuricemic (10 mg/dL) condition. n = 3-7 per group). All quantitative data are means  $\pm$  SD, ns = not significant, \* p < 0.05, \*\*\* P < 0.001 by one-way ANOVA.

---

Next, we investigated platelet activation and degranulation in the presence of soluble UA with or without CC stimulation in response to CRP and thrombin. For this, platelets were isolated from BL6N WT mice, pre-incubated with or without soluble UA (10mg/dL) and/or CC (2.5 mg/mL), and activated with CRP or thrombin as described in section 3.5.3. Platelets were stained with the P-selectin antibody, a  $\alpha$ -granule marker, to verify the efficiency of platelet degranulation and the expression levels are determined as median fluorescence intensity (MFI) using flow cytometry. The results showed that CC-induced degranulation in platelets after stimulation with CRP and thrombin significantly increased P-selectin exposure on the platelet surface, compared to resting platelets (Figure 32A and 32C). Interestingly, soluble UA had no additional effect on P-selectin exposure in CC-activated or untreated platelets compared to the control group (Figure 32A and 32C).

Next,  $\alpha$ IIB $\beta$ 3 integrin activation was measured in washed murine platelets *in vitro* using the JON/A-PE antibody. Flow cytometric analysis showed that CRP and thrombin could induce  $\alpha$ IIB $\beta$ 3 integrin activation, compared to resting platelets that were left untreated or treated with UA and/or CC (Figure 32B and 32D). However, we did not observe differences between soluble UA-treated or untreated platelets. These results indicate that soluble UA does not affect  $\alpha$ IIB $\beta$ 3 integrin activation and P-selectin exposure, triggered by PAR-Gq and GPVI-ITAM signalings.

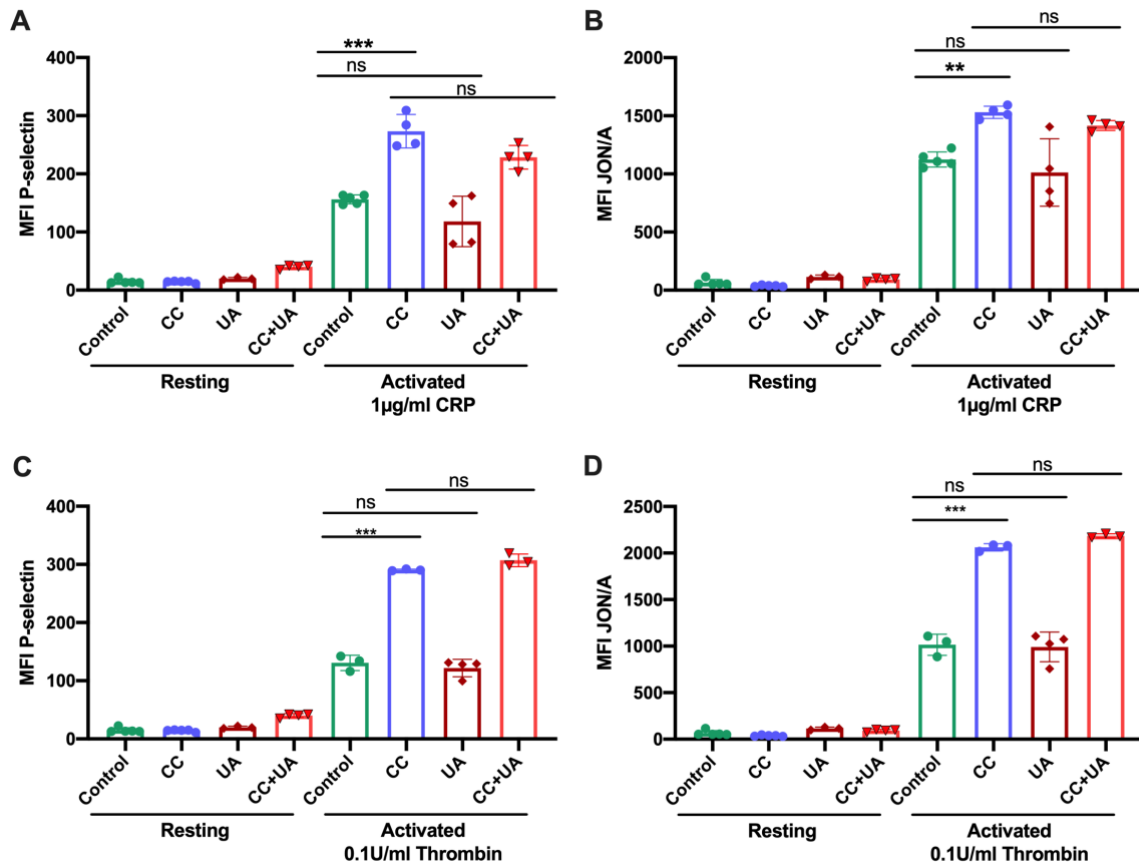


**Figure 32. Soluble uric acid has no effect on CC-induced platelet activation and degranulation *in vitro*.** (A-D) Washed platelets from BL6N WT mice were stimulated with soluble uric acid and/or CC *in vitro* as described in section 3.5.2. Median fluorescence intensity (MFI) was determined by flow cytometry. (A) P-selectin exposure on platelets stimulated with CRP agonist. (B) Platelet  $\alpha$ IIb $\beta$ 3 integrin activation stimulated with CRP agonist. (C) P-selectin exposure on platelets stimulated with thrombin. (D) Platelet  $\alpha$ IIb $\beta$ 3 integrin activation stimulated with thrombin. n = 3-5 per group. All quantitative data are means  $\pm$  SD, ns = not significant, \*\* p < 0.01, \*\*\* P < 0.001 by one-way ANOVA. CRP: collagen-related peptide.

To investigate whether platelets similar to other immune cells including monocytes and neutrophils express the urate transporter *Slc2a9* that is needed for the intracellular uptake of soluble UA, we isolated platelets from healthy individuals and incubated the cells in the presence or absence of soluble UA and performed RT-PCR as described in section 3.6 [164]. As shown in Figure 33A, human platelets express *SLC2A9* as indicated by the relative mRNA expression levels, while incubation with soluble UA did not change *SLC2A9* mRNA expression levels. In addition, we also determined the relative mRNA expression of *Slc2a9/Glut9* in platelets, megakaryocytes, liver and kidney isolated from healthy mice. As displayed in Figure 33B, mRNA expression of *Slc2a9/Glut9* was particularly low in murine platelets but also megakaryocytes compared with expression levels in the liver and kidney, tissues that are known to express *Slc2a9* in hepatocytes and tubular cells. Taken together, our *in vitro* findings support the *in vivo* results showing that asymptomatic hyperuricemia does not modulate platelet aggregation,  $\alpha$ IIb $\beta$ 3 integrin activation and  $\alpha$ -granule degranulation during CCE.

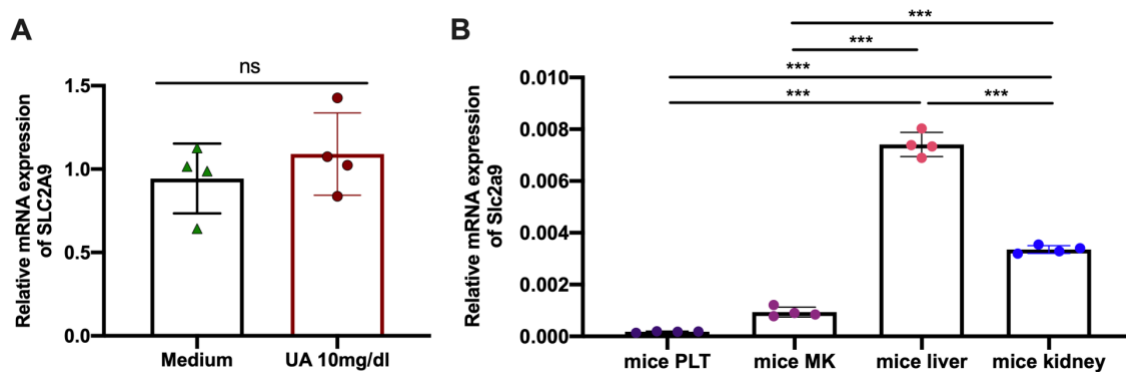


**Figure 33. Relative mRNA expression of *SLC2A9* and *Slc2a9* in platelets.** (A) Relative mRNA expression of *SLC2A9* from human platelets determined by RT-PCR after incubation in medium or with soluble UA (10 mg/dL) for 90 minutes (n = 4 per group, Student’s t-test). (B) Relative mRNA expression of *Slc2a9* from platelets, megakaryocytes, liver and kidney in C57BL/6N wild type mice (n = 4 per group, one-way ANOVA). All quantitative data are means ± SD, ns = not significant, \*\* p < 0.01, \*\*\* P < 0.001. PLT: platelets, MK: megakaryocytes.

### 4.2.9 Soluble uric acid protects HK2 cells from cell death during oxidative stress *in vitro*

As previously shown, asymptomatic hyperuricemia diminished tubular injury after CCE as illustrated on PAS-stained kidney sections (Figure 27 and 28). To confirm this protective effect of hyperuricemic on tubular cells also *in vitro*, we pre-incubated HK2 cells in the presence or absence of soluble UA (10 mg/dL) for 1 hour prior to stimulation with 10 mM H<sub>2</sub>O<sub>2</sub> for 3 hours to induce oxidative stress. Intracellular UA levels and cell cytotoxicity were analyzed as mentioned in section 3.3.2 and 3.4.4. As shown in Figure 34A, intracellular UA levels significantly increased in HK2 cells when cultured in the presence of soluble UA compared with untreated cells. Depleting UA from the medium with rasburicase decreased the intracellular UA levels in H<sub>2</sub>O<sub>2</sub> treated HK2 cells (Figure 34A). Soluble UA and rasburicase had no cytotoxic effect in unstimulated HK2 cells (Figure 34B). Only stimulation with H<sub>2</sub>O<sub>2</sub> induced a significant increase in cytotoxicity as compared to unstimulated cells (Figure 34B). Interestingly, soluble UA inhibited the cytotoxic effect of H<sub>2</sub>O<sub>2</sub> in HK2 cells, while rasburicase reversed this effect, confirming that soluble UA and asymptomatic hyperuricemia protect tubular cells from cell death *in vitro* and tubular injury *in vivo*.

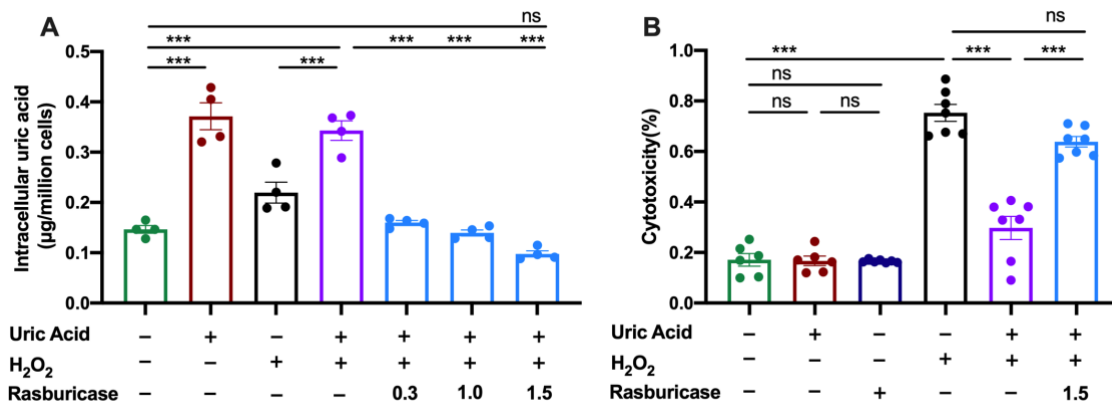


**Figure 34. Soluble UA protects HK2 cells from cell death during oxidative stress *in vitro*.** (A-B) HK2 cells were pre-incubated in presence or without soluble UA (10 mg/dL), and then rasburicase (0.3 mg/dL, 1 mg/dL and 1.5 mg/dL) was added to treatment groups 1 hour before 10 mM H<sub>2</sub>O<sub>2</sub> stimulation for 3 hours. (A) Intracellular uric acid in HK2 cells during oxidative stress in different groups (n = 4 per group). (B) HK2 cells cytotoxicity during oxidative stress in different conditons (n = 6 per group). All quantitative data are means ± SEM, ns = not significant, \*\*\* P < 0.001 by one-way ANOVA.

## 5. Discussion

### 5.1 Overview

In a new mouse model of CCE, we recently found that fibrin clots formed around obstructed peripheral arteries and cause ischemic tissue infarction, perilesional inflammation and organ failure [41]. However, the effect of metabolic disorders in CCE is currently unknown. The aim of this thesis was to investigate whether metabolic disorders such as T1D and asymptomatic hyperuricemia would impact on the outcomes of CC-induced AKI in mice. Our *in vivo* and *in vitro* data provide evidence that T1D and asymptomatic hyperuricemia altered kidney function, inflammation, occlusion and ischemic tissue infarction, albeit in different ways. While T1D worsens CC-induced AKI, asymptomatic hyperuricemia exhibited vasoactive and anti-inflammatory properties by reducing kidney infarct size and injury during the acute phase. These findings provide new insights in the pathomechanisms of immunothrombosis.

### 5.2 Type 1 diabetes worsens the outcomes in cholesterol crystal embolism

Using a mouse model of T1D with CCE, we showed for the first time that T1D contributes to a higher loss in GFR and a deteriorated pathology. Compared to the non-diabetic group (healthy control), mice with T1D had increased ischemic infarct lesions in the kidney and significantly more crystal clots in kidney arteries 24 hours after CCE. The number of Ly6B2+ leukocytes in the injured kidney and serum IL-6 levels increased 24 hours after CCE injury, suggesting that T1D drives leukocyte infiltration and exacerbates the inflammatory response to CC. Consistent with data from our group, fibrin positive crystal clots form inside the arteries after lodging of the CC emboli, while CC represent only a minor component of the crystal clot [41]. In fact, occlusion of kidney arteries occurs because of inflammation caused by crystals and the release of mediators from the surrounding injured tissue, which triggers immunothrombosis. Evidence suggested that hyperglycemia contributes to diffuse atherosclerosis and inflammatory immune cell infiltration including macrophages and neutrophils [175-177]. Especially advanced glycation endproducts can activate pro-inflammatory pathways by conjugating with its receptors on monocytes and macrophages [60]. Many inflammatory markers are increased during hyperglycemia such as IL-6, IL-1, TNF- $\alpha$  and C-reactive protein (CRP) in patients with diabetes [178, 179]. In addition, preclinical studies on SGLT2 inhibitors indicate a reduced

---

infarct size within one month after heart ischemia reperfusion and improved cardiac function during ischemic episodes [180]. A systematic review and meta-analysis showed that hyperglycemia increases infarct volume in middle cerebral artery occlusion models [181]. Consistent with this evidence diabetes exacerbates infarct size in tissue ischemia or occlusion primarily in the heart and brain [182, 183]. We now demonstrate that T1D has similar effects in CCE of the kidney, wherein T1D increases kidney infarct size leading to leukocyte infiltration and an exacerbated inflammatory response.

Kidney function, i.e., filtration in the glomerular compartment, depends on perfusion via the afferent glomerular arterioles. Due to the diffuse occluded kidney arteries and the large infarct areas after CCE, we believe that mice with T1D have more dysfunctional kidney nephrons compared to the non-diabetic control group. Indeed, the GFR decreased about 30% in T1D mice compared to mice without diabetes after CC-induced AKI. In fact, diabetes contributes to glomerular hyperfiltration during the early stage of the disease, for example the GFR was elevated by 10%–67% in patients with T1D and 6%–73% in patients with T2D, respectively [184]. Although we did not observe a difference in GFR between T1D and control mice before surgery, it is possibly that STZ injection might be toxic and causes side effects in mice [185] because we noted a reduced body weight in mice with T1D. Thus, in humans with early diabetic kidney damage, it is still necessary to have more clinical data on the changes of GFR before and after CCE. Nevertheless, the outcomes depend primarily on the area and size of occlusion caused by CCE.

Another factor that influences kidney function is the number of functional nephrons after kidney infarction. The decline in GFR after CCE was consistent with the degree of kidney injury in diabetic mice, indicating less functional nephrons compared to non-diabetic mice. Previous studies reported that impaired mitochondrial DNA, increased oxidative stress and increased reactive oxygen species (ROS) generation are characteristic features in DKD patients, and therefore more cell apoptosis and necrosis of tubular and glomerular cells occurs [186]. SGLT2 inhibition improves kidney injury and reduces proteinuria by protecting from oxidative stress [187]. *In vitro* studies indicate that a high glucose concentration of 30 mmol/L induces apoptotic cell death in HK2 cells via an increase in oxidative stress [188]. This is consistent with our *in vitro* and *in vivo* studies showing that high glucose concentrations further

---

aggravated CC-induced cell death in HK2 cells and that hyperglycemia drives tubular necrosis in CCE.

Endothelium dysfunction is a major cause of vascular complications in patients with T2D such as ophthalmopathy, diabetic foot syndrome and renal vasculopathy [189]. Indeed, our cultured GEnC experiments demonstrated that high glucose concentrations enhance CC-induced GEnC cell death compared with normoglycemic condition. Similar results were reported in human retinal endothelial cells treated with CC (2mg/mL) for 24 hours and in retinal endothelium of db/db mice at 6 months of age [190]. However, we now show that T1D had no effect on CD31 expression of endothelial cells. This could be due to differences in the animal model. For example, CCs primarily cause damage to the kidney arteries, which may diminish the effect of hyperglycemia on endothelial cells. However, further studies are needed address the contribution of T1D on endothelial cells in CC-induced AKI.

Platelets, leukocytes and endothelial cells are all involved in immunothrombosis. In patients with diabetes, blood tests that measure coagulation factors such as fibrinogen and activated partial thromboplastin show often elevated levels [191]. Particular in T2D patients with comorbidities such as cardiovascular complications and diabetic nephropathy often have abnormal clot formation [192]. Hyperglycemia can promote clotting by stimulating the release of circulating inflammatory mediators in endothelial and immune cells that either can indirectly activate platelets or directly activate ADP and collagen-related signals in platelets to promote coagulation [193, 194]. Consistent with our previous study, CC can trigger integrin  $\alpha\text{IIb}\beta\text{3}$  activation and increase the expression of P-selectin in platelets, and thus promoting platelet aggregation, which ultimately contributes to clot formation [41]. We observed similar effects when platelets were stimulated with a high glucose concentration *in vitro* (Figure 18). However, stimulating platelets with both high glucose concentration and CC further enhanced collagen-related platelet aggregation, CRP-related integrin  $\alpha\text{IIb}\beta\text{3}$  activation and P-selectin expression *in vitro*. Our *in vitro* data are consistent with the *in vivo* data demonstrating that diabetic mice have more occluded kidney arteries due to rapid platelet activation, which accelerates platelet adhesion, release of tissue factors from injured endothelial cells and the recruitment of immune cells such as neutrophils compared with non-diabetic mice after CCE. This process of intraarterial CC thrombosis ultimately worsens ischemic tissue infarction and perilesional inflammation under hyperglycemic conditions (Figure 35).

Hyperglycemia also contributes to alterations in the balance between vasodilation and vasoconstriction. Many patients with T2D suffer from cardiovascular diseases including hypertension [195]. Mechanistic studies suggest that hyperglycemia activates the renin-angiotensin-aldosterone system (RAAS), increases endothelin-1 expression but decreases NO production in the aorta of diabetic rats and in coronary microvessels in humans [196]. In addition, T2D can cause vasoconstriction in mouse arteries through the upregulation of *TMEM16A* mRNA [197]. Whether hyperglycemia, especially T1D, would induce vasoconstriction in CCE is currently unknown. We now found that T1D does not contribute to vasoconstriction in both the CC-injured and contralateral kidney in mice. Support for this comes from a study showing that rats with STZ-induced T1D were lacking signs of hypoxic pulmonary vasoconstriction [198]. Nevertheless, it is possible that T1D and T2D exhibit different effects on the vasculature and regulation of blood flow. Further studies are needed to address changes in vasodilation and vasoconstriction after CCE.

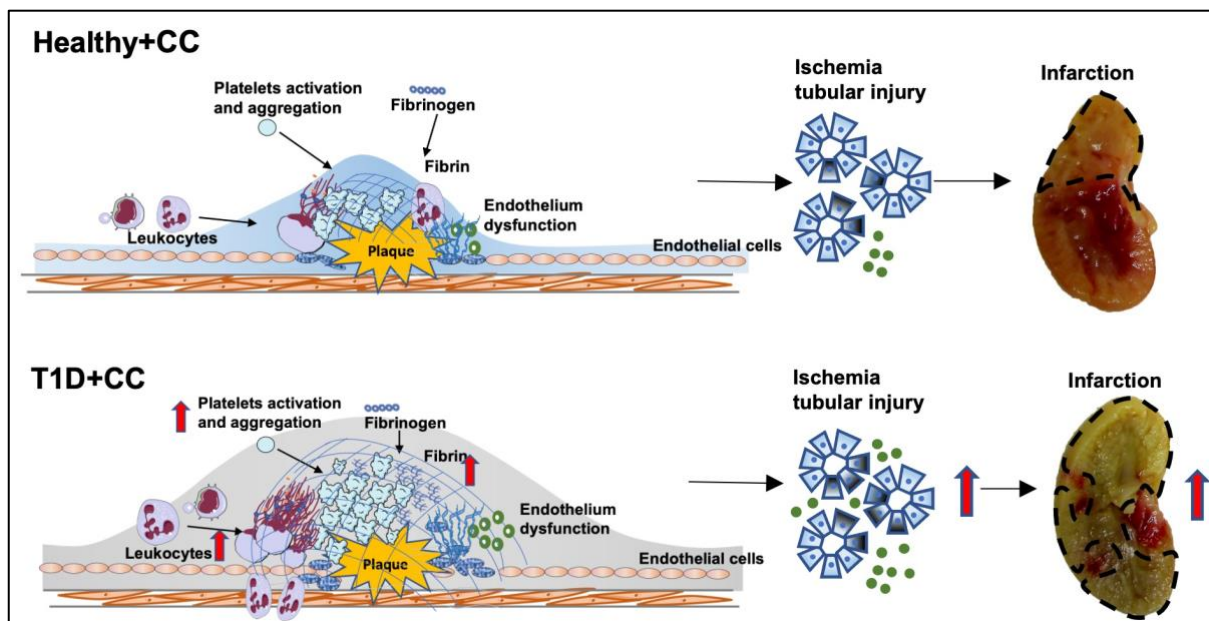


**Figure 35. Type 1 diabetes worsens the outcomes in cholesterol crystal embolism.** Hyperglycemia has more occlusion in the kidney arteries via increased platelet aggregation and activation, leukocyte accumulation and increased extracellular DNA. Increased ischemia tubular injury inducing infarction expands with obstruction in kidney arteries.

### 5.3 *Hyperuricemia has vasoactive effects in cholesterol crystal-induced acute kidney injury*

The focus of my second aim was to investigate whether asymptomatic hyperuricemia affects the outcomes after CC-induced AKI. Interestingly, the data implied that hyperuricemia contributes to a vast reduction in GFR upon CC-induced AKI but diminished kidney infarct size and tissue injury in mice suggesting a compensatory physiological mechanism of autoregulation to protect nephrons.

Evidence suggests that low serum UA levels (2-5 mg/dL) are associated with kidney vascular damage, vasoconstriction and tubulointerstitial injury in rats [199, 200]. We now found in a novel animal model of asymptomatic hyperuricemia with serum UA levels of 7-11 mg/dL [99] that hyperuricemia induced a rapid decline in GFR of more than 60% as compared to 30% in non-hyperuricemic mice after CC-induced kidney injury. This suggests that the strong GFR decline in hyperuricemic mice could be a consequence of vasoconstriction of the afferent arterioles of the non-injured nephrons in the CCE as well as the contralateral kidney. Indeed, the ratio of lumen versus artery area was significantly reduced in hyperuricemic compared with non-hyperuricemic mice upon CCE. Whether asymptomatic hyperuricemia is causally linked with cardiovascular diseases has been a matter of debate. Clinical studies suggest a strong association between hyperuricemia and hypertension. For example, longitudinal cohort studies showed that asymptomatic hyperuricemia without comorbidities predicts the development of hypertension [201]. Moreover, several randomized controlled trials reported that reducing hyperuricemia with allopurinol, a xanthine oxidase inhibitor, or probenecid, a uricosuric agent, reduced blood pressure in adolescents [202, 203]. In contrast, Preitner *et al.* found that low levels of serum UA (5 mg/dL) were not associated with hypertension in a mouse model of acute UA crystal-induced nephropathy [98] suggesting no direct role of hyperuricemia in the control of blood pressure. However, further studies are needed to investigate whether asymptomatic hyperuricemia related to vasoconstriction is associated with high blood pressure also in CCE.

Although asymptomatic hyperuricemia contributed to the strong decline in GFR, we observed that hyperuricemic mice had less ischemic tissue infarction and kidney injury without affecting the number of infiltrating Ly6B2<sup>+</sup> leukocytes and endothelial cell integrity compared with non-

hyperuricemic mice at day 1 after CC-induced AKI. One possible explanation could be that due to the vasoactive effect of hyperuricemia, the increased blood flow flushed smaller CC into arcuate and interlobular arteries of the kidney and therefore reduced the kidney infarct area (Figure 25). Another reason could be the anti-inflammatory and anti-oxidative effects of soluble UA and asymptomatic hyperuricemia. Recent *in vitro* and *in vivo* evidence suggests that soluble UA inhibits the pro-inflammatory function of monocytes and macrophages through the intracellular uptake of UA via urate transporters including SLC2A9/Glut9 and therefore diminishes acute injury and inflammation [103, 164]. In addition, asymptomatic hyperuricemia improves the recovery after acute organ injury, which is associated with a better tubular integrity by enhancing tubular mitochondrial dynamics (mitochondria fusion) [103]. Consistent with this, we found that soluble UA protects tubular epithelial cells from cell death by reducing oxidative stress-related cytotoxicity suggesting an anti-oxidative effect of soluble UA. In contrast, many *in vitro* and *in vivo* studies indicate pro-inflammatory functions of UA and hyperuricemia. For example, it was reported that UA increased the level of interleukin-1 $\beta$  and activated the NLRP3 inflammasome in murine macrophages, which occurred due to microcrystal contaminants in the UA preparation solution [139, 140, 204]. While UA microcrystals are known to trigger a pro-inflammatory response [205], a microcrystal-free UA solution prepared with sodium hydroxide and adjusted pH of 7 rather reveals immunomodulatory (anti-inflammatory) effects in human CD14<sup>+</sup> blood monocytes [164], which is in line with our data on HK2 cells. Consistent with other *in vivo* studies, asymptomatic hyperuricemia does not induce kidney injury [99, 141, 142] but rather promotes the recovery after AKI [103].

Several *in vitro* studies in 1970s showed that stimulating platelets with high concentrations of UA crystals triggers platelet activation [206-208]. In a recent clinical study the authors demonstrated that the concentration of serum UA could serve a negative predictor of platelet reactivity [174]. However, whether asymptomatic hyperuricemia or soluble UA have effects on platelet function and activity is currently unknown. We now show for the first time that asymptomatic hyperuricemia and soluble UA do not directly alter platelet aggregation,  $\alpha$ IIb $\beta$ 3 integrin activation and  $\alpha$ -granule degranulation in response to CC *in vitro* and may not directly affect platelet-mediated CC clot formation in mice. Thus, treating kidney disease-related hyperuricemia should have no effect on immunotrombosis.

From an evolutionary perspective, some evidence suggests that high serum UA levels facilitated humans to maintain blood pressure in ancient times when salt intake was low, body fat was needed to protect from the cold and/or fruit were not available [209]. Other studies reported that UA acts as an antioxidant to improve human survival in a low-oxygen environment such as the nervous system and in the kidney after acute ischemic injury [103, 143, 210]. Thus, the deletion of the uricase gene is favorably evolved in a hostile environment but causes metabolic abnormalities when humans have sufficient food and fat reserve capacity. Our results suggest that hyperuricemia contributes to a vast reduction in GFR due to vasoactive effects but diminished kidney infarct size and tissue injury in CC-induced AKI suggesting a compensatory physiological mechanism of autoregulation to protect nephrons. On the other hand, in patients with chronic kidney disease, hyperuricemia-related vasoconstriction might lead to increased arterial blood pressure, thus increasing the risk for cardiovascular complications.

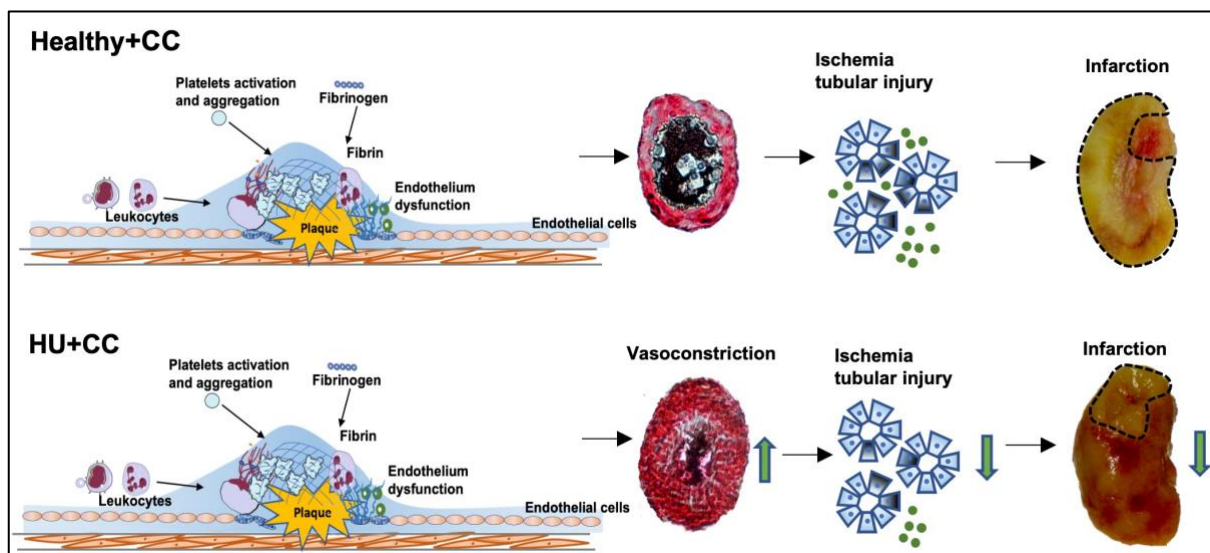


**Figure 36. Asymptomatic hyperuricemia affects the outcomes of cholesterol crystal-induced acute kidney injury.** Hyperuricemia does not affect either endothelial injury or alter platelet function, however, hyperuricemia exhibits vasoconstrictive effects in both contralateral and injured kidney together with a vast decline in GFR, as well as protects mice from ischemic tissue infarction via anti-oxidative effects on tubular epithelial cells after CC-induced AKI.

#### 5.4 Limitations of this study

One limitation of this project is that we manufactured a CCE-induced AKI model with CC injection into the kidney artery in mice, however, the synthetic CC might be different from the materials of detached atherosclerotic plaques. In aim 1, we observed only in STZ-induced T1D

mice but not in T2D mice such as db/db mice to detect hyperglycemia effects in CC-induced kidney injury. Regarding the phenotype, there may be changes between the different forms of diabetes. In addition, we did not collect data at later time points after CCE injury in T1D mice. For aim 2, we did not have enough serum to characterize the renin-angiotensin-aldosterone system and to collect more evidence for the vasoactive effects in HU mice. We also were not set-up to measure blood pressure. Therefore, whether the vasoconstrictive effects in HU mice were accompanied by systemic hypertension after CCE injury remains unknown.

### **5.5 Summary and Conclusion**

In summary, the research presented within this thesis focused on the role of hyperglycemia and asymptomatic hyperuricemia in CCE-induced AKI in mice. Our findings clearly demonstrated that metabolic disorders can differentially affect the outcomes after CCE-induced AKI. In particular ...

1. Hyperglycemia impaired kidney function in CCE as demonstrated by a decline in GFR, an increase in UACR levels and aggravated CC clot formation (platelet activation and aggregation), ischemic tissue infarction (accelerated death of renal tubular and endothelial cells) and perilesional inflammation (leukocyte infiltration).
2. In contrast, hyperuricemia exhibits vasoconstrictive effects in the contralateral and injured kidney as evidenced by a vast decline in GFR but protects mice from ischemic tissue infarction probably via anti-oxidative effects on tubular epithelial cells after CC-induced AKI suggesting a compensatory physiological mechanism of autoregulation to protect nephrons.

Taken together, our research provides new insights on metabolic comorbidities effects on kidney CCE and gives clinical suggestions that highly prevalent comorbidities independently contribute to the severity of AKI and the extent of kidney infarction in CCE. Diabetes is a risk factor for extended immunothrombosis and ischemic infarction, thus, control of hyperglycemia is essential to minimize these consequences. For hyperuricemia, the degree of acute kidney dysfunction may not fully reflect the severity of kidney injury. And due to the tissue protective effects of hyperuricemia, patients may better keep a high serum uric acid level to protect the tissue from CCE injury in advanced atherosclerosis.

## 6. References

1. Mulay, S.R. and H.J. Anders, *Crystallopathies*. N Engl J Med, 2016. **374**(25): p. 2465-76.
2. Paraskevas, K.I., et al., *Cholesterol crystal embolization: a possible complication of peripheral endovascular interventions*. J Endovasc Ther, 2008. **15**(5): p. 614-25.
3. Li, X., G. Bayliss, and S. Zhuang, *Cholesterol Crystal Embolism and Chronic Kidney Disease*. Int J Mol Sci, 2017. **18**(6).
4. Flory, C.M., *Arterial Occlusions Produced by Emboli from Eroded Aortic Atheromatous Plaques*. Am J Pathol, 1945. **21**(3): p. 549-65.
5. Scolari, F. and P. Ravani, *Atheroembolic renal disease*. Lancet, 2010. **375**(9726): p. 1650-60.
6. Tunick, P.A., et al., *Effect of treatment on the incidence of stroke and other emboli in 519 patients with severe thoracic aortic plaque*. Am J Cardiol, 2002. **90**(12): p. 1320-5.
7. Fukumoto, Y., et al., *The incidence and risk factors of cholesterol embolization syndrome, a complication of cardiac catheterization: a prospective study*. J Am Coll Cardiol, 2003. **42**(2): p. 211-6.
8. Carroccio, A., et al., *The role of aortic stent grafting in the treatment of atheromatous embolization syndrome: results after a mean of 15 months follow-up*. J Vasc Surg, 2004. **40**(3): p. 424-9.
9. Haas, M., et al., *Etiologies and outcome of acute renal insufficiency in older adults: a renal biopsy study of 259 cases*. Am J Kidney Dis, 2000. **35**(3): p. 433-47.
10. Scolari, F., et al., *The challenge of diagnosing atheroembolic renal disease: clinical features and prognostic factors*. Circulation, 2007. **116**(3): p. 298-304.
11. Fine, M.J., W. Kapoor, and V. Falanga, *Cholesterol crystal embolization: a review of 221 cases in the English literature*. Angiology, 1987. **38**(10): p. 769-84.
12. Belenfant, X., A. Meyrier, and C. Jacquot, *Supportive treatment improves survival in multivisceral cholesterol crystal embolism*. Am J Kidney Dis, 1999. **33**(5): p. 840-50.
13. Scolari, F., et al., *Cholesterol crystal embolism: A recognizable cause of renal disease*. Am J Kidney Dis, 2000. **36**(6): p. 1089-109.
14. Modi, K.S. and V.K. Rao, *Atheroembolic renal disease*. J Am Soc Nephrol, 2001. **12**(8): p. 1781-1787.
15. Goldman, M., et al., *Necrotising glomerulonephritis associated with cholesterol microemboli*. Br Med J (Clin Res Ed), 1985. **290**(6463): p. 205-6.
16. Granata, A., et al., *Atheroembolism renal disease: diagnosis and etiologic factors*. Clin Ter, 2012. **163**(4): p. 313-22.
17. Vidt, D.G., *Cholesterol emboli: a common cause of renal failure*. Annu Rev Med, 1997. **48**: p. 375-85.
18. Graff-Radford, J., C.J. Boes, and R.D. Brown, Jr., *History of Hollenhorst plaques*. Stroke, 2015. **46**(4): p. e82-4.
19. Thurlbeck, W.M. and B. Castleman, *Atheromatous emboli to the kidneys after aortic surgery*. N Engl J Med, 1957. **257**(10): p. 442-7.
20. Yudd M, L.F., *Disorders of renal arteries and veins: Atheroembolic Renal Disease*. Brenner B M. Brenner & Rector's the Kidney Disorder. 7 th, 2004. Elsevier: Saunders: p. 1580-1584.
21. AM., R., *Perforation of the jejunum: a complication of atheromatous embolisation*. Am J Gastroenterol, 1983. **78**: p. 77-82.
22. Kronzon, I. and M. Saric, *Cholesterol embolization syndrome*. Circulation, 2010. **122**(6): p. 631-41.
23. Quintart, C., et al., *Penile necrosis following cholesterol embolism*. Br J Urol, 1997. **80**(2): p. 347-8.
24. Sabatine, M.S., et al., *Pulmonary cholesterol crystal embolization*. Chest, 1997. **112**(6): p. 1687-92.

25. Jucgla, A., et al., *Cholesterol embolism: still an unrecognized entity with a high mortality rate.* J Am Acad Dermatol, 2006. **55**(5): p. 786-93.
26. Dickens, M.A., C.M. Greven, and M.M. Slusher, *Retinal-artery embolism after directional coronary atherectomy.* N Engl J Med, 1994. **331**(4): p. 278-9.
27. Kasinath, B.S. and E.J. Lewis, *Eosinophilia as a clue to the diagnosis of atheroembolic renal disease.* Arch Intern Med, 1987. **147**(8): p. 1384-5.
28. Cecioni, I., et al., *Eosinophilia in cholesterol atheroembolic disease.* J Allergy Clin Immunol, 2007. **120**(6): p. 1470-1; author reply 1471.
29. Mundi, S., et al., *Endothelial permeability, LDL deposition, and cardiovascular risk factors-a review.* Cardiovasc Res, 2018. **114**(1): p. 35-52.
30. Libby, P., et al., *Atherosclerosis.* Nat Rev Dis Primers, 2019. **5**(1): p. 56.
31. Boren, J. and K.J. Williams, *The central role of arterial retention of cholesterol-rich apolipoprotein-B-containing lipoproteins in the pathogenesis of atherosclerosis: a triumph of simplicity.* Curr Opin Lipidol, 2016. **27**(5): p. 473-83.
32. Llorente-Cortes, V., J. Martinez-Gonzalez, and L. Badimon, *LDL receptor-related protein mediates uptake of aggregated LDL in human vascular smooth muscle cells.* Arterioscler Thromb Vasc Biol, 2000. **20**(6): p. 1572-9.
33. Colin, S., G. Chinetti-Gbaguidi, and B. Staels, *Macrophage phenotypes in atherosclerosis.* Immunol Rev, 2014. **262**(1): p. 153-66.
34. Adamson, S. and N. Leitinger, *Phenotypic modulation of macrophages in response to plaque lipids.* Curr Opin Lipidol, 2011. **22**(5): p. 335-42.
35. Cybulsky, M.I. and M.A. Gimbrone, Jr., *Endothelial expression of a mononuclear leukocyte adhesion molecule during atherogenesis.* Science, 1991. **251**(4995): p. 788-91.
36. Li, H., et al., *An atherogenic diet rapidly induces VCAM-1, a cytokine-regulatable mononuclear leukocyte adhesion molecule, in rabbit aortic endothelium.* Arterioscler Thromb, 1993. **13**(2): p. 197-204.
37. Tonetti, M.S., et al., *Treatment of periodontitis and endothelial function.* N Engl J Med, 2007. **356**(9): p. 911-20.
38. Baena-Diez, J.M., et al., *Association between chronic immune-mediated inflammatory diseases and cardiovascular risk.* Heart, 2018. **104**(2): p. 119-126.
39. D'Aiuto, F., et al., *Systemic effects of periodontitis treatment in patients with type 2 diabetes: a 12 month, single-centre, investigator-masked, randomised trial.* Lancet Diabetes Endocrinol, 2018. **6**(12): p. 954-965.
40. D'Aiuto, F. and J.E. Deanfield, *Intensive periodontal therapy and type 2 diabetes - Authors' reply.* Lancet Diabetes Endocrinol, 2019. **7**(3): p. 175-176.
41. Shi, C., et al., *Crystal Clots as Therapeutic Target in Cholesterol Crystal Embolism.* Circ Res, 2020. **126**(8): p. e37-e52.
42. Ozaki, Y., et al., *Thin-cap fibroatheroma as high-risk plaque for microvascular obstruction in patients with acute coronary syndrome.* Circ Cardiovasc Imaging, 2011. **4**(6): p. 620-7.
43. Kessler, V., et al., *AAA Revisited: A Comprehensive Review of Risk Factors, Management, and Hallmarks of Pathogenesis.* Biomedicines, 2022. **10**(1).
44. Falanga, V., M.J. Fine, and W.N. Kapoor, *The cutaneous manifestations of cholesterol crystal embolization.* Arch Dermatol, 1986. **122**(10): p. 1194-8.
45. Gore, I., H.L. McCombs, and R.L. Lindquist, *Observations on the Fate of Cholesterol Emboli.* J Atheroscler Res, 1964. **4**: p. 527-35.
46. Kronzon, I. and P.A. Tunick, *Aortic atherosclerotic disease and stroke.* Circulation, 2006. **114**(1): p. 63-75.
47. Lyaker, M.R., et al., *Arterial embolism.* Int J Crit Illn Inj Sci, 2013. **3**(1): p. 77-87.
48. Pilely, K., et al., *Cholesterol Crystals Activate the Lectin Complement Pathway via Ficolin-2 and Mannose-Binding Lectin: Implications for the Progression of Atherosclerosis.* J Immunol, 2016. **196**(12): p. 5064-74.
49. Agnes B. Fogo, M.K., *Diagnostic atlas of renal pathology.* 3 ed. 2017. P359.

50. Eckel, R.H., S.M. Grundy, and P.Z. Zimmet, *The metabolic syndrome*. Lancet, 2005. **365**(9468): p. 1415-28.
51. Saltiel, A.R., *Insulin signaling in health and disease*. J Clin Invest, 2021. **131**(1).
52. E., K., *Hypertonie-Hyperglykämie-Hyperurikämiesyndrome*. Zentralblatt für innere Medizin, 1923. **44**.
53. Ranasinghe, P., et al., *Prevalence and trends of metabolic syndrome among adults in the asia-pacific region: a systematic review*. BMC Public Health, 2017. **17**(1): p. 101.
54. do Vale Moreira, N.C., et al., *Prevalence of Metabolic Syndrome by different definitions, and its association with type 2 diabetes, pre-diabetes, and cardiovascular disease risk in Brazil*. Diabetes Metab Syndr, 2020. **14**(5): p. 1217-1224.
55. Qiao, Q., et al., *Metabolic syndrome and cardiovascular disease*. Ann Clin Biochem, 2007. **44**(Pt 3): p. 232-63.
56. Mottillo, S., et al., *The metabolic syndrome and cardiovascular risk a systematic review and meta-analysis*. J Am Coll Cardiol, 2010. **56**(14): p. 1113-32.
57. Cankurtaran, M., et al., *Prevalence and correlates of metabolic syndrome (MS) in older adults*. Arch Gerontol Geriatr, 2006. **42**(1): p. 35-45.
58. Belete, R., et al., *Global prevalence of metabolic syndrome among patients with type 1 diabetes mellitus: a systematic review and meta-analysis*. Diabetol Metab Syndr, 2021. **13**(1): p. 25.
59. ; Available from: [https://www.who.int/health-topics/diabetes#tab=tab\\_1](https://www.who.int/health-topics/diabetes#tab=tab_1).
60. Poznyak, A., et al., *The Diabetes Mellitus-Atherosclerosis Connection: The Role of Lipid and Glucose Metabolism and Chronic Inflammation*. Int J Mol Sci, 2020. **21**(5).
61. Beckman, J.A., M.A. Creager, and P. Libby, *Diabetes and atherosclerosis: epidemiology, pathophysiology, and management*. JAMA, 2002. **287**(19): p. 2570-81.
62. Dahl-Jorgensen, K., J.R. Larsen, and K.F. Hanssen, *Atherosclerosis in childhood and adolescent type 1 diabetes: early disease, early treatment?* Diabetologia, 2005. **48**(8): p. 1445-53.
63. Diabetes, C., I. Complications Trial /Epidemiology of Diabetes, and G. Complications Study Research, *Intensive Diabetes Treatment and Cardiovascular Outcomes in Type 1 Diabetes: The DCCT/EDIC Study 30-Year Follow-up*. Diabetes Care, 2016. **39**(5): p. 686-93.
64. Summerhill, V.I., et al., *The Atherogenic Role of Circulating Modified Lipids in Atherosclerosis*. Int J Mol Sci, 2019. **20**(14).
65. Berneis, K.K. and R.M. Krauss, *Metabolic origins and clinical significance of LDL heterogeneity*. J Lipid Res, 2002. **43**(9): p. 1363-79.
66. Hagensen, M.K., et al., *Increased retention of LDL from type 1 diabetic patients in atherosclerosis-prone areas of the murine arterial wall*. Atherosclerosis, 2019. **286**: p. 156-162.
67. Albers, J.J., et al., *Prevalence and determinants of elevated apolipoprotein B and dense low-density lipoprotein in youths with type 1 and type 2 diabetes*. J Clin Endocrinol Metab, 2008. **93**(3): p. 735-42.
68. Vaidyula, V.R., et al., *Effects of hyperglycemia and hyperinsulinemia on circulating tissue factor procoagulant activity and platelet CD40 ligand*. Diabetes, 2006. **55**(1): p. 202-8.
69. Vaidyula, V.R., G. Boden, and A.K. Rao, *Platelet and monocyte activation by hyperglycemia and hyperinsulinemia in healthy subjects*. Platelets, 2006. **17**(8): p. 577-85.
70. Assert, R., et al., *Regulation of protein kinase C by short term hyperglycaemia in human platelets in vivo and in vitro*. Diabetologia, 2001. **44**(2): p. 188-95.
71. Winocour, P.D., et al., *Decreased platelet membrane fluidity due to glycation or acetylation of membrane proteins*. Thromb Haemost, 1992. **68**(5): p. 577-82.
72. Yngen, M., et al., *Enhanced P-selectin expression and increased soluble CD40 Ligand in patients with Type 1 diabetes mellitus and microangiopathy: evidence for platelet hyperactivity and chronic inflammation*. Diabetologia, 2004. **47**(3): p. 537-540.
73. Han, X., et al., *Sexual dimorphism in rat aortic endothelial function of streptozotocin-induced diabetes: possible involvement of superoxide and nitric oxide production*. Eur J Pharmacol, 2014. **723**: p. 442-50.
74. Zhou, H., X. Zhang, and J. Lu, *Progress on diabetic cerebrovascular diseases*. Bosn J Basic Med Sci, 2014. **14**(4): p. 185-90.

75. Otter, W., et al., *Hospital outcome of acute myocardial infarction in patients with and without diabetes mellitus*. *Diabet Med*, 2004. **21**(2): p. 183-7.
76. Booth, G.L., et al., *Relation between age and cardiovascular disease in men and women with diabetes compared with non-diabetic people: a population-based retrospective cohort study*. *Lancet*, 2006. **368**(9529): p. 29-36.
77. Banerjee, C., et al., *Duration of diabetes and risk of ischemic stroke: the Northern Manhattan Study*. *Stroke*, 2012. **43**(5): p. 1212-7.
78. Piccoli, G.B., et al., *Cholesterol emboli syndrome in type 2 diabetes: the disease history of a case evaluated with renal scintigraphy*. *Rev Diabet Stud*, 2005. **2**(2): p. 92-6.
79. Sandra S, H.D., McFarland; Nina, Bornemann; Cristiano P, Vieira; George, Abela; Maria B, Grant; Julia, Busik, *Cholesterol crystals promote diabetic retinopathy (DR) pathology*. *Investigative ophthalmology & visual science*, 2020. **63**(2): p. 1771a.
80. Patschan, D. and G.A. Muller, *Acute Kidney Injury in Diabetes Mellitus*. *Int J Nephrol*, 2016. **2016**: p. 6232909.
81. Hapca, S., et al., *The Relationship between AKI and CKD in Patients with Type 2 Diabetes: An Observational Cohort Study*. *J Am Soc Nephrol*, 2021. **32**(1): p. 138-150.
82. James, M.T., et al., *A Meta-analysis of the Association of Estimated GFR, Albuminuria, Diabetes Mellitus, and Hypertension With Acute Kidney Injury*. *Am J Kidney Dis*, 2015. **66**(4): p. 602-12.
83. Ahmad, A.A., S.O. Draves, and M. Rosca, *Mitochondria in Diabetic Kidney Disease*. *Cells*, 2021. **10**(11).
84. Ziyadeh, F.N., et al., *Effect of myo-inositol on cell proliferation and collagen transcription and secretion in proximal tubule cells cultured in elevated glucose*. *J Am Soc Nephrol*, 1991. **1**(11): p. 1220-9.
85. Cai, T., et al., *Sodium-glucose cotransporter 2 inhibition suppresses HIF-1alpha-mediated metabolic switch from lipid oxidation to glycolysis in kidney tubule cells of diabetic mice*. *Cell Death Dis*, 2020. **11**(5): p. 390.
86. Gorelik, Y., et al., *Hyperglycemia on Admission Predicts Acute Kidney Failure and Renal Functional Recovery among Inpatients*. *J Clin Med*, 2021. **11**(1).
87. Ougaard, M.E., et al., *Inhibitors of the renin-angiotensin system ameliorates clinical and pathological aspects of experimentally induced nephrotoxic serum nephritis*. *Ren Fail*, 2018. **40**(1): p. 640-648.
88. Nadkarni, G.N., et al., *Acute Kidney Injury in Patients on SGLT2 Inhibitors: A Propensity-Matched Analysis*. *Diabetes Care*, 2017. **40**(11): p. 1479-1485.
89. Hsiao, C.Y., et al., *Risk Factors for Development of Acute Kidney Injury in Patients with Urinary Tract Infection*. *PLoS One*, 2015. **10**(7): p. e0133835.
90. Mallat, S.G., et al., *Hyperuricemia, Hypertension, and Chronic Kidney Disease: an Emerging Association*. *Curr Hypertens Rep*, 2016. **18**(10): p. 74.
91. Song, M., et al., *Longitudinal association between serum uric acid levels and multiterritorial atherosclerosis*. *J Cell Mol Med*, 2019. **23**(8): p. 4970-4979.
92. Krishnan, E., et al., *Hyperuricemia and the risk for subclinical coronary atherosclerosis--data from a prospective observational cohort study*. *Arthritis Res Ther*, 2011. **13**(2): p. R66.
93. Hou, Y.L., et al., *Hypertriglyceridemia and hyperuricemia: a retrospective study of urban residents*. *Lipids Health Dis*, 2019. **18**(1): p. 81.
94. Peng, T.C., et al., *Relationship between hyperuricemia and lipid profiles in US adults*. *Biomed Res Int*, 2015. **2015**: p. 127596.
95. Binh, T.Q., et al., *First Report on Association of Hyperuricemia with Type 2 Diabetes in a Vietnamese Population*. *Int J Endocrinol*, 2019. **2019**: p. 5275071.
96. Kim, H., et al., *Asymptomatic hyperuricemia is independently associated with coronary artery calcification in the absence of overt coronary artery disease: A single-center cross-sectional study*. *Medicine (Baltimore)*, 2017. **96**(14): p. e6565.
97. DeBosch, B.J., et al., *Early-onset metabolic syndrome in mice lacking the intestinal uric acid transporter SLC2A9*. *Nat Commun*, 2014. **5**: p. 4642.

98. Preitner, F., et al., *No development of hypertension in the hyperuricemic liver-Glut9 knockout mouse*. *Kidney Int*, 2015. **87**(5): p. 940-7.
99. Sellmayr, M., et al., *Only Hyperuricemia with Crystalluria, but not Asymptomatic Hyperuricemia, Drives Progression of Chronic Kidney Disease*. *J Am Soc Nephrol*, 2020. **31**(12): p. 2773-2792.
100. Badve, S.V., et al., *Effects of Allopurinol on the Progression of Chronic Kidney Disease*. *N Engl J Med*, 2020. **382**(26): p. 2504-2513.
101. Afkarian, M., et al., *Preventing Early Renal Loss in Diabetes (PERL) Study: A Randomized Double-Blinded Trial of Allopurinol-Rationale, Design, and Baseline Data*. *Diabetes Care*, 2019. **42**(8): p. 1454-1463.
102. Steiger, S., Q. Ma, and H.J. Anders, *The case for evidence-based medicine for the association between hyperuricaemia and CKD*. *Nat Rev Nephrol*, 2020. **16**(7): p. 422.
103. Gnemmi V, L.Q., Ma Q,; De Chiara L,; Carangelo G,; Li C, Molina-Van den Bosch M,; Romagnani P,; Anders H-J,; Steiger S., *Asymptomatic Hyperuricemia Promotes Recovery from Ischemic Organ Injury by Modulating the Phenotype of Macrophages*. *Cells*, 2022. **11**: p. 646.
104. Anders, H.J., *Four danger response programs determine glomerular and tubulointerstitial kidney pathology: clotting, inflammation, epithelial and mesenchymal healing*. *Organogenesis*, 2012. **8**(2): p. 29-40.
105. Antonioli, L., et al., *CD39 and CD73 in immunity and inflammation*. *Trends Mol Med*, 2013. **19**(6): p. 355-67.
106. Sang, Y., et al., *Interplay between platelets and coagulation*. *Blood Rev*, 2021. **46**: p. 100733.
107. Varga-Szabo, D., I. Pleines, and B. Nieswandt, *Cell adhesion mechanisms in platelets*. *Arterioscler Thromb Vasc Biol*, 2008. **28**(3): p. 403-12.
108. Yun, S.H., et al., *Platelet Activation: The Mechanisms and Potential Biomarkers*. *Biomed Res Int*, 2016. **2016**: p. 9060143.
109. Campbell, R.A., et al., *Clots Are Potent Triggers of Inflammatory Cell Gene Expression: Indications for Timely Fibrinolysis*. *Arterioscler Thromb Vasc Biol*, 2017. **37**(10): p. 1819-1827.
110. Esmon, C.T., J. Xu, and F. Lupu, *Innate immunity and coagulation*. *J Thromb Haemost*, 2011. **9 Suppl 1**: p. 182-8.
111. Shi, C., et al., *Extracellular DNA-A Danger Signal Triggering Immunothrombosis*. *Front Immunol*, 2020. **11**: p. 568513.
112. Koupenova, M., et al., *Circulating Platelets as Mediators of Immunity, Inflammation, and Thrombosis*. *Circ Res*, 2018. **122**(2): p. 337-351.
113. Schmidt, E.P., et al., *On, around, and through: neutrophil-endothelial interactions in innate immunity*. *Physiology (Bethesda)*, 2011. **26**(5): p. 334-47.
114. Leppanen, A., et al., *Binding of glycosulfopeptides to P-selectin requires stereospecific contributions of individual tyrosine sulfate and sugar residues*. *J Biol Chem*, 2000. **275**(50): p. 39569-78.
115. Pervushina, O., et al., *Platelet factor 4/CXCL4 induces phagocytosis and the generation of reactive oxygen metabolites in mononuclear phagocytes independently of Gi protein activation or intracellular calcium transients*. *J Immunol*, 2004. **173**(3): p. 2060-7.
116. Smith, D.F., et al., *GRO family chemokines are specialized for monocyte arrest from flow*. *Am J Physiol Heart Circ Physiol*, 2005. **289**(5): p. H1976-84.
117. Ward, P.A., et al., *Regulatory effects of adenosine and adenine nucleotides on oxygen radical responses of neutrophils*. *Lab Invest*, 1988. **58**(4): p. 438-47.
118. Di Virgilio, F., P.A. Borea, and P. Illes, *P2 receptors meet the immune system*. *Trends Pharmacol Sci*, 2001. **22**(1): p. 5-7.
119. Papayannopoulos, V., *Neutrophil extracellular traps in immunity and disease*. *Nat Rev Immunol*, 2018. **18**(2): p. 134-147.
120. Castanheira, F.V.S. and P. Kubes, *Neutrophils and NETs in modulating acute and chronic inflammation*. *Blood*, 2019. **133**(20): p. 2178-2185.
121. Martinod, K. and D.D. Wagner, *Thrombosis: tangled up in NETs*. *Blood*, 2014. **123**(18): p. 2768-76.

122. Caudrillier, A., et al., *Platelets induce neutrophil extracellular traps in transfusion-related acute lung injury*. J Clin Invest, 2012. **122**(7): p. 2661-71.
123. Saleh, J., et al., *Mitochondria and microbiota dysfunction in COVID-19 pathogenesis*. Mitochondrion, 2020. **54**: p. 1-7.
124. Watson, B.D., et al., *Induction of reproducible brain infarction by photochemically initiated thrombosis*. Ann Neurol, 1985. **17**(5): p. 497-504.
125. Dietrich, W.D., et al., *Photochemically induced cerebral infarction. I. Early microvascular alterations*. Acta Neuropathol, 1987. **72**(4): p. 315-25.
126. Lu, H., et al., *Induction and imaging of photothrombotic stroke in conscious and freely moving rats*. J Biomed Opt, 2014. **19**(9): p. 96013.
127. Wu, J. and L.J. Yan, *Streptozotocin-induced type 1 diabetes in rodents as a model for studying mitochondrial mechanisms of diabetic beta cell glucotoxicity*. Diabetes Metab Syndr Obes, 2015. **8**: p. 181-8.
128. Kilic, E., D.M. Hermann, and K.A. Hossmann, *A reproducible model of thromboembolic stroke in mice*. Neuroreport, 1998. **9**(13): p. 2967-70.
129. Hara, T., G. Mies, and K.A. Hossmann, *Effect of thrombolysis on the dynamics of infarct evolution after clot embolism of middle cerebral artery in mice*. J Cereb Blood Flow Metab, 2000. **20**(10): p. 1483-91.
130. Kilic, E., D.M. Hermann, and K.A. Hossmann, *Recombinant tissue-plasminogen activator-induced thrombolysis after cerebral thromboembolism in mice*. Acta Neuropathol, 2000. **99**(3): p. 219-22.
131. Orset, C., et al., *Mouse model of in situ thromboembolic stroke and reperfusion*. Stroke, 2007. **38**(10): p. 2771-8.
132. Miyake, K., S. Takeo, and H. Kaijihar, *Sustained decrease in brain regional blood flow after microsphere embolism in rats*. Stroke, 1993. **24**(3): p. 415-20.
133. Lu, J., et al., *Mouse models for human hyperuricaemia: a critical review*. Nat Rev Rheumatol, 2019. **15**(7): p. 413-426.
134. Wang, M.X., et al., *Nuciferine restores potassium oxonate-induced hyperuricemia and kidney inflammation in mice*. Eur J Pharmacol, 2015. **747**: p. 59-70.
135. Liu, Y.L., et al., *Betaine reduces serum uric acid levels and improves kidney function in hyperuricemic mice*. Planta Med, 2014. **80**(1): p. 39-47.
136. Yong, T., et al., *Actions of water extract from Cordyceps militaris in hyperuricemic mice induced by potassium oxonate combined with hypoxanthine*. J Ethnopharmacol, 2016. **194**: p. 403-411.
137. Li, J.M., et al., *Protective effects of cortex fraxini coumarines against oxonate-induced hyperuricemia and renal dysfunction in mice*. Eur J Pharmacol, 2011. **666**(1-3): p. 196-204.
138. Hu, Q.H., et al., *Quercetin regulates organic ion transporter and uromodulin expression and improves renal function in hyperuricemic mice*. Eur J Nutr, 2012. **51**(5): p. 593-606.
139. Braga, T.T., et al., *Soluble Uric Acid Activates the NLRP3 Inflammasome*. Sci Rep, 2017. **7**: p. 39884.
140. Kim, S.M., et al., *Hyperuricemia-induced NLRP3 activation of macrophages contributes to the progression of diabetic nephropathy*. Am J Physiol Renal Physiol, 2015. **308**(9): p. F993-F1003.
141. Wu, X., et al., *Hyperuricemia and urate nephropathy in urate oxidase-deficient mice*. Proc Natl Acad Sci U S A, 1994. **91**(2): p. 742-6.
142. Lu, J., et al., *Knockout of the urate oxidase gene provides a stable mouse model of hyperuricemia associated with metabolic disorders*. Kidney Int, 2018. **93**(1): p. 69-80.
143. Ichida, K., et al., *Decreased extra-renal urate excretion is a common cause of hyperuricemia*. Nat Commun, 2012. **3**: p. 764.
144. Preitner, F., et al., *Glut9 is a major regulator of urate homeostasis and its genetic inactivation induces hyperuricosuria and urate nephropathy*. Proc Natl Acad Sci U S A, 2009. **106**(36): p. 15501-6.
145. Preitner, F., et al., *Urate-induced acute renal failure and chronic inflammation in liver-specific Glut9 knockout mice*. Am J Physiol Renal Physiol, 2013. **305**(5): p. F786-95.

146. Hervey, G.R., *The effects of lesions in the hypothalamus in parabiotic rats*. J Physiol, 1959. **145**(2): p. 336-52.
147. Coleman, D.L. and K.P. Hummel, *Effects of parabiosis of normal with genetically diabetic mice*. Am J Physiol, 1969. **217**(5): p. 1298-304.
148. Coleman, D.L., *Effects of parabiosis of obese with diabetes and normal mice*. Diabetologia, 1973. **9**(4): p. 294-8.
149. Coleman, D.L., *Obese and diabetes: two mutant genes causing diabetes-obesity syndromes in mice*. Diabetologia, 1978. **14**(3): p. 141-8.
150. Maffei, M., et al., *Leptin levels in human and rodent: measurement of plasma leptin and ob RNA in obese and weight-reduced subjects*. Nat Med, 1995. **1**(11): p. 1155-61.
151. Alpers, C.E. and K.L. Hudkins, *Mouse models of diabetic nephropathy*. Curr Opin Nephrol Hypertens, 2011. **20**(3): p. 278-84.
152. Qi, Z., et al., *Characterization of susceptibility of inbred mouse strains to diabetic nephropathy*. Diabetes, 2005. **54**(9): p. 2628-37.
153. Furman, B.L., *Streptozotocin-Induced Diabetic Models in Mice and Rats*. Curr Protoc Pharmacol, 2015. **70**: p. 5 47 1-5 47 20.
154. Soler, M.J., et al., *ACE2 inhibition worsens glomerular injury in association with increased ACE expression in streptozotocin-induced diabetic mice*. Kidney Int, 2007. **72**(5): p. 614-23.
155. DeFronzo, R.A., et al., *Type 2 diabetes mellitus*. Nat Rev Dis Primers, 2015. **1**: p. 15019.
156. Forbes, J.M. and M.E. Cooper, *Mechanisms of diabetic complications*. Physiol Rev, 2013. **93**(1): p. 137-88.
157. Ghanem, F., et al., *Cholesterol crystal embolization following plaque rupture: a systemic disease with unusual features*. J Biomed Res, 2017. **31**(2): p. 82-94.
158. Percie du Sert, N., et al., *Reporting animal research: Explanation and elaboration for the ARRIVE guidelines 2.0*. PLOS Biology, 2020. **18**(7): p. e3000411.
159. Motrapu, M., et al., *Drug Testing for Residual Progression of Diabetic Kidney Disease in Mice Beyond Therapy with Metformin, Ramipril, and Empagliflozin*. J Am Soc Nephrol, 2020. **31**(8): p. 1729-1745.
160. Schreiber, A., et al., *Transcutaneous measurement of renal function in conscious mice*. Am J Physiol Renal Physiol, 2012. **303**(5): p. F783-8.
161. Lei, Y., et al., *A multicenter blinded preclinical randomized controlled trial on Jak1/2 inhibition in MRL/MpJ-Fas(lpr) mice with proliferative lupus nephritis predicts low effect size*. Kidney Int, 2021. **99**(6): p. 1331-1341.
162. Ma, Q., *The Effects of Hyperuricemia on Sterile Inflammation during Chronic Kidney Disease*. 2019, Ludwig-Maximilians-Universität.
163. Yeap, X.Y., et al., *Quantitation of acute necrosis after experimental myocardial infarction*. Methods Mol Biol, 2013. **1004**: p. 115-33.
164. Ma, Q., et al., *Soluble Uric Acid Is an Intrinsic Negative Regulator of Monocyte Activation in Monosodium Urate Crystal-Induced Tissue Inflammation*. J Immunol, 2020. **205**(3): p. 789-800.
165. Tang, W.H., et al., *Glucose and collagen regulate human platelet activity through aldose reductase induction of thromboxane*. J Clin Invest, 2011. **121**(11): p. 4462-76.
166. Naqvi, M.Z.S.N.-u.-H., *Effects of STZ-Induced Diabetes on the Relative Weights of Kidney, Liver and Pancreas in Albino Rats: A Comparative Study*. International Journal of Morphology, 2010. **28**(1): p. 135-142.
167. Benedek, A., et al., *Use of TTC staining for the evaluation of tissue injury in the early phases of reperfusion after focal cerebral ischemia in rats*. Brain Res, 2006. **1116**(1): p. 159-65.
168. Rask-Madsen, C. and G.L. King, *Vascular complications of diabetes: mechanisms of injury and protective factors*. Cell Metab, 2013. **17**(1): p. 20-33.
169. Deng, M., et al., *Metformin and Vascular Diseases: A Focused Review on Smooth Muscle Cell Function*. Front Pharmacol, 2020. **11**: p. 635.
170. Bautista-Becerril, B., et al., *Immunothrombosis in COVID-19: Implications of Neutrophil Extracellular Traps*. Biomolecules, 2021. **11**(5).

171. Nakazawa, D., et al., *Histones and Neutrophil Extracellular Traps Enhance Tubular Necrosis and Remote Organ Injury in Ischemic AKI*. J Am Soc Nephrol, 2017. **28**(6): p. 1753-1768.
172. Fidler, T.P., et al., *Deletion of GLUT1 and GLUT3 Reveals Multiple Roles for Glucose Metabolism in Platelet and Megakaryocyte Function*. Cell Rep, 2017. **20**(4): p. 881-894.
173. Shechter, M., et al., *Blood glucose and platelet-dependent thrombosis in patients with coronary artery disease*. J Am Coll Cardiol, 2000. **35**(2): p. 300-7.
174. Karolczak, K., et al., *Platelet and Red Blood Cell Counts, as well as the Concentrations of Uric Acid, but Not Homocysteinaemia or Oxidative Stress, Contribute Mostly to Platelet Reactivity in Older Adults*. Oxid Med Cell Longev, 2019. **2019**: p. 9467562.
175. Matuschik, L., et al., *Hyperglycemia Induces Inflammatory Response of Human Macrophages to CD163-Mediated Scavenging of Hemoglobin-Haptoglobin Complexes*. Int J Mol Sci, 2022. **23**(3).
176. Kanter, J.E., et al., *Diabetes promotes an inflammatory macrophage phenotype and atherosclerosis through acyl-CoA synthetase 1*. Proc Natl Acad Sci U S A, 2012. **109**(12): p. E715-24.
177. Josefs, T., et al., *Neutrophil extracellular traps promote macrophage inflammation and impair atherosclerosis resolution in diabetic mice*. JCI Insight, 2020. **5**(7).
178. Dogan, Y., et al., *Serum IL-1beta, IL-2, and IL-6 in insulin-dependent diabetic children*. Mediators Inflamm, 2006. **2006**(1): p. 59206.
179. Bashir, H., et al., *Role of inflammatory mediators (TNF-alpha, IL-6, CRP), biochemical and hematological parameters in type 2 diabetes mellitus patients of Kashmir, India*. Med J Islam Repub Iran, 2020. **34**: p. 5.
180. Andreadou, I., et al., *SGLT2 inhibitors reduce infarct size in reperfused ischemic heart and improve cardiac function during ischemic episodes in preclinical models*. Biochim Biophys Acta Mol Basis Dis, 2020. **1866**(7): p. 165770.
181. MacDougall, N.J. and K.W. Muir, *Hyperglycaemia and infarct size in animal models of middle cerebral artery occlusion: systematic review and meta-analysis*. J Cereb Blood Flow Metab, 2011. **31**(3): p. 807-18.
182. Izumi, Y., et al., *Insulin protects brain tissue against focal ischemia in rats*. Neurosci Lett, 1992. **144**(1-2): p. 121-3.
183. Miki, T., et al., *Effects of diabetes on myocardial infarct size and cardioprotection by preconditioning and postconditioning*. Cardiovasc Diabetol, 2012. **11**: p. 67.
184. Tonneijck, L., et al., *Glomerular Hyperfiltration in Diabetes: Mechanisms, Clinical Significance, and Treatment*. J Am Soc Nephrol, 2017. **28**(4): p. 1023-1039.
185. Noshahr, Z.S., et al., *Animal Models of Diabetes-Associated Renal Injury*. J Diabetes Res, 2020. **2020**: p. 9416419.
186. Jiang, H., et al., *The Mitochondria-Targeted Metabolic Tubular Injury in Diabetic Kidney Disease*. Cell Physiol Biochem, 2019. **52**(2): p. 156-171.
187. Tanaka, S., et al., *Sodium-glucose cotransporter 2 inhibition normalizes glucose metabolism and suppresses oxidative stress in the kidneys of diabetic mice*. Kidney Int, 2018. **94**(5): p. 912-925.
188. Verzola, D., et al., *Oxidative stress mediates apoptotic changes induced by hyperglycemia in human tubular kidney cells*. J Am Soc Nephrol, 2004. **15 Suppl 1**: p. S85-7.
189. Dhananjayan, R., et al., *Endothelial Dysfunction in Type 2 Diabetes Mellitus*. Indian J Clin Biochem, 2016. **31**(4): p. 372-9.
190. Hammer, S.S., et al., *Statins and  $\alpha$  cyclodextrin treatments prevent cholesterol crystal-induced pathology in human retinal endothelial cells and in db/db mice*. Investigative Ophthalmology & Visual Science, 2021. **62**(8): p. 2928-2928.
191. Zhao, Y., et al., *Diabetes mellitus is associated with shortened activated partial thromboplastin time and increased fibrinogen values*. PLoS One, 2011. **6**(1): p. e16470.
192. Alzahrani, S.H. and R.A. Ajjan, *Coagulation and fibrinolysis in diabetes*. Diab Vasc Dis Res, 2010. **7**(4): p. 260-73.

- 
193. Kaur, R., M. Kaur, and J. Singh, *Endothelial dysfunction and platelet hyperactivity in type 2 diabetes mellitus: molecular insights and therapeutic strategies*. Cardiovasc Diabetol, 2018. **17**(1): p. 121.
194. Pretorius, E., *Platelets as Potent Signaling Entities in Type 2 Diabetes Mellitus*. Trends Endocrinol Metab, 2019. **30**(8): p. 532-545.
195. Petrie, J.R., T.J. Guzik, and R.M. Touyz, *Diabetes, Hypertension, and Cardiovascular Disease: Clinical Insights and Vascular Mechanisms*. Can J Cardiol, 2018. **34**(5): p. 575-584.
196. Derosa, G. and P. Maffioli, *A review about biomarkers for the investigation of vascular function and impairment in diabetes mellitus*. Vasc Health Risk Manag, 2016. **12**: p. 415-419.
197. Leo, M.D., et al., *TMEM16A channel upregulation in arterial smooth muscle cells produces vasoconstriction during diabetes*. Am J Physiol Heart Circ Physiol, 2021. **320**(3): p. H1089-H1101.
198. Soloviev, A., et al., *Hypoxic pulmonary vasoconstriction is lacking in rats with type 1 diabetes*. Clin Exp Pharmacol Physiol, 2019. **46**(11): p. 1022-1029.
199. Sanchez-Lozada, L.G., et al., *Hemodynamics of hyperuricemia*. Semin Nephrol, 2005. **25**(1): p. 19-24.
200. Sanchez-Lozada, L.G., et al., *Mild hyperuricemia induces vasoconstriction and maintains glomerular hypertension in normal and remnant kidney rats*. Kidney Int, 2005. **67**(1): p. 237-47.
201. Kuwabara, M., et al., *Asymptomatic Hyperuricemia Without Comorbidities Predicts Cardiometabolic Diseases: Five-Year Japanese Cohort Study*. Hypertension, 2017. **69**(6): p. 1036-1044.
202. Soletsky, B. and D.I. Feig, *Uric acid reduction rectifies prehypertension in obese adolescents*. Hypertension, 2012. **60**(5): p. 1148-56.
203. Feig, D.I., B. Soletsky, and R.J. Johnson, *Effect of allopurinol on blood pressure of adolescents with newly diagnosed essential hypertension: a randomized trial*. JAMA, 2008. **300**(8): p. 924-32.
204. Braga, T.T., et al., *Sensing soluble uric acid by Naip1-Nlrp3 platform*. Cell Death Dis, 2021. **12**(2): p. 158.
205. Martinon, F., et al., *Gout-associated uric acid crystals activate the NALP3 inflammasome*. Nature, 2006. **440**(7081): p. 237-41.
206. Ginsberg, M.H., et al., *Release of platelet constituents by monosodium urate crystals*. J Clin Invest, 1977. **60**(5): p. 999-1007.
207. Ginsberg, M., et al., *Mechanisms of platelet response to monosodium urate crystals*. Am J Pathol, 1979. **94**(3): p. 549-68.
208. Boss, G.R. and J.E. Seegmiller, *Hyperuricemia and gout. Classification, complications and management*. N Engl J Med, 1979. **300**(26): p. 1459-68.
209. Alvarez-Lario, B. and J. Macarron-Vicente, *Uric acid and evolution*. Rheumatology (Oxford), 2010. **49**(11): p. 2010-5.
210. Amaro, S., et al., *A pilot study of dual treatment with recombinant tissue plasminogen activator and uric acid in acute ischemic stroke*. Stroke, 2007. **38**(7): p. 2173-5.
- rats. J Biomed Opt, 2014. **19**(9): p. 96013.
144. Wu, J. and L.J. Yan, *Streptozotocin-induced type 1 diabetes in rodents as a model for studying mitochondrial mechanisms of diabetic beta cell glucotoxicity*. Diabetes Metab Syndr Obes, 2015. **8**: p. 181-8.
145. Kilic, E., D.M. Hermann, and K.A. Hossmann, *A reproducible model of thromboembolic stroke in mice*. Neuroreport, 1998. **9**(13): p. 2967-70.
146. Hara, T., G. Mies, and K.A. Hossmann, *Effect of thrombolysis on the dynamics of infarct evolution after clot embolism of middle cerebral artery in mice*. J Cereb Blood Flow Metab, 2000. **20**(10): p. 1483-91.

147. Kilic, E., D.M. Hermann, and K.A. Hossmann, *Recombinant tissue-plasminogen activator-induced thrombolysis after cerebral thromboembolism in mice*. *Acta Neuropathol*, 2000. **99**(3): p. 219-22.
148. Orset, C., et al., *Mouse model of in situ thromboembolic stroke and reperfusion*. *Stroke*, 2007. **38**(10): p. 2771-8.
149. Miyake, K., S. Takeo, and H. Kaijihar, *Sustained decrease in brain regional blood flow after microsphere embolism in rats*. *Stroke*, 1993. **24**(3): p. 415-20.
150. Hervey, G.R., *The effects of lesions in the hypothalamus in parabiotic rats*. *J Physiol*, 1959. **145**(2): p. 336-52.
151. Coleman, D.L. and K.P. Hummel, *Effects of parabiosis of normal with genetically diabetic mice*. *Am J Physiol*, 1969. **217**(5): p. 1298-304.
152. Coleman, D.L., *Effects of parabiosis of obese with diabetes and normal mice*. *Diabetologia*, 1973. **9**(4): p. 294-8.
153. Coleman, D.L., *Obese and diabetes: two mutant genes causing diabetes-obesity syndromes in mice*. *Diabetologia*, 1978. **14**(3): p. 141-8.
154. Maffei, M., et al., *Leptin levels in human and rodent: measurement of plasma leptin and ob RNA in obese and weight-reduced subjects*. *Nat Med*, 1995. **1**(11): p. 1155-61.
155. Alpers, C.E. and K.L. Hudkins, *Mouse models of diabetic nephropathy*. *Curr Opin Nephrol Hypertens*, 2011. **20**(3): p. 278-84.
156. Qi, Z., et al., *Characterization of susceptibility of inbred mouse strains to diabetic nephropathy*. *Diabetes*, 2005. **54**(9): p. 2628-37.
157. Furman, B.L., *Streptozotocin-Induced Diabetic Models in Mice and Rats*. *Curr Protoc Pharmacol*, 2015. **70**: p. 5 47 1-5 47 20.
158. Soler, M.J., et al., *ACE2 inhibition worsens glomerular injury in association with increased ACE expression in streptozotocin-induced diabetic mice*. *Kidney Int*, 2007. **72**(5): p. 614-23.
159. DeFronzo, R.A., et al., *Type 2 diabetes mellitus*. *Nat Rev Dis Primers*, 2015. **1**: p. 15019.
160. Forbes, J.M. and M.E. Cooper, *Mechanisms of diabetic complications*. *Physiol Rev*, 2013. **93**(1): p. 137-88.
161. Ghanem, F., et al., *Cholesterol crystal embolization following plaque rupture: a systemic disease with unusual features*. *J Biomed Res*, 2017. **31**(2): p. 82-94.
162. Percie du Sert, N., et al., *Reporting animal research: Explanation and elaboration for the ARRIVE guidelines 2.0*. *PLOS Biology*, 2020. **18**(7): p. e3000411.
163. Motrapu, M., et al., *Drug Testing for Residual Progression of Diabetic Kidney Disease in Mice Beyond Therapy with Metformin, Ramipril, and Empagliflozin*. *J Am Soc Nephrol*, 2020. **31**(8): p. 1729-1745.
164. Schreiber, A., et al., *Transcutaneous measurement of renal function in conscious mice*. *Am J Physiol Renal Physiol*, 2012. **303**(5): p. F783-8.
165. Lei, Y., et al., *A multicenter blinded preclinical randomized controlled trial on Jak1/2 inhibition in MRL/MpJ-Fas(lpr) mice with proliferative lupus nephritis predicts low effect size*. *Kidney Int*, 2021. **99**(6): p. 1331-1341.
166. Ma, Q., *The Effects of Hyperuricemia on Sterile Inflammation during Chronic Kidney Disease*. 2019, Ludwig-Maximilians-Universität.
167. Yeap, X.Y., et al., *Quantitation of acute necrosis after experimental myocardial infarction*. *Methods Mol Biol*, 2013. **1004**: p. 115-33.
168. Ma, Q., et al., *Soluble Uric Acid Is an Intrinsic Negative Regulator of Monocyte Activation in Monosodium Urate Crystal-Induced Tissue Inflammation*. *J Immunol*, 2020. **205**(3): p. 789-800.
169. Tang, W.H., et al., *Glucose and collagen regulate human platelet activity through aldose reductase induction of thromboxane*. *J Clin Invest*, 2011. **121**(11): p. 4462-76.
170. Naqvi, M.Z.S.N.-u.-H., *Effects of STZ-Induced Diabetes on the Relative Weights of Kidney, Liver and Pancreas in Albino Rats: A Comparative Study*. *International Journal of Morphology*, 2010. **28**(1): p. 135-142.
171. Benedek, A., et al., *Use of TTC staining for the evaluation of tissue injury in the early phases of reperfusion after focal cerebral ischemia in rats*. *Brain Res*, 2006. **1116**(1): p. 159-65.

172. Rask-Madsen, C. and G.L. King, *Vascular complications of diabetes: mechanisms of injury and protective factors*. *Cell Metab*, 2013. **17**(1): p. 20-33.
173. Deng, M., et al., *Metformin and Vascular Diseases: A Focused Review on Smooth Muscle Cell Function*. *Front Pharmacol*, 2020. **11**: p. 635.
174. Bautista-Becerril, B., et al., *Immunothrombosis in COVID-19: Implications of Neutrophil Extracellular Traps*. *Biomolecules*, 2021. **11**(5).
175. Nakazawa, D., et al., *Histones and Neutrophil Extracellular Traps Enhance Tubular Necrosis and Remote Organ Injury in Ischemic AKI*. *J Am Soc Nephrol*, 2017. **28**(6): p. 1753-1768.
176. Fidler, T.P., et al., *Deletion of GLUT1 and GLUT3 Reveals Multiple Roles for Glucose Metabolism in Platelet and Megakaryocyte Function*. *Cell Rep*, 2017. **20**(4): p. 881-894.
177. Shechter, M., et al., *Blood glucose and platelet-dependent thrombosis in patients with coronary artery disease*. *J Am Coll Cardiol*, 2000. **35**(2): p. 300-7.
178. Karolczak, K., et al., *Platelet and Red Blood Cell Counts, as well as the Concentrations of Uric Acid, but Not Homocysteinaemia or Oxidative Stress, Contribute Mostly to Platelet Reactivity in Older Adults*. *Oxid Med Cell Longev*, 2019. **2019**: p. 9467562.
179. Matuschik, L., et al., *Hyperglycemia Induces Inflammatory Response of Human Macrophages to CD163-Mediated Scavenging of Hemoglobin-Haptoglobin Complexes*. *Int J Mol Sci*, 2022. **23**(3).
180. Kanter, J.E., et al., *Diabetes promotes an inflammatory macrophage phenotype and atherosclerosis through acyl-CoA synthetase 1*. *Proc Natl Acad Sci U S A*, 2012. **109**(12): p. E715-24.
181. Josefs, T., et al., *Neutrophil extracellular traps promote macrophage inflammation and impair atherosclerosis resolution in diabetic mice*. *JCI Insight*, 2020. **5**(7).
182. Dogan, Y., et al., *Serum IL-1beta, IL-2, and IL-6 in insulin-dependent diabetic children*. *Mediators Inflamm*, 2006. **2006**(1): p. 59206.
183. Bashir, H., et al., *Role of inflammatory mediators (TNF-alpha, IL-6, CRP), biochemical and hematological parameters in type 2 diabetes mellitus patients of Kashmir, India*. *Med J Islam Repub Iran*, 2020. **34**: p. 5.
184. Niiya, Y., et al., *Advanced glycation end products increase permeability of brain microvascular endothelial cells through reactive oxygen species-induced vascular endothelial growth factor expression*. *J Stroke Cerebrovasc Dis*, 2012. **21**(4): p. 293-8.
185. Hirose, A., et al., *Advanced glycation end products increase endothelial permeability through the RAGE/Rho signaling pathway*. *FEBS Lett*, 2010. **584**(1): p. 61-6.
186. Ishibashi, Y., et al., *Advanced glycation end products potentiate citrated plasma-evoked oxidative and inflammatory reactions in endothelial cells by up-regulating protease-activated receptor-1 expression*. *Cardiovasc Diabetol*, 2014. **13**: p. 60.
187. Andreadou, I., et al., *SGLT2 inhibitors reduce infarct size in reperfused ischemic heart and improve cardiac function during ischemic episodes in preclinical models*. *Biochim Biophys Acta Mol Basis Dis*, 2020. **1866**(7): p. 165770.
188. MacDougall, N.J. and K.W. Muir, *Hyperglycaemia and infarct size in animal models of middle cerebral artery occlusion: systematic review and meta-analysis*. *J Cereb Blood Flow Metab*, 2011. **31**(3): p. 807-18.
189. Izumi, Y., et al., *Insulin protects brain tissue against focal ischemia in rats*. *Neurosci Lett*, 1992. **144**(1-2): p. 121-3.
190. Miki, T., et al., *Effects of diabetes on myocardial infarct size and cardioprotection by preconditioning and postconditioning*. *Cardiovasc Diabetol*, 2012. **11**: p. 67.
191. Tonneijck, L., et al., *Glomerular Hyperfiltration in Diabetes: Mechanisms, Clinical Significance, and Treatment*. *J Am Soc Nephrol*, 2017. **28**(4): p. 1023-1039.
192. Noshahr, Z.S., et al., *Animal Models of Diabetes-Associated Renal Injury*. *J Diabetes Res*, 2020. **2020**: p. 9416419.
193. Jiang, H., et al., *The Mitochondria-Targeted Metabolic Tubular Injury in Diabetic Kidney Disease*. *Cell Physiol Biochem*, 2019. **52**(2): p. 156-171.

194. Tanaka, S., et al., *Sodium-glucose cotransporter 2 inhibition normalizes glucose metabolism and suppresses oxidative stress in the kidneys of diabetic mice*. *Kidney Int*, 2018. **94**(5): p. 912-925.
195. Verzola, D., et al., *Oxidative stress mediates apoptotic changes induced by hyperglycemia in human tubular kidney cells*. *J Am Soc Nephrol*, 2004. **15 Suppl 1**: p. S85-7.
196. Dhananjayan, R., et al., *Endothelial Dysfunction in Type 2 Diabetes Mellitus*. *Indian J Clin Biochem*, 2016. **31**(4): p. 372-9.
197. Hammer, S.S., et al., *Statins and  $\alpha$  cyclodextrin treatments prevent cholesterol crystal-induced pathology in human retinal endothelial cells and in db/db mice*. *Investigative Ophthalmology & Visual Science*, 2021. **62**(8): p. 2928-2928.
198. Zhao, Y., et al., *Diabetes mellitus is associated with shortened activated partial thromboplastin time and increased fibrinogen values*. *PLoS One*, 2011. **6**(1): p. e16470.
199. Alzahrani, S.H. and R.A. Ajjan, *Coagulation and fibrinolysis in diabetes*. *Diab Vasc Dis Res*, 2010. **7**(4): p. 260-73.
200. Kaur, R., M. Kaur, and J. Singh, *Endothelial dysfunction and platelet hyperactivity in type 2 diabetes mellitus: molecular insights and therapeutic strategies*. *Cardiovasc Diabetol*, 2018. **17**(1): p. 121.
201. Pretorius, E., *Platelets as Potent Signaling Entities in Type 2 Diabetes Mellitus*. *Trends Endocrinol Metab*, 2019. **30**(8): p. 532-545.
202. Petrie, J.R., T.J. Guzik, and R.M. Touyz, *Diabetes, Hypertension, and Cardiovascular Disease: Clinical Insights and Vascular Mechanisms*. *Can J Cardiol*, 2018. **34**(5): p. 575-584.
203. Derosa, G. and P. Maffioli, *A review about biomarkers for the investigation of vascular function and impairment in diabetes mellitus*. *Vasc Health Risk Manag*, 2016. **12**: p. 415-419.
204. Leo, M.D., et al., *TMEM16A channel upregulation in arterial smooth muscle cells produces vasoconstriction during diabetes*. *Am J Physiol Heart Circ Physiol*, 2021. **320**(3): p. H1089-H1101.
205. Soloviev, A., et al., *Hypoxic pulmonary vasoconstriction is lacking in rats with type 1 diabetes*. *Clin Exp Pharmacol Physiol*, 2019. **46**(11): p. 1022-1029.
206. Sanchez-Lozada, L.G., et al., *Hemodynamics of hyperuricemia*. *Semin Nephrol*, 2005. **25**(1): p. 19-24.
207. Sanchez-Lozada, L.G., et al., *Mild hyperuricemia induces vasoconstriction and maintains glomerular hypertension in normal and remnant kidney rats*. *Kidney Int*, 2005. **67**(1): p. 237-47.
208. Kuwabara, M., et al., *Asymptomatic Hyperuricemia Without Comorbidities Predicts Cardiometabolic Diseases: Five-Year Japanese Cohort Study*. *Hypertension*, 2017. **69**(6): p. 1036-1044.
209. Soletsky, B. and D.I. Feig, *Uric acid reduction rectifies prehypertension in obese adolescents*. *Hypertension*, 2012. **60**(5): p. 1148-56.
210. Feig, D.I., B. Soletsky, and R.J. Johnson, *Effect of allopurinol on blood pressure of adolescents with newly diagnosed essential hypertension: a randomized trial*. *JAMA*, 2008. **300**(8): p. 924-32

---

## 7. *Abbreviations*

<b>ACR</b>	Albumin-creatinine ratio
<b>ADP</b>	Adenosine diphosphate
<b>AGE</b>	Advanced glycation end products
<b>AKI</b>	Acute kidney injury
<b>ATP</b>	Adenosine triphosphate
<b><math>\alpha</math>-SMA</b>	Alpha smooth muscle actin
<b>BUN</b>	Blood urea nitrogen
<b>CC</b>	Cholesterol crystal
<b>CCE</b>	Cholesterol crystal embolism
<b>CDC</b>	Center of Disease Control
<b>CKD</b>	Chronic kidney disease
<b>CRP</b>	Collagen-related peptide
<b>CXCL</b>	Chemokine (C-X-C motif) ligand
<b>CXCR</b>	C-X-C motif chemokine receptor
<b>DAMPs</b>	Damage-associated molecular patterns
<b>DKD</b>	Diabetic kidney disease
<b>DMEM</b>	Dulbecco's Modified Eagle Medium
<b>ELISA</b>	Enzyme linked immunosorbent assay
<b>FCS</b>	Fetal calf serum
<b>FITC</b>	Fluorescein-isothiocyanate
<b>GE<sub>n</sub>C</b>	Mouse glomerular endothelial cells
<b>GFR</b>	Glomerular filtration rate
<b>GPVI</b>	Glycoprotein VI
<b>GPIb</b>	Glycoprotein Ib
<b>HG</b>	High glucose
<b>HK2</b>	Human renal proximal tubular epithelial cells
<b>HU</b>	Hyperuricemic mice
<b>ITAM</b>	Immunoreceptor tyrosine-based activation motif
<b>IL</b>	Interleukins
<b>LDL</b>	Low-density lipoprotein
<b>NETs</b>	Neutrophil extracellular traps
<b>OD</b>	Optical density

---

<b>PAS</b>	Periodic acid Schiff staining
<b>PAR-Gq</b>	Protease-activated receptor-G $\alpha_q$
<b>PGI2</b>	Prostaglandin I2
<b>PS</b>	Penicillin-streptomycin
<b>PSGL-1</b>	P-selectin glycoprotein ligand-1
<b>sdLDL</b>	Small dense LDL
<b>SGLT2</b>	Sodium-glucose cotransporter-2
<b>STZ</b>	Streptozotocin
<b>T1D</b>	Type 1 diabetes
<b>T2D</b>	Type 2 diabetes
<b>TF</b>	Tissue factor
<b>TTC</b>	2,3,5-triphenyl tetrazolium chloride
<b>UA</b>	Uric acid
<b>UACR</b>	Urinary albumin to creatinine ratio
<b>vWF</b>	von Willebrand factor
<b>WHO</b>	World Health Organization

## **8. Acknowledgment**

There are many colleagues who have contributed to this project, helped and inspired me during my study. I would like to convey my gratitude to all of them.

First, I would like to thank my supervisor Prof. Dr. Hans-Joachim Anders. He patiently provided the vision, encouragement and advice for me to proceed through the doctoral program. Thank you very much for giving me the opportunity to work at Anders Lab. I would like to thank my co-supervisor Priv. Doz. Dr. Stefanie Steiger. Thank you for your sharing, guidance, and encouragement.

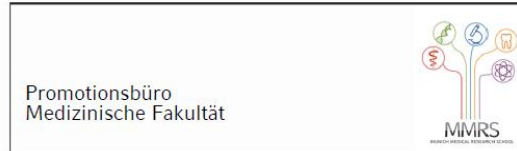
I would also like to thank people for their work and cooperation to complete this thesis. Thank Dr. Attila Braun and Dr. Elmina Mammadova-Bach in Walther-Straub-Institute, LMU, Germany for collaborate with the platelet part. Thank Yvonne Minor, Anna Anfimiadou and Janina Mandelbaum for their technique support and assistance of animal study.

I thank all my lab members. Thank Yutian, Lidia, Mohsen, Qiuyue, Shishi, Taka, Manga, Chenyu, Dangyang, Meisi, Li Li, Zhibo, Qiubo, Cong for their teaching, sharing, help, and encouragement. Thank all the lab buddies, who I could not enumerate here, for generating such a friendly and scientific environment. Thank Bruno, Kathi, Thi, Maciej, Jana and Anna for all the organization and management of our lab.

I would like to thank CSC-LMU scholarship for their financial support and giving me an opportunity to study abroad.

I would like to thank my family and friends, who are the pillar of my life and whose advice and encouragement I greatly appreciate.

It is my duty to express my humble respect to the animals, which had to involved in the experiment for the betterment of human being.



## Affidavit

Luying Yang

\_\_\_\_\_  
Surname, first name

Goethestraße 31

\_\_\_\_\_  
Street

80336 München, Germany

\_\_\_\_\_  
Zip code, town, country

I hereby declare, that the submitted thesis entitled:

**Metabolic comorbidities modulate kidney cholesterol crystal embolism**

is my work. I have only used the sources indicated and have not made unauthorised use of services of a third party. Where the work of others has been quoted or reproduced, the source is always given.

I further declare that the submitted thesis or parts thereof have not been presented as part of an examination degree to any other university.

Munich, 03,04,2023.

\_\_\_\_\_  
place, date

Luying Yang

\_\_\_\_\_  
Signature doctoral candidate